PRELIMINARY SHUTTLE STRUCTURAL DYNAMICS MODELING DESIGN STUDY

GRUMMAN

N73-13911
NASA CR 112196

PRELIMINARY SHUTTLE STRUCTURAL DYNAMICS MODELING DESIGN STUDY

Prepared Under Contract NAS1-10635-4 by
Grumman Aerospace Corporation
Bethpage, New York 11714

NOVEMBER 1972

for

Langley Research Center
Hampton, Virginia 23365

NATIONAL AERONAUTICS AND SPACE ADMINISTRATION

FOREWORD

The work presented in this report was the combined effort of TRW Systems Group Incorporated and Grumman Aerospace Corporation. Sections 2, 3, and 8 were prepared by TRW (A. E. Galef, Dr. P. B. Grote, and D. H. Mitchell respectively). Sections 4 and 6 were prepared by J. B. Smedfjeld, and Section II was prepared by R. L. Goldstein following suggestions by S. Goldenberg. The remainder of the report and all the revisions and addition of updated information were prepared by M. Bernstein.

The design study of the 1/10th scale model details was conducted by A. P. LaValle, F. L. Halfen, and P. J. Coschignano.

This work was administered by the Dynamic Loads Branch, Loads Division, NASA Langley Research Center, Hampton, Virginia.

This report has been approved by:

Eugene F. Baird

Eugene F. Baird
Program Manager

TABLE OF CONTENTS

INTRODUCTION AND CHRONOLOGY

INTRODUCTION AND CHRONOLOGY

Structural dynamics problems during the Apollo program were very important and required considerable technology development concurrent with the design and flights of the various vehicles. Problems caused by POGO in particular required a high level of effort in very short time span. Increased analytical and test capability has since been developed and should help to reduce the impact of these problems on the Shuttle program. However, the Shuttle configuration will have more complex structural dynamic characteristics than previous launch vehicles primarily because of the high modal density at low frequencies and the high degree of coupling between lateral and longitudinal motions. A preliminary structural dynamics model will provide for the early study of many structural dynamics problems, a means of evaluating the accuracy of the structural and hydroelastic analysis methods on a shuttle-like test vehicle, and a means for efficiently evaluating potential cost savings in structural dynamic testing techniques.

This task was originally established in June 1971 to determine the optimum configuration for such a preliminary model. The original requirements for the study included the following:

(1) Determination of requirements based upon a review of significant dynamics analyses (POGO, Control System Stability, Dynamic Loads)
(2) Selection of a generalized model configuration
(3) Study of two candidate scale factors
(4) Study of initial structural details and material substitutions
(5) Preparation of Test Plans and Schedules

The requirements study based upon the Shuttle configurations under consideration at that time was completed and reviewed on August 12, 1971. Copies of the report were submitted to the Technical Monitor on September 20, 1971.

As a result of changes in the Shuttle Configuration and at the request of the Technical Monitor, the effort on the remaining portions of the study was suspended until more definitive configuration information became available.

An additional study, authorized by Modification No. 1, to further evaluate modal component synthesis techniques was completed in November 1971, and submitted to the NASA Technical Monitor on December 13, 1971. This study verified that the analytical treatment of measured data was feasible for the existing 1/15 scale NASA Langly Shuttle Model, and that further analysis was warranted. As part of the same effort, a review of the measurements required to compute a damping matrix from test data was conducted at TRW. The procedure proposed is described in an AIAA Journal note "Method for Constructing a Full Modal Damping Matrix From Experimental Measurements" by T. K. Hasselman, April 1972. The attempt at using this method on available NASA and TRW test data showed that the presence of off-resonant modes in the responses made the data unsuitable, and additional processing was required. This effort was transferred to Task NAS 1-10635-8 for processing vibration test data.

Modification No. 3 authorized a change in the basic objectives of the task by directing that a general arrangement and some structural details of a 1/10 scale model design for the series-burn pressure-fed booster, which had been selected as the baseline configuration, be developed. In accordance with this direction, model structural studies and an accompanying stress analysis was undertaken starting in January 1971. Proposed details of the LO_2 tank, intertank skirt, and LH_2 tank were discussed with the NASA Technical Monitor in January 1971. The preliminary design and analysis was completed and submitted on March 31, 1972.

This completed the model design effort under this Task Order. The design details for the tanks and orbiter developed during this effort are presently being used as part of the design of a complete model under NASA 1-10635-11.

An additional brief study of the suitability of the proposed model design details for obtaining structural dynamics data for use in verifying POGO analytical methods was completed by TRW in August 1972.

All the work accomplished under this Task Order, as described above, has been included in this report. Several of the sections have been revised slightly from their original submission to include additional available information.

1. RATIONALE FOR MODEL AND PROPOSED MODEL FEATURES

1. RATIONALE FOR MODEL AND PROPOSED MODEL FEATURES

1.1 Necessity for a Preliminary Shuttle Dynamic Model

Structural dynamic effects will be much more important for the Shuttle than for past launch vehicles because the configurations evolving from the various studies all possess large numbers of low-frequency modes with considerable amounts of coupling between motions in orthogonal directions. These effects are analytically accounted for by using mathematical models derived from a large-scale finite-element representation. Experience on less complex vehicles such as Saturn, LM, and F-14 has shown instances where important differences occurred between analysis and test results, for example, between the calculated and measured mode shapes and frequencies. It is imperative, therefore, that shuttle analytical procedures be checked (and modified or supplemented as required) by comparing typical results from these procedures with corresponding test data from a structure containing as many of the significant prototype features as is feasible. A preliminary dynamic model provides the only means of obtaining this complementary experimental data on a timely and cost-effective basis. Specific contributions of the dynamic-model program are:

- Enhancement and verification of analytical modeling procedures in areas where these are reasonably well developed (e.g., definition of finite-element structures models and lumped mass dynamics models)
- Complementary empirical data in areas where analyses are relatively weak (e.g., representation of fluid/tank-wall interactions for highly flexible thin shell tanks, or modeling of partially buckled structural elements)
- Investigation of effects of system nonlinearities (e.g., preloaded interstage restraint systems)

In addition to these analysis-related requirements for a dynamic model, some further benefits include:

- Early verification of important preliminary vehicle dynamic characteristics of a typical shuttle design
- Disclosure of previously unanticipated dynamics problem areas

- Definition of optimum configuration changes for eliminating critical problem areas
- Development and demonstration of efficient full-scale prototype testing procedures.

In summary, while fulfilling its primary mission of providing vitally needed supporting data in key analysis areas, the model will also furnish means for investigating critical design and testing problems.

1.2 Rationale for Selecting Configuration Features

The primary purpose of the preliminary dynamic model is to verify the procedures used in analyses. Therefore the major emphasis in this limited study establishing model requirements was to review each of important analytical procedures in detail and determine the necessary structural dynamics information. In most instances this consisted of determining the modes in which major input forces and responses occurred, and the significant structural details in these modes. The frequency ranges required were determined principally from analyses conducted during shuttle configuration studies or from Saturn V results.

The model is also required to incorporate as many significant typical prototype features as possible so as to reveal the maximum number of problem areas. In order to limit costs, however, these features should be simplified and idealized while still simulating the dynamic behavior.

1.3 Summary of Recommended Configuration Features

The significant structural features required for the major elements of a model to be representative of a prototype for each analysis reviewed and most likely to reveal problem areas are summarized in Section 10. Based upon these considerations, it is recommended that a preliminary dynamic model incorporate the features listed below.

- Orbiter

  The orbiter fuselage should be represented by three sections consisting of a forward portion containing the crew area and forward payload attachments, a mid-section containing the wing carry-through and the aft payload attachments, and an aft section containing the engine and fin support structures. The crew compartment should be a simple closed

shell containing extensions of the two side longerons with provisions for attachment of weights representing equipment. The mid section should have removable payload doors which have torsion carrying capability but add no bending stiffness. The basic U shape frame for the mid section should be used along the entire fuselage.

- External Tanks

  The external tank should consist of a representation of an LO_2 tank designed to hold water, an intertank skirt with provisions for attaching SRM's, an LH_2 tank with internal frames and external fittings to attach the Orbiter, and an aft skirt with provisions for attaching the booster. The LO_2 tank should be represented by a monocoque shell of uniform thickness. The bottom dome should be of uniform thickness with attachment for measuring pressure and for drain and fill capability. No provision is required for slosh baffles or simulated feedlines. Internal pressurization can be limited to a low value (2 psi).

  The intertank skirt should be of monocoque construction with no chem milling. Any frames or struts used to distribute loads internally should be represented by the proper geometry, however, in order to keep the design simple, the members should be designed to avoid buckling without requiring added stiffening. Interstage attachment members may be of simple cross-sectional shape rather than scaled down prototype values. Fittings may be oversized and simplified to limit costs.

  The LH_2 tank should be of monocoque construction with a minimum of chem milling. Skin gages should be heavy enough to avoid buckling under model handling loads without requiring any additional stiffeners. The internal frames which transmit the orbiter loads should have the proper geometry but the members may be of simpler cross sectional shape and should be designed to avoid buckling without stiffening. Fittings may be oversized and simplified to limit costs.

  The aft skirt should be of simple monocoque construction, similar to the inter-tank skirt described above.

2. POGO CONSIDERATIONS IN A SPACE-SHUTTLE STRUCTURAL DYNAMIC MODEL

2. POGO CONSIDERATIONS IN SPACE-SHUTTLE STRUCTURAL DYNAMIC MODEL

2.1 Brief Description of Analysis Procedures

POGO is a self-excited oscillation that results from coupling of structure, propellant, the pumps and the motors of a rocket propelled vehicle.

Qualitatively, the POGO phenomenon occurs because vehicle accelerations and associated accelerations of the propellants in tanks and feedlines cause pressure changes in the propellant at the pump inlet. These pressure changes result in changes of net thrust of the rocket motors. The phase of these thrust changes is usually such as to cause structural accelerations in the same direction as those initially postulated. There is then "positive feedback," and the system is potentially capable of self-excited vibration.

A determination for a particular configuration of a specific vehicle of whether POGO is likely to occur, may be made from an evaluation of the closed-loop eigenvalues of the coupled engine-structure-line system or, alternately, by a calculation of the open-loop frequency response of the same system with the loop opened at pertinent points. Regardless of whether open-loop or closed-loop analysis is selected, it is necessary to enter the same parameters in the analysis. These parameters are:

(1) Structural response, as functions of magnitude and frequency of exciting force at engine locations

   a. Engine motions
   b. Pump motions
   c. Motions of fluids in fuel and oxidizer tanks, or alternately
   d. Pressure of fluids at tank-feedline interfaces

(2) Feedline Characteristics

   a. Pressure at pump inlets caused by pressure at tank-feedline interfaces and motion of lines and pumps*

*This pressure is often influenced strongly by the naturally occurring or artifically provided compliance at the pump inlet, and is therefore determined separately from Item 1-d, above.

(3) Pump-Engine Characteristics

a. Variations in net thrust caused by variations in pressure and flow rates at the pump inlet

b. Compliance at pump inlets

All these parameters may be determined, with more or less accuracy and confidence, by analysis at early stages of the vehicle design. But they must all be test-verified prior to flight in order to improve confidence in results of POGO stability calculations.

The structural characteristics should be test-verified as early as possible because of the tremendous schedule and cost impact that could result from unforeseen structural characteristics that are sufficiently unfavorable to indicate a need for significant changes. A structural dynamic scale model, which may be considered as a hybrid between analysis and a full scale structure, can be of great help in confirming the analytic techniques used to calculate structural characteristics.

The feedline characteristics, as functions of the compliance prevailing at the pump inlet, have been considered in the past to be the characteristics which are most amenable to analysis and therefore to require the least test verification. However, the convolutions of presently proposed space-shuttle feedlines are such that confidence in analysis is reduced, and test-verification prior to building of actual hardware will be appropriate. Models of feedlines will be valuable, but these need not be incorporated in the overall model for the reasons discussed later in Section 2.4.3. Instead, the effect of the lines, when known from analysis and test can be incorporated in the overall mathematical model by reliable modal synthesis techniques.

The pump and engine characteristics, including the cavitation compliance at the pump inlet which has been stipulated often to have strong effects upon the feedline characteristics, are dependent upon both fluid velocities and accelerations, which cannot be scaled simultaneously. Therefore, these characteristics cannot be derived from scale models and a scale model cannot be used to provide a complete determination of the POGO stability of the space-shuttle. But because a structural dynamic scale model can provide some important information in a timely manner, it can be a very valuable tool for

determination of POGO stability. Such a model is recommended.

In the remainder of this section, considerations entering into the cost-effective and timely fabrication of such a model are discussed. Specific recommendations are made when possible, and areas requiring further studies are identified.

2.2 Tanks and Fluids

2.2.1 Tank Structure

Tank bulging influences all longitudinal modes, and has a direct effect on the modal pressures at the tank-feedline interface.

Tank bulging is affected primarily by the density of the fluid in the tank and by the stiffness of the tank walls and bottom. The density of the walls and bottom is of negligible concern, as is the stiffness (bulk modulus) of the fluids.

The stiffness of concern for thin-walled tanks as will exist in space-shuttle is primarily extensional stiffness; shell bending stiffness has purely local effects which are overwhelmed by the extensional stiffness. As a result, it will be permissible to model the tank walls and bottom with any material of appropriate thickness having stiffness (EA) equivalent to the composite stiffness of the proposed tank design. This permits the use of reinforced plastic for the model tank wall, and this may be particularly convenient if the full scale design should incorporate different circumferential and longitudinal stiffness. An appropriate selection of amount of reinforcing material in the warp and woof of the selected reinforcing fabric will permit adequate simulation of tank walls.

2.2.2 Fluids

Present planning involves fueling the external tanks with liquid hydrogen and liquid oxygen.

A mixture of water and alcohol could be made to provide precise density simulation of liquid oxygen, as could many other combinations of miscible fluids. Any such mixture would have substantially greater acoustic velocity than the highly compressible liquid oxygen but, as was noted, this difference is not significant for tank bulging modes.

The very low density of liquid hydrogen, which makes it difficult to simulate with a room-temperature fluid, usually makes it precise simulation unnecessary. Thus, when testing the "Apollo" full scale Dynamic Test Vehicle it was conclused that negligible accuracy would be lost if the liquid hydrogen were replaced in the scale model by an equivalent weight of water. An equivalent conclusion may well be reached for the proposed space-shuttle model.

If the lack of need for simulation of the liquid hydrogen cannot be demonstrated for space-shuttle, then it will be possible to provide reasonable density simulation with a uniform grid of closed-cell plastic foam blocks, constrained against floating to the surface, displacing appropriate amounts of water. Appropriate density plastic beads, either foam or phenolic "micro-ballons," might prove to be acceptable without any fluid.

Finally it is noted that while simulation of fluids by spring masses will be useful in some model studies, particularly those involving slosh modes where gravity scaling is impossible, such simulations do not appear to be either necessary or sufficient for a model designed to yield POGO information.

2.3 Structural Transfer Functions Required

The structural characteristics which have been noted as necessary for quantitative POGO analysis have been stipulated to be frequency-dependent functions. As a result, the structure is most conveniently described for POGO analysis by sets of characteristics of its normal modes. The pertinent characteristics are:

(1) Modal frequency
(2) Modal damping
(3) Generalized modal mass
(4) Modal motions of engines, pumps, feedlines, and propellant in tanks, normalized to the same point used for normalization in calculation of the modal mass

The modes of concern are those having substantial engine motion in the direction of engine thrust, and having modal frequencies near oxidizer* feedline resonant frequencies. In the case of the External Tank and SRM configuration, the frequency of the lowest feedline resonance of concern may be as low as 2.5 Hz, and only those structural modes with frequency less than approximately 25 Hz need be considered. For the Orbiter and External Tank configuration, or for a proposed configuration which has oxidizer tanks aft, however, it will not be possible to define a usefully low "upper limit of concern" until after accumulators have been assigned to the pump inlets, and reasonably sized. The "upper limit" for the orbiter, or for a booster with oxidizer tank aft, may be higher than 30 Hz.

2.3.1 Structural Details

Low "maximum" frequencies in the actual vehicle are desirable from the viewpoint of designing and building a model, for only those local assemblies having subsystem frequencies less than approximately one octave above the "maximum" frequency need be modeled in detail. Stiffer subassemblies are adequately modeled when their rigid body inertial properties are reproduced in scale. Conversely, some structure will be adequately modeled if its stiffness alone is reproduced in scale; an example would be the interconnecting structure between the booster and the orbiter.

2.3.1.1 Thrust Structure

The thrust structure, which interconnects the engines and attaches to the orbiter, may be a dominant factor in POGO-significant modes if the maximum frequency of concern extends reasonably high, and plans should be made for careful modeling of that structure. The expected simplicity of the orbiter thrust structure is fortunate in light of the possibly substantially higher frequency regime of concern which may require valid simulation of modes as high as 30 Hz. This implied the need for a scaled replica of orbiter thrust structure if the objective is a model with good fidelity to the prototype.

*Fuel feedlines are presently expected to have little influence on POGO sensitivity of the space shuttle because of the relatively short lengths of the fuel feedlines and because of the mass flow rate of liquid hydrogen will be of the order of 20% the flow rate of the liquid oxygen. These factors make large reductions in thrust oscillations for fuel side velocity changes as against oxidizer-side oscillations, and therefore make fuel natural frequencies of less concern.

Unless oxygen feedline accumulators should be firmly incorporated in the design, it is recommended that plans be made for including a scaled replica of this subsystem.

2.3.1.2 Lines

An important subassembly, whose modal frequency is by definition within the frequency regime of concern, is the oxidizer feedline system. This is discussed separately in Section 2.4, following.

2.3.1.3 Joints

Good design of joints usually aims for 100% joint efficiency, which means that the joint will fail under the same load as skin adjacent to the joint. In order to approach the goal of 100% efficiency, it is generally necessary to weld a reinforcing ring to the skin, so that the local stiffness and weight of the joint will differ from that of adjacent continuous structure even when the structural efficiency reaches the desired 100 percent.

Purely local increases in stiffness, even when quite large, have negligible effect upon structural modes. If analysis shows that any of the doublers hypothesized above increase local stiffness, their weight effects may be accounted for by adding some local weight to the model, and their stiffness effects may be neglected.

Local reductions in stiffness have more effect on modal characteristics than do stiffness increases, but the effects remain small in the absolute sense unless the stiffness reduction is large and this is not likely to occur in the case of a normally designed joint. If, however, calculations indicate that the stiffness reduction is indeed large, this can be simulated by cutting away a small region of skin much more easily and economically than by attempting to reproduce the joint.

2.4 Propulsion Study

Transfer Function Requirements

The transfer functions which are required with the structural transfer functions to complete the POGO loop are:

1. $\partial P_c/\partial P_{sO}$, $\partial P_c/P_{sf}$, $\partial P_c/\partial \dot{W}_{DO}$, $\partial P_c/\dot{W}_{Df}$
2. $\partial P_{sO}/\partial P_t$, $\partial P_{sO}/Y_e$, $\partial P_{sO}/\partial Y_\ell$, $\partial P_{sf}/\partial P_t$, $\partial P_{sf}/Y_e$, $\partial P_{sf}/Y_\ell$

Where P_c is engine chamber pressure
P_{sO}, P_{sf}, are inlet pressures of oxidizer, fuel, pumps, respectively
P_t is pressure at tank bottoms
$\dot{W}_{Df}$, $\dot{W}_{DO}$ is fluctuating flow rate in fuel, oxidizer, pumps respectively
Y_e, Y_ℓ, is motion of pump and line support points, respectively

2.4.1 Engine

The first set of functions, providing the chamber pressure and hence the thrust, are characteristics of the pumps and engines. As has been previously stated, these cannot be derived from scale models.

2.4.2 Lines

The second set of functions, yielding the pressures at the pump inlets, are functions of the geometry and stiffness of the feedline structure, the density and bulk modulus of the propellants, and the location and stiffness of naturally occurring or artifically provided lumped compliance at any point of the line. Direct replica simulation of this set of parameters in model scale will be exceedingly difficult if possible, because:

1. Line walls would have to have thickness as low as .002 inches even if the model were made as large as 1/10 scale
2. The bulk modulus of cryogenic fluids tends to be very low in comparison to that of room temperature fluids
3. Reynolds number (viscosity) considerations will probably enter, because of both the diameter reduction of a scale model and the necessary absence of "steady state" flow rate in a model

Some of these considerations can be overcome by, for example, using a highly compliant material for pipe walls and thereby arriving at a reasonably correct overall "effective" bulk modulus, $\hat{B}$, where

$$\hat{B} = \left(\frac{1}{B} + \frac{D}{tE}\right)^{-1}$$

where B is the bulk modulus of the fluid
D is local line diameter
E is line wall stiffness
t is line wass thickness

However, we recommend against such procedures and therefore against including simulated lines in the structural dynamic scale model because of the complexities and uncertainties of doing so.

Additionally, in deriving a mathematical model of a structure for POGO purposes, it customary to exclude the feedlines and their fluid from the basic structural model and later to couple the line modes with structural modes in the stability analysis. This has the important advantage of avoiding the need for calculation of new sets of structural modes for each change in feedline characteristics.

Exclusion of lines from a structural dynamic scale model would have an equivalent, and cost effectwise, probably more cogent advantage since it would not be necessary to retest the overall scale model each time a different line configuration is considered. Based upon past experience in Titan and Apollo POGO studies, where improvement of POGO characteristics involved primarily changes to local lumped line compliances, this will be a great advantage indeed in the Space Shuttle model.

The argument against including feedlines in the structural model is reinforced by experience on the 1/10 scale replica model of Apollo-Saturn V. Lines were carefully reproduced to scale on that model, but no useful data was achieved from this inclusion because the model test procedures could not include any provisions to reproduce the effect of fluid flow and cavitation at the pump entrance. Consequently line modes did not interact with structural modes in a realistic manner and useful correlation between feedline pressures and forces and motions could not be attained.

It will, however, be useful to build models of the lines alone, or a cold-flow facility which simulates the pump dynamics as well. Such models could help refine techniques for analytic calculations of line modes, as functions of cavitation and/or accumulator compliance, of the complicated line configuration presently planned.

A model of lines-alone would not be constrained by the scaling factor selected for the overall model, or by the material of the walls. Further, since the model would be for the purpose of verifying analytic techniques rather than achieving specific directly applicable numerical results, detailed geometry would not have to be reproduced. Thus a subassembly model with lines of sufficient diameter to facilitate making pressure measurements and to minimize viscosity effects could be built without the need to have straight sections of lines as long as the scale factor or diameters would require if detailed geometry were to be maintained. This would substantially facilitate testing.

2.5 POGO Related Test Objectives and Data for Proposed Model Tests(1)

2.5.1 Introduction

The structural dynamic complexity of the Space Shuttle configuration poses potential problems of a greater magnitude than have heretofore been experienced on spacecraft/launch systems. To enhance the understanding and assess the problems envisioned, a structural dynamic scale model has been proposed upon which a variety of tests could be performed. In a very general sense the objectives of this model test program can be grouped in three broad categories as follows:

- Enhancement and verification of analytic modelling techniques and procedures
- Disclosure and identification of unanticipated structural dynamic interactions and/or coupling problems
- Development and demonstration of appropriate testing techniques/procedures and data acquisition/evaluation techniques applicable to full scale prototype testing.

One of the prime outputs of the model test program will be the determination of the modal characteristics of the scale model against which analytic models will be evaluated. The complexity of the Space Shuttle configuration

(1) This section was added in August 1972 after the proposed model configuration for the parallel-burn Shuttle (with SRM's) was reviewed.

may require that the analytic modal characteristics be determined using component mode techniques, wherein subsystems such as the solid rocket motors, the H/O tankage, and the orbiter are individually and separately analytically modelled and then combined to generate shuttle system modal characteristics. An overall model test/analysis program as generally depicted in Figure 2-1 is envisioned. In support of such a program, the proposed design of the scale model H/O tankage (Reference 2-1) has been examined relative to the determination of modal tank bottom pressure coefficients necessary for a POGO analysis of the Space Shuttle.

2.5.2 Background

In longitudinal stability (POGO) analyses, an important set of parameters can be the "tank bottom pressure coefficients" (Reference 2-2). Such coefficients relate the oscillatory fluid pressure in the tank at the outlet to the feed system to a reference modal displacement or acceleration. The resulting tank bottom pressures are applied as a driving force to the feedline providing one of the coupling terms between the structural and propulsion systems in the closed loop interaction (POGO). The proper determination of these terms has only recently come under investigation as launch vehicle systems have become more complex (References 2-3, 2-4, 2-5).

Reference 2-4 gives a summary of dynamic modelling technology for liquid propellant launch vehicles circa 1969-70. At that time, approximate methods were developed to more adequately represent the interaction between liquid and structure in the propellant tanks. These techniques were sufficient for calculating the longitudinal modes of the vehicle, but Reference 2-4 states, "The method is not applicable where higher tank modes or local liquid effects, such as tank bottom pressures, must be predicted accurately."

Accordingly, an improved technique was used (Reference 2-3) to calculate tank bottom pressures for POGO analyses. The state of the fluid continuum is defined in terms of a velocity potential and finite elements are used to model the flexible tank. Surface wave effects are neglected and the liquid surface is assumed to remain flat. The analysis was compared with model tests but the experimental data were rather limited.

Another finite element technique (Reference 2-8) is similar to that of Reference 2-3 in that the fluid is treated as a continuum, but the problem is formulated in terms of an integral equation and discrete elements are used on the fluid boundaries. By using washer-like, annualr elements on the free surface, axisymmetric liquid sloshing effects are included (i.e., surface waves).

After the Saturn V experienced POGO on the S-II stage, vibration tests were conducted on an S-II Lox tank (termed the mini-stage). These experiments were compared with an analysis to determine tank modes and tank bottom pressure coefficients (Reference 2-5) which used the above mentioned finite element program. This recent paper (Reference 2-5, January 1972) presents a comparison between test and analysis. Although there are only limited tank bottom pressure data the modes and pressures compare reasonably well with the computer model.

In prior scale model testing of both the Titan III (Reference 2-6) and Saturn (Reference 2-7), the need for tank bottom pressuee coefficients was not compelling and no significant information was obtained although an attempt was apparently made to determine tank pressures. A similar situation prevailed during the full scale testing of Saturn V and no useful pressure information was obtained from these tests (Reference 2-4).

Presuming that the Shuttle scale model test program will contain, in some sense, the elements as depicted in Figure 2-1, the following sections provide objectives and data requirements pertinent to H/O tankage tank bottom pressures for POGO analyses. Similar examinations should be made for the other subsystems (solid rocket motors, and orbiter) and for the other dynamic analyses (controls, transient loads, separation dynamics, etc.).

2.5.3 Test Objectives

These objectives pertain to the H/O tankage as a component and as a part of the total Space Shuttle system, and are oriented specifically toward obtaining data necessary for POGO analyses.

For the H/O tankage alone, as a Space Shuttle subsystem or component, the prime test objective is:

(1) The determination of LO_2 tank bulging/aft dome longitudinal mode shapes and frequencies and corresponding modal tank bottom pressures under several propellant loading conditions. Modes up to approximately 20 Hz (prototype) with the tankage excited at the LO_2 tank "Y" ring are required.

For the H/O tankage integrated with the other subsystems (orbiter; with and without solid rocket motors) the objectives are:

(1) Determine the free-free coupled modal characteristics of the total Shuttle system (up to 20 Hz prototype) under several propellant loading conditions.

(2) Determine tank bottom pressure coefficients for each of the system modes identified. Both LO_2 and LH_2 tank bottom pressure coefficients should be determined, but any compromises should be resolved in favor of the LO_2 tank measurements.

2.5.4 Data Requirements

For the H/O tankage as a component or subsystem both accelerometer and pressure data are required. Placement of three rays of 4 accelerometers on the LO_2 tank aft dome is a possible scheme to determine the first few dome mode shapes (Figure 2-2). The three rays of accelerometers will permit averaging around the dome to help define the modes and the lateral accelerometers above the "Y" will permit detection of tank bulging. The intent is to define a dome mode shape that can be correlated with analytic results and to obtain a tank bottom pressure coefficient (psi/g or psi/in) for correlation with analytic predictions.

For the Space Shuttle system model, both tank bottom pressure transducers along with sufficient accelerometers such that system modes up to 10-15 Hz (prototype) can be defined are required. In particular modal data are required at the following locations for POGO analyses:

- 3 axis accelerometers at the orbiter engine location(s)
- 3 axis accelerometers at the LO_2 feedline attach points to the structure (in both orbiter and H/O tankage)

- both LO_2 and LH_2 tank bottom pressures and accelerations
- 3 axis accelerometers at the turbopump location(s) (if different from the engines)

Pressure transducers and accelerometers should have flat phase and amplitude response characteristics in the range of approximately 20-300 Hz. Oscillatory pressures will probably be less than 5 psi. (Static pressure in an unpressurized LO_2 tank full of water is $\sim$ 2.5 psi.) The detail of the tank bottom deflections may not be required if good correlation can be obtained in component or subsystem tests.

These data are required at several propellant loading configurations a minimum of which are (assuming an approximate 350 second powered flight and a 100 second solid rocket motor burn):

$t = 0$	Lift off
$t \simeq 100$	Booster burnout (booster attached)
$t \simeq 100$	Booster burnout (booster released)
$t \simeq 350$	Main engine burnout

All data should include amplitude, phase and frequency, as a function of input amplitude and frequency.

2.5.5 Configuration Considerations

Since one of the prime objectives is the analytic/test correlation relating tank bottom pressures and modal deflections (or accelerations) rather than obtaining directly scaleable results to the prototype, several cost effective compromises seem appropriate. Tapered thickness of the lower bulkheads is not necessary for the test/analytic comparison as long as the bulkhead modes remain in the proper frequency range relative to the overall system modes. Local stiffening and mass effects such as the tank outlet fittings/line or reinforcement structure should be included in the model. Water can be used as an LO_2 simulant. Light weight plastic spheres have been used before to simulate the mass distribution of the LH_2 (Reference 7), but the adequacy of this simulation of a liquid for obtaining tank bottom pressure measurements is unknown. Because the LH_2 propellant and feedline dynamics are not expected to contribute significantly to potential POGO problems due to the low density of

LH_2, the uncertainties resulting from the use of such spheres will probably not be important. However, this choice is probably adequate for the overall system modal definition.

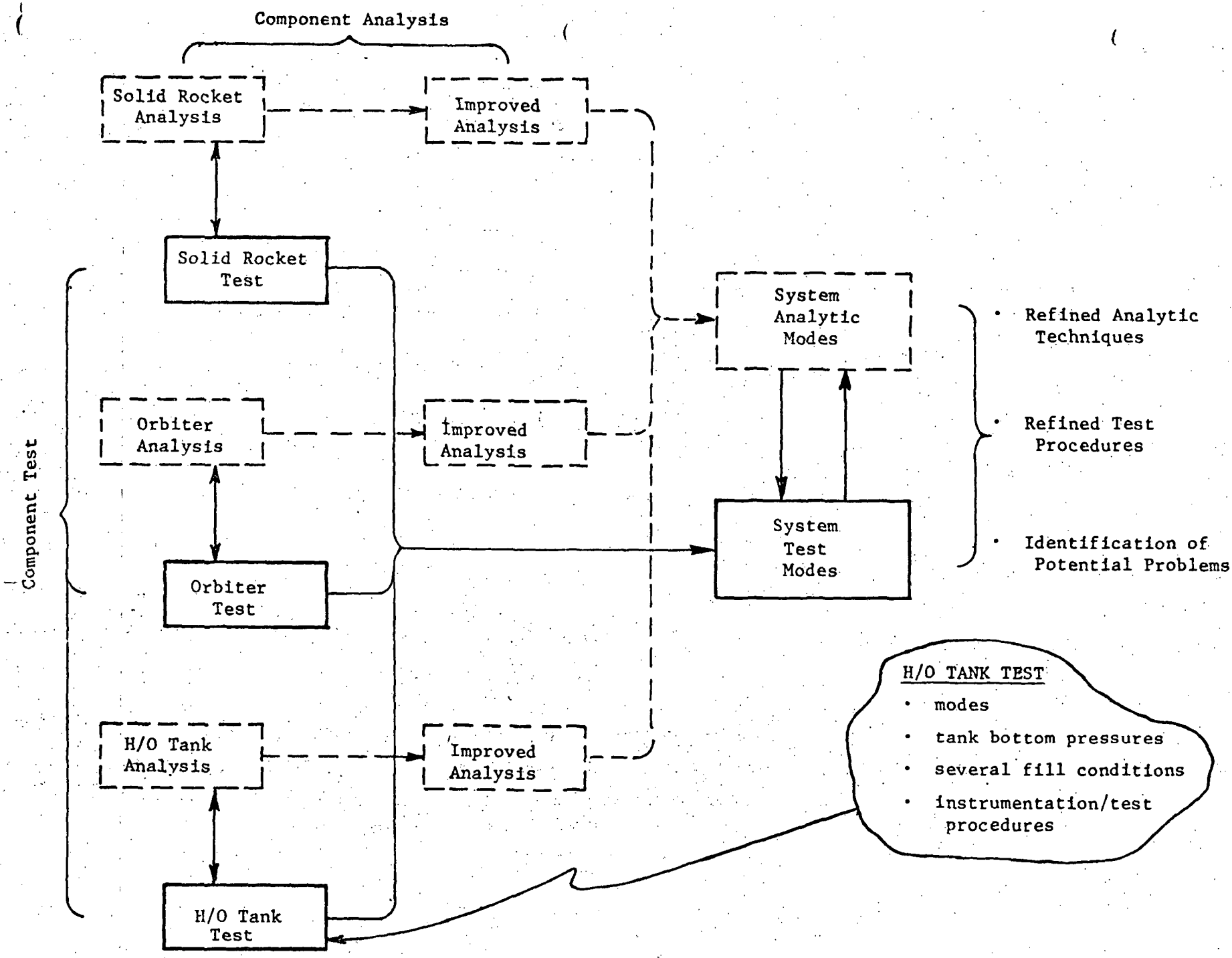

Figure 2-1 Test/Analysis Flow

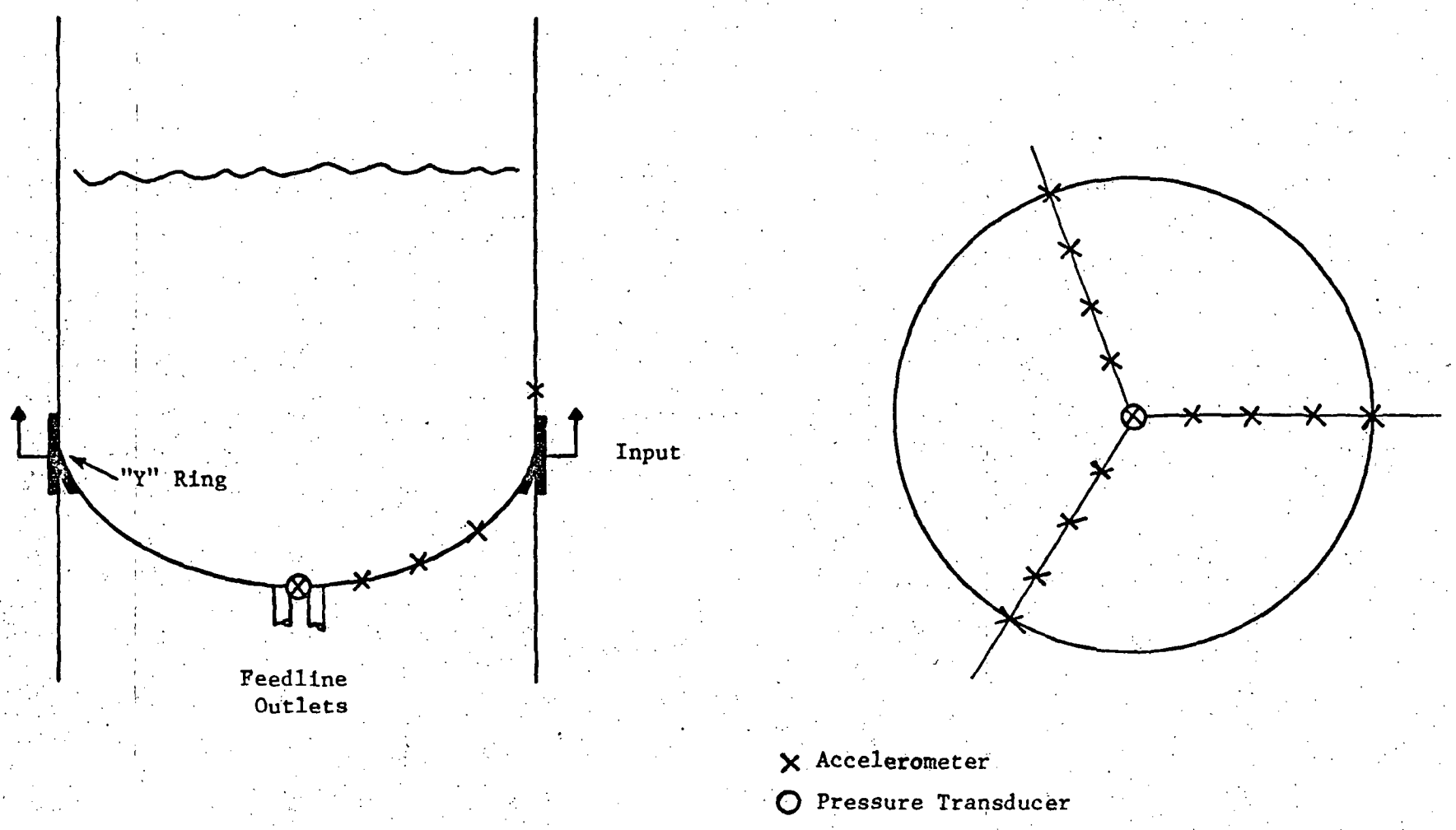

Figure 2-2 Tank Bottom Instrumentation

3. CONTROL SYSTEM CONSIDERATIONS

3. CONTROL SYSTEM ANALYSIS

3.1 Brief Description of Analysis Procedures

The shuttle flight control system design necessitates an investigation of the interaction among the shuttle rigid and flexible body dynamics, the control system sensors and actuators and the external disturbances to which the vehicle is subjected. The coupling between the controls, dynamics and the disturbances is described analytically via a closed loop formulation of the equations of motion such as depicted in Figure 3.1. The stability of the control system and verification of the system performance in the time domain must be established for each of the many flight maneuvers of shuttle vehicle. These include lift-off, normal atmospheric and orbital flight, staging, and abort maneuvers which may occur throughout the vehicle's flight path. The performance of these analyses will begin with simplified analytical models (i.e., a rigid body depicting the vehicle dynamics subject to a linearized control system) and culminate with complex models which include the flexible degrees of freedom coupled into the rigid body motion and including the highly non-linear control system.

The success of the advanced control system analysis of the shuttle vehicle depends in part on obtaining a realistic description of the vehicle's structural dynamics. The size and complexity of the proposed shuttle structure requires that much of this information be derived from sub-scale model testing. Some of important aspects of the controls-dynamics interaction of the shuttle vehicle are discussed individually below.

The structural feedback into the control system affects both sensors and actuators. Sensors (rate gyros and accelerometers) are primarily intended to sense rigid body rotations and accelerations, but their output includes errors due to structural bending rotations and linear flexible body accelerations. These flexible body effects are minimized by judiciously placing the sensors so that the local structural dynamics response will on the whole be minimal, and by using several sensors placed at various points on the system such that a comparison or averaging of these sensor outputs by onboard computers allows an accurate prediction of rigid body rotations and accelerations.

In order to evaluate sensor error, accurate modal data (modes, frequencies, generalized masses) are required. Secondly, the existance of local modes must be examined to ensure that the gross vehicle modes provide a sufficient basis for error processing. In the same manner, the flexibility of the points of action of control actuators must be considered in the analysis of structural feedback.

Control actuators include booster and orbiter engines which may be gimballed or have variable thrust, attitude control jets and aerodynamic control surfaces. Engine mount point and engine actuator flexibility must be considered as well as the flexibility of points of attachment of control surfaces.

Propellant slosh effects on the control system are of major importance due to the predominance of propellant fluids in the total mass distribution of the shuttle vehicle. Slosh modes may interact with one or more of the control system frequencies during both steady state and transient maneuvers. The slingshot effect is an example of the latter category. It may take place at the end of an engine burn when energy stored in the deformation of fuel tanks during high acceleration periods is suddenly released causing liquid residuals to be propelled towards the forward bulkhead at high velocity.

Other mechanisms of structural feedback involve aeroelastic effects which may couple the rigid and flexible body dynamics and localized deformation due to the mass and inertia distribution of major components.

A sub-scale model of the shuttle vehicle can be readily used to obtain the gross natural modes of vibration within the control system band-pass ($\sim$ 7 Hz). Yet, the complexity of structure makes it very difficult and costly to attempt a replica scaling of local flexibility and structural damping effects which, as was noted above, play a major part in the controls-dynamics interaction. Furthermore, some phenomena, such as fuel sloshing are subject to different scaling laws than the natural modes of vibration (i.e., slosh frequency typically is scaled by the square root of the length ratio) and thus are difficult to scale accurately.

Fortunately, replica scaling representing identical geometric scaling and using prototype material throughout the model is not necessary to establish the validity of the analytical simulation of the dynamic interaction of the shuttle vehicle. Instead, general geometric scaling may be employed, where the localized flexibility and a number of slosh modes are expressed in terms of "distortion parameters" that indicate the degree of distortion of the individual parameters used. An analytical simulation of the closed-loop controls-dynamics interaction of the sub-scale model is then performed and the results are compared with a laboratory test performed on the scale model. Good agreement between the analytical and the test results permits extension of the simulation, using the aforementioned "distortion parameters" whenever possible, to cover the shuttle flight configuration.

3.2 Structural Information Required

The structural dynamics data required or validated from the sub-scale model of the shuttle vehicle are as follows:

(1) Lift-Off Configuration

- (a) First three natural frequencies and modes of vibration of the cantilevered booster/orbiter combined structure
- (b) Modal displacement at engines and accelerometer locations
- (c) Modal rotation at the mount point of each rate-gyro

(2) In-Flight Configuration

- (a) Natural frequencies and modes of vibration of the free-free booster/orbiter combination and the orbiter alone within a frequency band up to 7 Hz
- (b) Modal displacement at engines and accelerometer mount point
- (c) Modal rotations of the mount point of each thruster and rate gyro
- (d) Localized stiffness coefficients of major components measured statically
- (e) Structural damping coefficients of all major modes of vibration
- (f) Discrete damping at constrained hinges
- (g) Slosh modes and frequencies up to 7 Hz

These data should be obtained for several vehicle configurations including:

- Booster/orbiter configuration with booster propellant loading of 100%, 75%, 50%, 25%, and 0%
- Orbiter configuration with propellant loading of 100%, 75%, and 50%, 25% and 0%

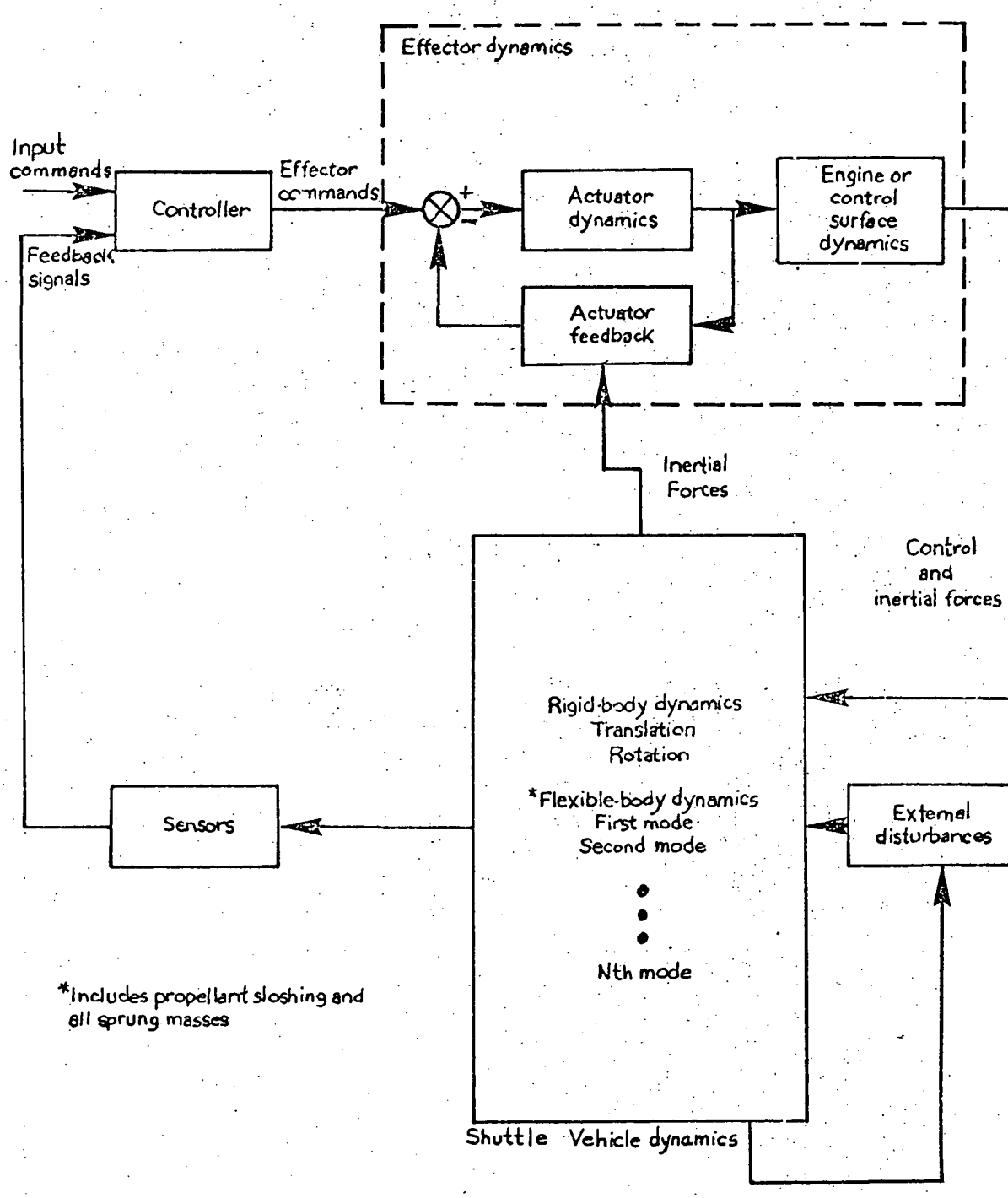

Figure 3 1. Block Diagram of the Shuttle Control Loop with Flexible Body Dynamics

4. GROUND WIND LOADS CONSIDERATIONS

4. GROUND WIND LOADS ANALYSIS

4.1 Brief Description of Analysis Procedures

Dynamic loads due to ground winds may be caused by one or more of several phenomena: responses to turbulence-induced unsteady drag forces, oscillatory lateral forces due to vortex shedding, galloping instability, and stop-sign flutter.

Turbulence-induced loads may be determined analyticallying using a model of the environment such as that contained in Reference (4-1) together with vehicle distributed drag data and structural dynamic characteristics. The approach used would be a cross-spectral analysis such as that described in Reference (4-2). Since a shuttle-type vehicle could be excited by turbulence in both translation (bending) and roll (torsion), antisymmetric as well as symmetric modes would have to be considered.

An alternate scheme for obtaining ground-wind gust loads would be to utilize elastic models in a wind tunnel which includes a simulation of the atmospheric turbulence as discussed in Reference (4-3). Power spectra of the shears, bending moments, and accelerations would then be obtained directly from the models. For more detailed design information than might be available from the model instrumentation, the measured results could be compared with the analytical results obtained in accordance with the procedure of the previous paragraph; these comparisons at selected locations could then be used as factors to be applied to the remainder of the analytical results. It should be noted that this subject is still in the developmental stage, and difficulties in reproducing the desired spectra and spatial correlations may be significant.

4.2 Structural Transfer Functions Required

Analyses and/or wind-tunnel tests to determine dynamic loads due to ground winds will require a knowledge of the cantilever modes of the shuttle restrained on the launch pad by the hold-down structure. As noted above, both symmetric and antisymmetric modes are of interest.

Turbulence-induced loads will occur primarily at low frequencies - in part due to the spectral distribution of energy in the atmosphere, in part because the vehicle restraint prevents the alleviation of very-low-frequency gust inputs by rigid-body vehicle motions, and in part due to the partial cancellation of positive and negative generalized forces for mode shapes higher than the fundamental. Past experience with essentially cylindrical launch vehicles has shown that only the fundamental cantilever mode makes a significant contribution to the total mean-square response. In extending this experience to the space shuttle, the concept of a "fundamental mode" requires some generalization. First, as stated above, both symmetric and antisymmetric modes will have to be considered, i.e., bending normal to the wing plane, lateral bending, and torsion (roll). Also, since the wings will give rise to much of the aerodynamic loading, the fundamental wing modes, as well as the fundamental cantilever fuselage modes may have to be considered.

The phenomena of vortex shedding, galloping instability, and stop-sign flutter all involve overall vehicle oscillations in the fundamental cantilever modes. Wing flexibility may influence the last two phenomena, but in any event the degree of dynamic similarity discussed in the previous paragraph on turbulence should also be adequate for these other considerations.

The approach to determining loads due to vortex shedding will be largely experimental and/or empirical with several different variations being possible. The one which would utilize the most analysis would involve wind-tunnel testing of essentially rigid models to determine only the oscillatory lift forces. A power-spectral response analysis would then be used in conjunction with a structural dynamic mathematical model to determine dynamic loads. Another approach would be to test a dynamically similar wind-tunnel model to obtain responses and loads directly. Regardless of what type of model is used, however, careful attention must be paid to the effects of Reynolds number differences between the wind-tunnel and full-scale conditions.

Since the shuttle configurations are symmetric only with respect to one plane, and since vortex shedding could produce lift forces normal to this plane, both symmetric and asymmetric modes will have to be considered. On the other hand, for the complex noncylindrical configurations that characterize the shuttle designs, the extent of vortex shedding is still in doubt.

The phenomena of galloping instability and stop-sign flutter are in one sense similar to vortex shedding and in another sense opposite to vortex shedding. All three phenomena must be studied primarily by experimental and/or emperical methods, but whereas the significance of vortex shedding is probably diminished in changing from a cylindrical to a shuttle configuration, the other two problems were not important previously and now may be very significant. Again, asymmetries in the vehicle configuration require that both symmetric and antisymmetric structural vibration modes be considered in any mathematical or physical model.

5. LIFT-OFF LOADS ANALYSIS

5. LIFT-OFF LOADS ANALYSIS

5.1 Brief Description of Analysis Procedures

Dynamic loads at lift-off are calculated as the response of a vehicle, initially deflected by wind loads and engines, to the forces induced as the hold-down restraints are released. The initial deflected position can be determined from the response of the cantilivered vehicle to the combination of appropriate engine-induced forces, steady winds, and turbulence, obtaining an equivalent static deflection using the matching technique of reference (5-1). An elastic wind tunnel model can be used as an alternative means of determining responses to appropriate winds.

For purposes of analyses the vehicle is represented by the free elastic modes, with initial conditions being described in terms of deflections in free modes plus rigid rotations. An alternate approach which in some cases is less difficult than matching deflections is to determine the reaction forces while the vehicle is restrained by the hold-down and apply these as forces to the free modes. Transient forces representing the continued net difference between thrust build up and hold-down releases are then applied along with steady peak wind forces, and the maximum member loads are determined. The dynamic loads due to turbulence at lift-off are determined separately, with the flexible vehicle again represented by the free modes. The force applied in this case is the spectrum representing the horizontal wind turbulence. Again, the matching-condition technique of reference (5-2) can be used to convert member loads representing a 3-sigma response to the turbulence to a static load distribution. These results are then added to those due to lift-off transient and steady wind to determine total load magnitudes.

5.2 Structural Characteristics Required

The loads at lift-off are expected to design the aft portion of the SRM. Dynamic loads at lift-off affecting members in this area would therefore be most significant. These would be determined by motions of the major mass items in the free modes below 4 Hz, the most important probably being the liquid oxygen tank and solid rocket motors. The interstage flexibility and LO_2 tank to interstage flexibility are therefore important.

In this analysis the major forces are those applied principally in the axial direction through the vehicle engines and hold-down release system. The engine ignition start up transient is expected to have a relatively slow rise time. Current specifications limit the thrust buildup in each liquid rocket engine to a rate of less than 700,000 lbs/sec and the engines are expected to be started sequentially so that the time from 10 percent to full thrust should be relatively long. The solid rocket motor start-up time is also relatively slow, about .3 seconds. The hold-down release forces could be applied rapidly since the Saturn V system originally permitted release in .01 to .02 seconds. However, in the present system the release time is about 0.6 seconds, and a similar device might be used for the shuttle to limit dynamic response. The axial forces therefore will not contain many high frequency components, and the low frequency modes with appreciable axial motion at the engine thrust structure would be most significant. In the Grumman GIII configuration for example only 1 symmetric mode of the lowest 20 had appreciable deflection (above 0.1) at the SRM engine and hold-down location, and this occurred at 2.5 hz. Many of the modes did have appreciable motion at the orbiter engines; however, the fluctuating thrust at higher frequencies will not add much to primary structure loads as mentioned in Section 7.

Lateral forces are applied principally by the potential energy stored in the deflected cantilevered vehicle. The modes most significant in this context would be those in which static and dynamic response to ground winds and orbiter engines are highest.

In order to obtain some insight into the frequency range corresponding to this criterion, the cantilevered modes at lift-off calculated for a 4.9 million pound parallel burn (orbiter/external tank/SRM's) configuration (Grumman Design GIII) were reviewed. A description of the mode shapes is listed in Table 5-1. The modes which are expected to be most significant are the 1st, 3rd, and 4th, and 8th. The wing and fin modes for this vehicle are summarized in Table 5-2, and it may be noted that the fundamental frequencies are low and that the 2nd wing bending mode which is probably the upper limiting frequency for appreciable wind induced loads is at 8 hz.

TABLE 5-1

CANTILEVERED SYMMETRIC MODES - GIII LIFT-OFF CONFIGURATION

MODE NO.	FREQ. HZ	GENLZD. WT.-LBS.	MODAL DEFORMATION PATTERN				
			MAX. MOTION	EXT. TANK	SRM	ORB. FUSELAGE	ORB. WING
1	.22	1.514 M	LO_2 Tank Nose Z	Pitch	Z-1st Cantilevered	Pitch	Pitch
2	1.05	1.541 M	SRM Nose Z	Pitch, Z-1st Bending	Z-2nd Cantilevered Y-1st Cantilevered	Pitch	Plunge
3	1.18	1.357 M	LO_2 Tank Nose Z	Z-1st Bend. LO_2, LH_2 Axial	Z-2nd Cantilevered	Axial	Plunge
4	1.59	.188 M	Fin Tip Z	Axial, Z-1st Bend. LO_2, LH_2 Axial	Little Motion	Axial, Z-1st Bend.	Pitch, Z-1st Bend.
5	1.69	.067 M	RCS Pod (Wing Tip)Z	Z-1st Bend.	Little Motion	Z-1st Bend.	Z-1st Bend.
6	2.08	.025 M	RCS Pod (Wing Tip)Z	Little Motion	Little Motion	Z-1st Bend.	Pitch, Z-1st Bend.
7	2.36	.0315M	RCS Pod (Wing Tip)Z	Little Motion	Little Motion	Axial, Pitch	Z-1st Bend.
8	2.85	.0276M	Fuselage Nose-Z	Little Motion	Little Motion	X-1st Longit. Z-1st Bend.	Pitch
9	3.32	.671 M	Fin Tip-X	Little Motion LH_2 Axial	Little Motion	Z-1st Bend. Axial, X-1st Long.	Axial, Pitch
10	3.47	.934 M	Fuselage Nose-Z	Z-2nd Bend, LH_2 Axial	Z-2nd Cantilevered	Z-1st Bend. Axial,X-1st Long.	Axial Pitch, Z-1st Bend.

Note: Rigid Modes denoted by Pitch, Axial, Plunge. Flexible by Z-1st Cantil., X-1st Long. etc.

TABLE 5-2

GIII ORBITER WING AND FIN MODES

FREQUENCY Hz	RESTRAINT AT ROOT	MODAL DEFORMATION PATTERN
1.59	Antisymmetric	Wing 1st Bending
1.81	Symmetric	Wing 1st Bending
3.5	Flexible	Fin 1st Bending
3.92	Antisymmetric	Wing Tip (RCS Pod) Pitch
4.45	Antisymmetric	Wing Tip (RCS Pod) Pitch
4.96	Antisymmetric	Wing Tip (RCS Pod) Yaw
5.01	Rigid	Fin 1st Bending
5.73	Symmetric	Wing Tip (RCS Pod) Yaw
7.53	Antisymmetric	Wing 2nd Bending
8.27	Symmetric	Wing 2nd Bending
9.52	Antisymmetric	Wing 1st Torsion
10.18	Symmetric	Wing 1st Torsion
11.51	Flexible	Fin 2nd Bending
16.24	Rigid	Fin 2nd Bending
18.31	Flexible	Fin 1st Torsion
19.21	Rigid	Fin 1st Torsion

Note: Antisymmetric restraint allows no deflection at fuselage side wall and centerline. Symmetric restraint allows no deflection at fuselage side wall and zero slope at fuselage centerline.

6. GUST LOADS CONSIDERATIONS

6. GUST-LOADS ANALYSIS

6.1 Brief Description of Analysis Procedure

Space-shuttle flexible-vehicle gust-response calculations will generally be of three different types: (1) a power-spectral analysis for the maximum-dynamic-pressure portions of the ascent and entry phases of a mission using a gust spectrum representative of the high-frequency content of measured wind profiles; (2) a time-history ascent analysis in which the high-frequency content is retained in the wind profile; (3) a power spectral analysis for the near-horizontal-flight phases of the vehicle usage. Of the various portions of a mission profile, the gust loads during ascent are expected to be the most severe. Also, during this flight phase, the structural-mode frequencies will be the lowest and the wing loading will be the highest. Thus, the contributions of the structural-mode responses relative to the rigid-body responses will be a maximum for this flight phase. Accordingly, in evaluating the importance of higher-frequency structural modes from a gust-response viewpoint, it was this flight regime that was considered. Details of this work are contained in Section 6.3, but the conclusion is that about 10 to 15 of the first 30 symmetric modes will have responses of sufficient magnitude in a gust-loads analysis of reasonable engineering accuracy.

6.2 Structural Transfer Functions Required

The structural modeling, from a gust-response viewpoint, should give emphasis to those modes which: (1) are readily excited by a gust normal to the vehicle, i.e., have large displacements of lifting surfaces predominantly in one direction; (2) have large motions of nonaerodynamic components with large mass, so that the generalized mass is high and the total percent of critical damping (aerodynamic plus structural) is low; (3) have large motions at critical vehicle locations, e.g., crew compartments and payload area; and (4) are lightly damped aerodynamically due to proximity to a flutter condition. Of course, few if any modes will exhibit all these characteristics, and hence a good preliminary vibration and gust-response analysis will be required to delineate the critical modes. Therefore, considerable knowledge about a vehicle's mass and structural characteristics must be available before a definitive selective judgement can be made along these lines. Generally

speaking, however, the implications of the above criteria are that a good simulation is required for: (1) the lifting surfaces; (2) the most flexible portions of the fuselages; (3) the interstage structure; (4) the crew-compartment, payload, and tank support structures; and (5) the engine and sensor support structures. This simulation is required not only to provide the desired modal data, but also to provide data on internal structural loads due to inertia loadings associated with each mode. The simulation should emphasize those flexibilities that give rise to transverse rather than longitudinal deformations. Also, since liquid motions will give rise to large fractions of many of the generalized masses and internal loads, these must be represented carefully.

6.3 Evaluation of Importance of Higher-Frequency Modes on Gust Response

To obtain a preliminary quantitative evaluation of the number of modes for which data would be required to perform space-shuttle gust-response calculations of reasonable engineering accuracy, an external hydrogen tank orbiter heat sink booster, the Grumman/Boeing H3T design in the ascent configuration corresponding to maximum dynamic pressure was analyzed using 22 of the first 30 symmetric modes of the combined orbiter/booster. The 22 modes used were selected based on the criteria in the previous paragraph, and covered a frequency range from 1.5 to 8 Hz (see Table 6-1). The rigid body short-period mode was about 0.35 Hz. Frequency-response functions and power spectra were computed for the accelerations at 10 locations, 5 on the orbiter and 5 on the booster. Table 6-2 which summarizes the results, gives the order of importance of the various significant modes according to their contributions to the mean square acceleration at each location. In attempting to correlate the peaks of the power spectra in Appendix A with the mode numbers listed in Table 6-2, the shifts in the modal frequencies due to the aerodynamic forces must be considered. This was done with aid of modal response curves such as those shown in Figures A-5 through A-8. As might be expected, the first mode is by far the most important of the various structural modes considered. However, there are 11 different modes which have contributions greater than the rigid-body accelerations at least one location. Furthermore, the 21st mode has the greatest contribution at two locations, and even the 29th mode has a significant contribution at one location.

In evaluating the significance of these findings from the viewpoint of dynamic modeling requirements, the limited scope of this preliminary study must be considered. Of the 22 modes chosen for inclusion in the calculations, 13 were found to have significant contributions at least one of only ten locations. Thus, it is likely that there are other modes that would have significant contributions someplace on the vehicle. It appears, therefore, that the calculations performed thus far are approaching the definition of an upper limit, but that this limit cannot yet be stated with confidence. At this point, a best guess at a conclusion would be that a space shuttle structural dynamic model for gust-response purposes should probably be capable of representing modes up to about 8 Hz. A representation up to about 6.5 Hz is definitely required.

TABLE 6-1 H3T COMBINED ORBITER/BOOSTER

SYMMETRIC VIBRATION MODES

MAX Q ALPHA

Mode No.	Freq. (Hz)	Gen. Weight (lbs.)	Mode Normalized to:	Used in Gust-Response Analysis
1	1.48	25,240	Orb Fin Z	X
2	1.57	9,032	Boost Wing Z	X
3	2.16	569,811	Orb Lo_2 Z	X
4	2.31	181,346	Orb Lo_2 Y	X
5	2.37	51,781	Orb Fin X	X
6	2.51	133,363	Orb LH_2 Z	X
7	2.73	18,355	Orb Fin X	X
8	2.90	23,564	Orb Fin X	X
9	2.99	5,215	Orb Wing Z	X
10	3.06	4,724	Boost Fin Z	X
11	3.22	15,305	Orb Fin X	X
12	3.28	24,540	Orb Wing Z	X
13	3.55	62,687	Orb LH_2 Y	X
14	3.79	27,574	Boost Fin X	X
15	3.92	10,129	Boost Wing X	
16	4.13	16,868	Orb Eng Z	
17	4.37	47,880	Boost Fin X	X
18	4.63	43,349	Boost Nose X	X
19	4.99	20,240	Boost Stab Z	
20	5.42	5,247	Boost Stab X	
21	5.57	37,682	Orb Nose Z	X
22	6.13	27,335	Orb Nose Z	X
23	6.22	56,611	Boost Wing Z	X
24	6.45	9,969	Orb Nose Z	X
25	6.59	201,599	Orb Lo_2 Y	
26	7.07	17,127	Orb OMS X	
27	7.33	9,618	Orb Nose Z	
28	7.68	41,576	Boost Nose Z	
29	7.76	6,847	Orb Wing Z	X
30	8.00	2,890	Orb Wing Z	X

TABLE 6-2 - RELATIVE MODAL CONTRIBUTIONS

TO REPRESENTATIVE LOCAL ACCELERATIONS,

H3T COMBINED ORBITER/BOOSTER

Location	Order of Significant Modal Contributions
Orbiter	
Crew Compartment, (Coord 57)	21, 1, RB *, 18
Payload, (60)	21, 23, RB, 22, 10, 12, 29
Oxygen Tank, (39)	1, RB, 3
Hydrogen Tank, (84)	1, 21, 7, 22, RB, 23
Wing Tip, (110)	1, 9, 6
Booster	
Crew Compartment, (126)	18, RB, 7, 10, 3, 1
Oxygen Tank, (150)	RB, 1, 7, 21
Hydrogen Tank, (136)	RB, 1, 7, 3, 21
Wing Tip, (173)	2, 1, 22, 23
Engine, (196)	1, 7, RB

* RB = rigid-body short-period mode

7. ENGINE INDUCED RESPONSE CONSIDERATIONS

7. ENGINE INDUCED RESPONSE

7.1 Brief Description of Analysis Procedure

Dynamic loads due to engine induced forces are generally determined by calculating the response of unrestrained vehicles represented by a selected set of free modes of vibration. Time integration is used for transient loading, and harmonic and random vibration analysis procedures are used for oscillatory loading conditions. The start-up forces for the shuttle will probably employ sequential ignition to reduce dynamic loads and can therefore be represented by a series of steps, each with a rise time of about 0.6 seconds for the liquid engines and 0.3 seconds for the solids. The time from 10 percent to full thrust is probably greater than .6 seconds. Engine shutdown forces will be more rapid, but the total sequence will probably occur over half a second. The SRM abort thrust termination could occur rapidly but the process could be controlled to occur over .2 sec.

The random engine induced forces will cover a broad frequency range. Currently requirements limit the harmonic content of engine thrust to 450 pounds for each liquid rocket engine in the frequency range from 1.5 to 25 Hz and permit slightly higher levels outside this band up to 100 Hz.

7.2 Structural Transfer Functions Required

The transient and steady-state thrust irregularities occur primarily in the axial direction. Thus the strongest excitation arises for modes involving substantial axial engine motions. The largest overall loads derive from the lower frequency modes in which large sections of the vehicle move in phase, and which also involve significant engine axial motion. However, the acceleration response particularly on the orbiter tends to occur at frequencies close to the engine support resonance. This effect is illustrated by the responses calculated on the Grumman GIII model of the Shuttle. Most of the higher frequency response occurred at 12.4 Hz, as shown on Table 7-1. In order to calculate responses and loads both, modes up to about 20 Hz would be required. If only loads were required, a lower cut-off frequency would be acceptable.

G111 SYMMETRIC MATH MODEL

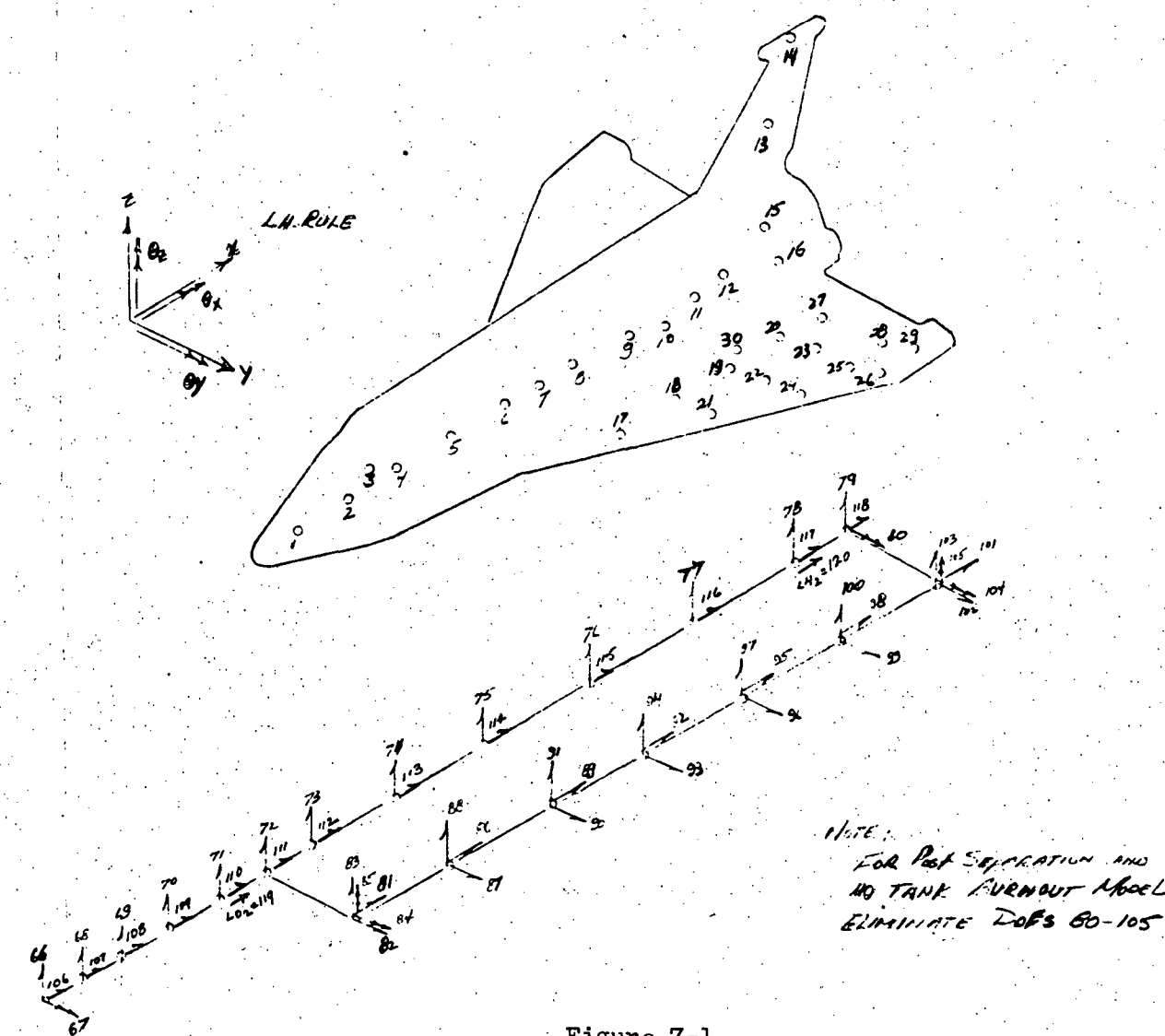

MASS	NODE	X	Y	Z	θ_x	θ_y	θ_z
1	1			2			3
2	4			5			
3	6			7			8
4	9			10			
5	11			12			
6	13			14			
7	15			16			
8	17			18			
9	19			20			
10	21			22			
11	23			24			
12	25			26			27
13	28						
14	29						
15	30			31			
16	32	33		34			
17				35	36		37
18				38			
19	39			40			
20				41			
21				42	43		44
22	45			46			
23				47			
24	48			49	50		51
25				52			
26				53	54		55
27				56			
28				57			
29	58	59		60			61 62
30	63	64		65			

Figure 7-1

TABLE 7-1

ACCELERATION RESPONSE OF SHUTTLE CONFIGURATION GIII TO 450LBS/ENGINE OSCILLATING THRUST AT LIFTOFF

	g MAXIMUM	FREQUENCY
1	4.9100E-01	1.2445E 01
2	7.0924E-01	2.8430E 00
3	2.5150E-03	1.2445E 01
4	5.0747E-01	1.2445E 01
5	4.5341E-01	2.8430E 00
6	5.1237E-01	1.2445E 01
7	3.4840E-01	2.8430E 00
8	1.8023E-03	2.8430E 00
9	1.8217E-01	1.2445E 01
10	2.3307E-01	2.8430E 00
11	2.3403E-01	1.2445E 01
12	1.5795E-01	1.2445E 01
13	1.5593E-01	1.2445E 01
14	2.3294E-01	1.2445E 01
15	1.0064E-01	1.2445E 01
16	2.1428E-01	1.2445E 01
17	9.1180E-02	2.8430E 00
18	1.5803E-01	1.2445E 01
19	9.9121E-02	2.8430E 00
20	9.2746E-03	1.6577E 00
21	1.2153E-01	1.2445E 01
22	8.7447E-03	1.6577E 00
23	1.7069E-01	1.2445E 01
24	1.0796E-01	1.2445E 01
25	2.2706E-01	1.2445E 01
26	9.3156E-02	1.2445E 01
27	5.2251E-04	1.2445E 01
28	3.2274E-01	1.2445E 01
29	3.2624E-01	6.0883E 00
30	5.8307E-01	1.2445E 01
31	1.7849E-01	1.3515E 01
32	2.4724E-01	1.2445E 01
33	3.1444E-03	1.3515E 01
34	1.3710E-01	1.3515E 01
35	4.7336E-01	1.2445E 01
36	4.9745E-03	1.2445E 01
37	2.3010E-03	1.2445E 01
38	2.8329E-01	1.2445E 01
39	2.0272E-01	1.2445E 01
40	1.7260E-01	1.3515E 01
41	2.1360E-01	1.2445E 01
42	6.8405E-01	1.2445E 01
43	4.3859E-03	1.2445E 01
44	1.4557E-03	1.2445E 01
45	3.1913E-01	1.2445E 01
46	4.3097E-01	1.3515E 01
47	3.4523E-01	1.2445E 01
48	4.2248E-01	1.2445E 01
49	3.9115E-01	1.2445E 01
50	4.9710E-03	1.3515E 01

	g MAXIMUM	FREQUENCY
51	3.1241E-03	1.2445E 01
52	2.4850E-01	1.2445E 01
53	2.9404E-01	1.9307E 00
54	9.3084E-03	1.1377E 01
55	2.7581E-03	1.9307E 00
56	6.3302E-01	1.2445E 01
57	1.1527E 00	1.2445E 01
58	5.7151E-01	1.2445E 01
59	3.3337E-01	4.5335E 00
60	5.4262E-01	1.9307E 00
61	6.6205E-03	1.2445E 01
62	4.1499E-03	1.2445E 01
63	1.0205E-01	2.8430E 00
64	1.1353E-01	1.2445E 01
65	1.7611E-01	1.2445E 01
66	3.4414E-02	3.8814E 00
67	1.7240E-04	3.8814E 00
68	2.4950E-02	1.3589E 00
69	1.8789E-02	1.3589E 00
70	1.4006E-02	3.8814E 00
71	2.8106E-02	3.8814E 00
72	3.7710E-02	3.8814E 00
73	4.8487E-02	1.6577E 00
74	6.5377E-02	1.6577E 00
75	7.6898E-02	1.6577E 00
76	7.9435E-02	1.6577E 00
77	6.9774E-02	1.6577E 00
78	5.3436E-02	7.7035E 00
79	5.1230E-02	7.7035E 00
80	9.7929E-05	1.6577E 00
81	1.0225E-02	2.3054E 00
82	2.2041E-02	2.3054E 00
83	2.9270E-02	1.3589E 00
84	3.4967E-05	1.9307E 00
85	3.8878E-05	2.3054E 00
86	1.0457E-02	2.3054E 00
87	1.3442E-02	2.3054E 00
88	2.2757E-02	1.3589E 00
89	1.0651E-02	2.3054E 00
90	5.8163E-03	2.3054E 00
91	2.3735E-02	1.6577E 00
92	1.0805E-02	2.3054E 00
93	6.4916E-03	1.6577E 00
94	2.4635E-02	1.6577E 00
95	1.0914E-02	2.3054E 00
96	6.8281E-03	2.3054E 00
97	2.1906E-02	1.6577E 00
98	1.0983E-02	2.3054E 00
99	1.1439E-02	2.3054E 00
100	1.6971E-02	1.9307E 00

	g MAXIMUM	FREQUENCY
101	1.1009E-02	2.7074E 00
102	1.5164E-02	2.3054E 00
103	2.2726E-02	1.9307E 00
104	3.9430E-05	1.3589E 00
105	4.2699E-05	1.2445E 01
106	1.6400E-02	1.2445E 01
107	1.6136E-02	1.2445E 01
108	1.6951E-02	1.2445E 01
109	1.5678E-02	1.2445E 01
110	1.5405E-02	1.2445E 01
111	1.4850E-02	1.2445E 01
112	1.3868E-02	1.2445E 01
113	2.4416E-02	1.2445E 01
114	2.9904E-02	1.2445E 01
115	3.5696E-02	1.2445E 01
116	4.0533E-02	1.2445E 01
117	3.9512E-02	4.2012E 00
118	3.9606E-02	4.2012E 00
119	3.3043E-02	2.8430E 00
120	1.3092E-01	4.2012E 00
121	1.2570E-01	1.3515E 01
122	1.0440E-01	1.2445E 01
123	9.0998E-02	1.2445E 01

Note: Coordinate Locations Shown in Fig. 7-1

8. STAGING CONSIDERATIONS

8. STAGING

8.1 Staging Analysis

Staging of the shuttle vehicle will normally occur at an altitude of approximately 130,000 feet and a velocity of about Mach 4. Under nominal staging conditions, the boosters are essentially empty while the liquid propellant tanks are about 2/3 full. In contrast, abort staging may occur at any intermediate altitude and associated velocity and propellant loading. The number of abort conditions is intrinsically large and will demand a larger share of the analysis effort.

During nominal staging or in an abort staging, loads are input to the system from a variety of sources, all of which must be accounted for in the staging analysis. Initial conditions form a second input to the staging analysis. The inputs and other factors must be considered in the analysis, including:

- Stage separation systems which are kinematically constrained. These devices may be pre-loaded and include spring elements or active devices such as pistons.
- Thrust transients arising from shut down of booster engines. The booster engine thrust may not tail down uniformly which could give rise to differential thrust and require ME gimballing to counteract the motions.
- Stored elastic energy in the orbiter and booster which is released upon staging.
- Flight loads from aerodynamic and control effects.
- Liquid propellant motions.

The analytical structural dynamics model to determine staging response of the orbiter and booster will include the following elements:

- Bending, longitudinal, and torsional deformations.
- Slosh effects will be included implicitly in the modes if slosh amplitudes or masses are small. The large amplitude slosh motions which may arise during abort staging, such as propellant sidewall impact, can

be bounded using existing experimental data. A more precise determination of this effect will depend on data obtained from the structural dynamic model.

- Detailed booster and orbiter thrust time-histories, including the thrust of each engine and the orientation of each gimballed thruster as a function of time.
- Initial conditions such as angular rates, and velocities, which arise from pre-loads, detonation of pyrotechnics, and actuators.
- Analytical models of the gasdynamic and aerodynamic effects.
- Analytical model of stage separation system kinematics, stiffnesses, power sources, and release mechanisms.

The above inputs will be combined in a numerical simulation of the stage separation process. The equations of motion will be synthesized from the equations of motion for the orbiter and booster written in terms of the flexible body modes and rigid body modes and the equations of motion of the link mechanism. The synthesization is achieved by invoking the boundary conditions between the stage separation system and the orbiter and between the booster and the stage separation system linkage. Because of the large angle motions of the booster and orbiter that may arise during some staging maneuvers, the large amplitude propellant motions, and the nonlinearity of the stage separation system, the equations of motion for the system will be nonlinear, necessitating a numerical integration of the equations of motion.

Three major concepts for the stage separation system are presently being studied. These are a reverse linkage mechanism, a piston device, and combination link-actuator system. Analyses have shown a major factor in establishing the forces and moments which arise during staging is the stiffness of the interconnection attachment points. Loads which arise during staging vary over orders of magnitude, depending on the stiffness of these points, and for some ranges of stiffness a "rocking" motion (pitch oscillation) can arise during staging.

The same considerations apply to abort staging. In addition, during abort staging (the worst conditions may exist at max $q\alpha$), large propellant loadings may be present. The fuel may accelerate rapidly and impact on the tops of the tanks, causing large upsetting moments and large bulkhead loads.

At the present time, uncertainties in stage separation system design including stiffness, geometry (kinematics), release times, damping, and operation in conjunction with system control preclude a detailed modeling of the system. In any case, the properties of the vehicles at the points of attachment of the stage separation system linkage are the analytically uncertain quantities which are most readily established by means of the structural dynamic model. The actual stage separation system should be developed and tested by means of a separate structural scale model.

The structural dynamic model should provide a portion of the inputs for the staging analysis: the modes and frequencies of the orbiter and booster separately, with coordinates defined at the stage separation system linkage attach points, and a means of characterizing the large amplitude slosh motion which are likely to arise during some abort staging modes.

The experimentally established free-free modes and frequencies of the orbiter and booster will serve to validate the analytical procedures. These are used in conjunction with a separate dynamic model of the stage separation system and analytical models of loads and initial conditions to simulate staging dynamics.

8.2 Structural Transfer Functions Required

Depending on the design, the stage separation system will typically attach at 6 to 8 points. Modal data must be obtained at these points on the booster and orbiter structural dynamic models. Accelerometers will be required to measure linear accelerations and angular velocity transducers will be used to measure modal rotations at these points.

Since staging will occur over a time period of the order of 1/2 sec., the low frequency modes are most important to the staging analysis. A determination of all orbiter and booster modes below 5 Hz will be adequate for staging purposes.

The stage separation system linkage itself need not be included in the structural dynamic model. However, since attachment point stiffness is of critical importance in determining staging dynamics, portions of the stage separation system which contribute significantly to the stiffness of the linkage (or piston or actuator) attach points must be carefully included in the structural dynamic model.

A second area of major concern to the staging analysis is the modeling of the booster/orbiter thrust structures. Booster and orbiter angular and relative displacement rates which arise during the staging maneuver will be controlled to preclude structural damage to the booster and orbiter, as well as the constraints of crew safety and confort. Generally all booster and orbiter engines are thrusting during staging. Control is achieved by means of an appropriate transient variation in the thrust of the orbiter engines and by gimballing of the engines. Thus, flexibility of the thrust structures will strongly influence the angular and displacement rates each vehicle actually attains. Modal data must be defined for each engine (as also required on the basis of POGO analysis considerations) in addition to interconnection attachment points. The discussion "Requirements for POGO Analysis," pertaining to thrust structure modeling are equally applicable for staging analysis purposes.

Large amplitude sloshing and propellant impact play a major role in staging abort condition dynamics. In the case of nominal staging, the ullage of the External Tank could be about 1/3. Significant propellants mass may therefore undergo large amplitude angular motions during the staging maneuver or impact tank bulkheads. Further study should be given to determine if separate tests will be required to dynamically characterize these motions, or it should be established by analysis that their occurrence can be precluded in every abort mode by means of appropriate system control.

A study of the reverse link concept in an early Shuttle configuration has shown that during nominal staging the moment applied on the booster through the stage separation system is approximately 40×10^6 ft-lbs, the moment produced by plume impingement is on the order of 3×10^6 ft-lb, and the moment produced by thrust is approximately 40×10^6 ft-lb. Significant variations in these number will occur before the stage separation system design is fixed and the

staging process is defined in detail, however, they provide order of magnitude indications of the magnitude of the forces required to study staging transients in the laboratory.

The test configurations required for nominal staging are:

Modal Survey

- Free-free support of the booster with nominal staging equivalent propellant loading
- Free-free support of the orbiter with full propellant loading

The test configurations required for abort staging include:

- Free-free support of the booster with propellant load corresponding to max $q\alpha$
- Free-free support of the booster with intermediate propellant loadings, such as 25%, 50% and 75%

Slosh Test

A slosh test should be performed if the slosh response during abort staging can be shown by analysis to be large. These tests will consist of measuring vehicle and slosh response to simulate staging loads.

If abort staging response tests are deemed necessary, it will have significant impact on booster model test facility requirements. That is, this test may require special support fixtures, actuators for inputting simulated staging loads, and additional instrumentation to measure fluid and tank wall response and structural loads.

9. TEST REQUIREMENTS

9. TEST REQUIREMENTS

The test requirements for many of the analytical procedures are similar; therefore this topic is discussed in this one section to limit repetition.

9.1 Measurement Requirements and Instrumentation

For most of the mode surveys the following measurement locations are suggested.

Orbiter	Accel.
Wings	20
Elevon	5
Fin	8
Fuselage	8
Crew Area	3
Payload	12
Engine	9

Booster	Accel.
Nose	4
Fwd Mounting Skirt	4
Fuel Cylinder	16
Aft Mounting Skirt and Holddown	6

External Tank	Accel.	Strain	Pressure
LO_2 Tank Wall	12	12	
LO_2 Tank Dome	10	12	1
Intertank Skirt (SRM Attachment)	6		
LH_2 Tank Wall	10		
LH_2 Tank Frames (Orbiter Attachments)	6		
Aft Skirt (SRM Attachment)	6		

Instrumentation systems currently available, such as the automated mode survey data acquisition and reduction systems at Grumman and TRW are suitable for most tests. The Grumman system for example has capability for up to 300 measurements and can process accelerometer, strain gage, and force transducer signals. Automatic data plotting using computer assisted procedures are helpful in rapidly processing the data. Lightweight piezo electric accelerometers

suitable for model tests are available. Fluid reaction in LO_2 tanks would be determined from the strain gages provided sufficient sensitivity is available, alternatively, pressure transducers might be used.

9.2 Facilities

Facilities required for the model testing would include a low frequency suspension system to simulate free-free conditions, hoisting and handling facilities, tank fill and drain capability, and shaker control and support or suspension systems. For cantilevered tests, a base plate suitable for mounting hold-down latches is required. A shaker control system capable of operating 8 simultaneous shakers should be adequate.

9.3 Additional Requirements

Modifications or additions to the above test requirements are associated with data required for the following analyses.

9.3.1 POGO

The significant data to be acquired is the response to axially applied excitation at the engine. Configurations to be tested are the combined vehicle at 3 different levels of propellant in the SRM booster, and the orbiter and external tanks at 3 different propellant levels. Force inputs are required at the engine. Response of the fluid in the tank which can be used to determine tank bottom pressures should be measured. Data should be reduced to supply transfer functions between sinusoidal sweeps at the engine and response at the tank bottoms.

9.3.2 Flight Controls

Accelerometers and rate gyros should be located in the vicinity of proposed Flight Control System sensor mounting locations as well as at the points of attachment of the control surfaces. Mode surveys should be conducted at 3 propellant weight levels for the combined vehicle and for the orbiter alone.

9.3.3 Ground Wind Loads

Cantilevered modes of the combined vehicle are required. Test configurations probably should provide three values of hold-down latch stiffnesses. Four propellant configurations should be tested for each value of stiffness.

9.3.4 Lift-Off

Mode survey data for the combined vehicle on a soft suspension is the primary requirement. However, the response to transient inputs at the engine and hold-down points should also be measured. Techniques like the impulse transfer function tests would permit rapid and accurate calculation of the response to hold-down and engine transients which might be difficult to reproduce for a scaled model.

9.3.5 Gust

The most important configuration for which information is desired from a dynamic model for gust-response studies is the combined orbiter/booster in a vertical-flight position for a weight condition corresponding to the maximum-dynamic-pressure portion of the ascent trajectory. A secondary objective would be to obtain similar information for about three other points during the portion of the ascent trajectory from lift-off to about 50,000 feet. In addition, data would also be desirable for the orbiter independently for weight conditions corresponding to: (1) the maximum-dynamic-pressure portions of their re-entry trajectories; and (2) typical near-horizontal-flight configurations.

9.3.6 Engine Induced Loads

Test configurations should include the full combined vehicle, the maximum-dynamic-pressure configuration, booster burn-out, and orbiter/external tank at 3 different propellant quantities. Single point excitation at the engines should be used to determine transfer functions for both steady and transient loads. Impulse transfer function techniques would be useful for determining responses to transient applied loads not readily reproducible in test.

9.3.7 Staging

The booster and orbiter would be tested separately in free suspensions. The configurations for the booster would include the appropriate propellant weights for lift-off, maximum dynamic pressure, and burnout. The orbiter/external tank would only be tested with propellant weight at separation.

Measurements of accelerations and rotations should be made at the interconnection points in addition to the standard instrumentation.

Slosh tests of the vehicle in maximum dynamic pressure configuration may be required in which simulated staging transient loads are applied and the resulting tank responses and slosh amplitudes are measured.

10. SUMMARY OF REQUIREMENTS STUDY

10. SUMMARY OF REQUIREMENTS STUDY

10.1 Summary of Significant Structural Features for Each Dynamic Analysis Procedure

The specific aspects of the shuttle structure which are most important in each of the analyses procedures reviewed are summarized in this section. This information would be of direct use in designing an experimental model intended to simulate the structural dynamics of a specific prototype; however, it is also required to determine those features most significant and therefore likely to reveal problem areas.

10.1.1 POGO

- Tanks
  Sidewall and aft end dome bulging flexibility under fluid loading for LO_2 tank. Flexibility of intertank skirt and LH_2 tank to SRM and orbiter interstage locations.
- Engine
  Orbiter engine support structure flexibility
- Feedlines
  Not included
- Orbiter Fuselage
  Flexibility from engine support structure to interstage
- Booster
  Flexibility in lowest lateral mode
- Frequency Range
  Modes involving motion of major parts of the launch configuration up to about 5 Hz are required. Modes involving motion of the orbiter engine thrust structure, feedline support points, and LO_2 tank wall and bottom dome are desired to about 25 Hz.

10.1.2 Control System

- Engines
  Engine support structure flexibilities up to the first axial mode
- Aerodynamic Control Surfaces
  Surface support flexibility
- Reaction Control Thrust
  Flexibility of structure where thrusters are located
- Sensor Locations
  Flexibility in areas where sensors might be mounted
- Frequency Range
  Modes up to 7 Hz are desired for both the combined vehicle and orbiter alone.

10.1.3 Ground Wind Loads

- Launch Configurations
  Flexibility adequate to describe the first cantilever modes in bending normal to the wing plane, lateral bending, and torsion (roll).
- Aerodynamic Lifting Surfaces
  Wing flexibility adequate to describe the first symmetric mode
- Frequency Range
  Modes up to 2 Hz are desired for the full vehicle restrained at the base by the hold-down latches. This same frequency range is also considered adequate for the empty vehicle.

10.1.4 Lift-Off Loads

- Fuselage
  Orbiter flexibility between the engine and the interstage points
- Aerodynamic Lifting Surface
  Flexibility adequate to describe lowest two symmetric bending modes
- Tanks
  Sidewall and aft end dome bulging flexibility of LO_2 tank adequate to described lowest modes. Flexibility from LO_2 tank through LH_2 tank to Orbiter and SRM interstage points

- Booster Thrust and Hold-Down Structure
  Flexibility equivalent to the first axial mode
- Frequency Range
  Modes up to 4 Hz are desired for the full combined vehicle.

10.1.5 Gust Loads

- Wings
  Flexibility up to the equivalent of the second bending and first torsion modes
- Fuselage
  Orbiter flexibility equivalent to the first bending mode
- Tanks
  Flexibility from LO_2 tank through Orbiter interstage points to wing root
- Payload and Orbiter Crew Compartment
  The flexibility relative to the wing root
- Booster
  Flexibility equivalent to 1st axial mode
- Frequency Range
  Modes up to about 8 Hz are desired for the combined vehicle in maximum $q\alpha$ weight configuration.

10.1.6 Engine Induced Response

The same characteristics as required for POGO analyses would be suitable here, except that the frequency range of interest would extend somewhat higher.

10.1.7 Staging

- Engines
  Engine support structure flexibilities up to the first axial mode for both the orbiter and the booster
- Interstage Connection Points
  Flexibilities from these points to major inertia reaction items such as the LO_2 tanks

- Frequency Range

  Modes up to 5 Hz for each vehicle component separately - for a full orbiter and for an empty booster.

11. MODAL COUPLING APPLIED TO THE NASA LANGLEY 1/15 SCALE STRUCTURAL DYNAMICS MODEL TEST DATA

11. MODAL COUPLING APPLIED TO 1/15 SCALE MODEL TEST DATA

In accordance with the requirements of NAS1-10635-4 Modification 1, analytical coupling of the orbiter and booster dynamic model fuselage modes has been briefly investigated. This work was undertaken to evaluate a specific coupling procedure using test data from the 1/15 scale model described in References 11-1 and 11-2.

11.1 Description of Problem

An additional requirement to this task added by Modification No. 1 on 9/1/71 stated that "In order to more fully determine the requirements for the model configuration, additional study shall be conducted to further evaluate modal component synthesis techniques needed to attain an adequate understanding of the dynamic behavior of the involved structure." The objective was to evaluate an existing analytical approach and to study means for computing systems damping from component tests. Therefore the feasibility of analytically combining the experimentally determined component modes of a model of an early shuttle concept was investigated.

The model, described in Reference 11-1 and 11-2, consisted of tubular beams representing an orbiter and a booster in pitch plane motion. These beams are coupled by two interconnecting spring assemblies each of which had a stiffness of 1,000 lbs/in. The measured data and analysis only considered lateral motions.

11.2 Description of Coupling Procedure

The modal coupling procedure used assumed that the orbiter and booster fuselage models could be coupled by massless springs which add to the generalized stiffness of the combined beams. The potential energy of the coupled system would then have a contribution from the orbiter, described in terms of similar modes, and a contribution from the coupling springs between the two vehicle. It was assumed that the kinetic energy of the coupled system could be described terms of uncoupled orbiter and booster modes. The equations of motion of the combined system, in terms of model coordinates as determined from the energy expressions, were solved for the eigenvalues and eigenvectors, and the resulting vectors were translated back into the original coordinates. The following is a summary of the procedure.

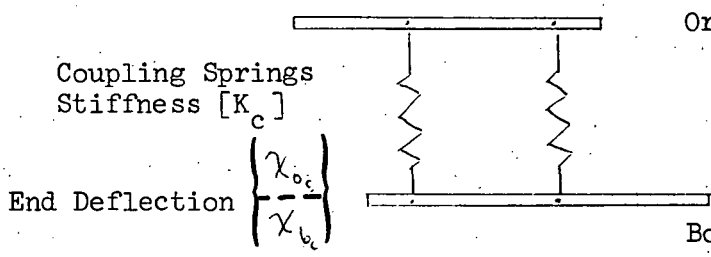

Kinetic Energy

$$V = \frac{1}{2}\{X_o\}^T[K_o]\{X_o\} + \frac{1}{2}\{X_b\}^T[K_b]\{X_b\} + \frac{1}{2}\begin{Bmatrix} X_{o_c} \\ \hline X_{b_c} \end{Bmatrix}^T [K_c] \begin{Bmatrix} X_{o_c} \\ \hline X_{b_c} \end{Bmatrix}$$

Express deflections as $X = \varphi\xi$ where φ are modal vectors and ξ modal displacements.

$$V = \frac{1}{2}\{\phi_o\xi_o\}^T[K_o]\{\phi_o\xi_o\} + \frac{1}{2}\{\phi_b\xi_b\}^T[K_b]\{\phi_b\xi_b\} + \frac{1}{2}\begin{Bmatrix} \phi_{o_c}\xi_{o_c} \\ \hline \phi_{b_c}\xi_{b_c} \end{Bmatrix}^T [K_c] \begin{Bmatrix} \phi_{o_c}\xi_{o_c} \\ \hline \phi_{o_b}\xi_b \end{Bmatrix}$$

Since $[\varphi_O]^T [K_O]\{\varphi_O\} = [M_O\omega_{n_O}^2]$, where M_O are the orbiter generalized masses and ω_{nO}^2 are the square of the resonant frequencies and since a similar relationship holds for the booster, then $\left\{\frac{\partial V}{\partial \xi}\right\}$, which is the form required for the equations of motion, becomes:

$$\frac{\partial V}{\partial \xi} = \left[\begin{array}{c|c} M_b\omega_b^2 & 0 \\ \hline 0 & M_o\omega_o^2 \end{array}\right] \left\{\begin{array}{c} \xi_b \\ \hline \xi_o \end{array}\right\} + \left[\begin{array}{c|c} \phi_{b_c}^T & \\ \hline & \phi_{o_c}^T \end{array}\right] K_c \left[\begin{array}{c|c} \phi_{b_c} & \\ \hline & \phi_{o_c} \end{array}\right] \left\{\begin{array}{c} \xi_b \\ \hline \xi_o \end{array}\right\}$$

For the specific problem considered here, coupling 2 flexibile and 2 rigid orbiter modes to 5 flexible and 2 rigid booster modes, the size of the matrices involved are shown. Also, for equal rate coupling springs, the form of (K_c) is:

$$\begin{bmatrix} K & 0 & -K & 0 \\ 0 & K & 0 & -K \\ -K & 0 & K & 0 \\ 0 & -K & 0 & K \end{bmatrix}$$

Similarly, the term required for the equations of motion from the kinetic energy becomes:

$$\frac{d}{dt}\left(\frac{\partial T}{\partial \dot{\xi}}\right) = \left[\begin{array}{c|c} M_b & \\ \hline & M_o \end{array}\right] \left\{\begin{array}{c} \ddot{\xi}_b \\ \hline \ddot{\xi}_o \end{array}\right\}$$

11.3 Verification of Coupling Procedure

To verify the procedure, the simple two-beam, three-spring, arrangement shown below was examined. Each beam was allowed 14 degrees of freedom and had a fundamental (free-free) frequency of about 86 Hz. Two sets of equal rate springs were studied (10^4 and 10^5 lbs/in.).

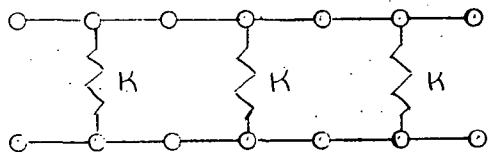

A review of the calculations indicated that when 14 modes were used to describe each beam (two rigid body and 12 flexible) all 28 coupled-system frequencies agreed with those calculated directly for the entire system. The frequency comparisons are included as Tables 11-1 and 11-2. The effect of using fewer modes in the coupling process was also explored and it was determined that reproducibility of frequencies appeared to be better with a higher number of modes. For example, coupling the 10 lowest frequency modes of each beam gave correct total system frequencies up to the 20th mode; whereas, coupling 3 modes of each beam gave only 3 correct total system frequencies. This result was influenced by the value of the coupling spring and generalizations do not appear warranted. Mode shapes are also compared in Table 11-3.

The agreement shown in the above problem provided the desired check of the analytical method.

11.4 Processing of Data from Langley 1/15 Scale Model

The separate modes of the orbiter and booster fuselage models obtained by test in October , 1971 were used in the coupling analyses. The 2 elastic and 2 rigid body orbiter modes used are shown in Table 11-4. Only motion in the pitch plane was considered. It was most convenient to keep the modal displacements at the locations of the concentrated weights separate from those for the distributed weights, therefore the first 7 coordinates are for distributed weight locations and the succeeding 16 are for the concentrated weights. The distance along the beam, from the orbiter nose, for each coordinate may be obtained by subtracting 8 in. (the reference distance) from the value for mode 4, the rigid body pitch mode. The weight associated with each coordinate is shown in the column matrix on the right under WEIGHT 0. In order to check

the orthogonality of these modes, the matrix of terms $M_{ij}^2/M_{ii}M_{jj}$ was formed from the generalized mass matrix $M = (\varphi)^T (m) (\varphi)$. In evaluating experimentally measured modes, the orthogonality between them is generally considered adequate if the off-diagonal terms in this matrix are less than 0.1. This is the case for the orbiter elastic modes, the first two rows and columns in matrix ORTHO shown on the bottom of Table 11-4. The last two rows and columns show the coupling between rigid body translation and pitch modes which is high as anticipated because the rigid body pitch is taken about a reference point 8" forward of the nose.

The 5 elastic and 2 rigid body booster modes used are shown in Table 11-5. The first 13 coordinates represent the distributed weight location, while the remaining 18 represent the booster concentrated weights. The weight associated with each coordinate is shown in the last column on the right under WEIGHT 8. The distance of each coordinate from the booster nose reference point may be obtained by subtracting 15.7 from the values in the 7th mode (rigid body pitch). The orthogonality check shown at the bottom indicates that only orthogonality between the 4th and 5th elastic modes is not within the desirable limit.

The generalized mass matrix was formed from the measured flexible and the computed rigid body mode shapes. All off diagonal terms (except for the coupling between rigid body translation and pitch) were eliminated. The form of the matrix used is shown in Table 11-6.

The generalized stiffness matrix was formed as indicated previously. The off-diagonal terms were eliminated from the separate body generalized mass matrix before multiplying by the square of the resonant frequencies. The coupling generalized spring matrix which was a full 11 by 11, was then added.

The resulting 11 x 11 eignevalue problem was then solved and the resulting eigenvectors were translated into the original booster and orbiter coordinate system, and then rearranged for easier plotting. Tabulated values of the modes and frequencies of the coupled system are shown on Table 11-7. The frequencies are shown at the top of each vector column. The location of each coordinate may be obtained from the 0.19 Hz mode which turns out to be the rigid body pitch about some point just forward of the orbiter. The non-zero frequency of this rigid body mode results from the numerics of the eigenvalue calculation. The components of this modal vector represent the relative

distance of each coordinate, and multiplying them by 150 in. gives the absolute distance. For example, coordinate 15 is .517 of the distance from the reference point to the back end of the beam representing the booster, or 150 (.517) = 78". The first 31 coordinates represent the booster, the next 23 represent the orbiter and the last 4 represent the location of the coupling springs on the orbiter and booster.

11.5 Review of Results

Five of the flexible modes for which comparisons between analytical coupling and direct measurement could be made were plotted as shown in Figures 11-2 through 11-6. One mode measured experimentally, the 4th flexible at 48.3 Hz did not appear at all in the analytically coupled modes but is shown in Figure 11-7. This mode shape resembles that for the second flexible mode with considerably more orbiter bending. An orthogonality check of the measured coupled system modes, as shown in Table 8, indicated that the 2nd and 4th flexible modes were highly coupled (note that the 2, 4 term in the matrix is 0.85). Both modes are apparently orthogonal with all the others measured.

Modes above 103.5 Hz were not plotted because a review of the data in Table 11-7 indicated that the 4 remaining higher frequency modes were similar to the input modes for the individual uncoupled model in both frequency and shape. In fact, the sixth measured flexible coupled mode shown in Figure 6 actually appears to be the first orbiter bending with little motion of the booster and the measured frequency of 101.9 Hz is close to the 98.8 Hz measured for the orbiter model alone. This effective uncoupling of higher frequency modes is due to the relatively low stiffness of the connecting springs. A similar effect was noted in the analytical work described in reference 11-2. The coupled pitch mode at 104.9 Hz shown in Figure 22(i) of this reference is similar to the first mode of the orbiter fuselage at 103.5 Hz shown in Figure 13 (a) of the same reference. Also, the next higher pitch mode at 118.7 Hz shown in Figure 22(l) is similar to the second mode of the booster fuselage at 117.7 Hz shown in Figure 12(b).

11.6 Discussion and Recommendation

The coupling procedure employed in the investigation demonstrated the feasibility of predicting coupled system modes using vibration measurements made during tests on the separate vehicles. The inability of this procedure to predict the fourth mode (48.3 Hz), however, demonstrates the difficulties in making assumptions as to the type of restraint at interfaces between vehicles. In subsequent work reported by Dr. R. W. Fralich (Reference 11-3), the assumption that the interconnecting springs were pinned to the tubes was modified to permit a finite rotational restraint, and the assumption of lateral motion only was modified to permit axial motion as well. With these changes, the calculated and measured frequencies for the fourth as well as the other modes were very close.

The case studied here involved physical models of relatively simple form, i.e., two stiff beams represented by these free-free modes coupled by relatively soft discrete springs. The evaluation of other coupling techniques which might be used on the shuttle should consider more representative model configuration and a wider variety of testing and coupling combinations. The existing model, if it is to be used further, could be modified to account for more rigid interstage connections (including redundant ties) and for motions other than in the pitch plane. Close coordination between analyses and test should be maintained to insure the careful investigation of discrepancies. Analytical coupling procedures which accommodate separate vehicle tests under other than free-free support conditions should also be investigated.

SAMPLE BEAM PROBLEM - COMPARISON OF FREQUENCIES ($K=10^5$ #/IN)

MODE NO.	CALCULATED FREQ (rad/sec.)	RUN 1 14* - 14*	RUN 2 3-3	RUN 3 4-4	RUN 4 5-5	RUN 5 6-6	RUN 6 7-7	RUN 7 9-9	RUN 8 10+10	RUN 9 12+12
1	4.048	2.193	—	.568	—	1.18	—	—	3.159	—
2	9.448	5.52	2.917	.951	.570	1.54	2.27	2.34	4.473	3.58
3	543.28	543.31	543.56	543.55	543.28	543.27	543.27	543.27	543.28	543.27
4	1087.5	1085.3	2244.8	1114.28	1106.8	1088.8	1088.7	1087.9	1086.3	1085.5
5	1157.7	1158.5	3083.	1413.7	1163.0	1163.	1162.1	1161.5	1161.3	1158.6
6	1415.8	1415.8	3741.	2247.1	1416.4	1416.	1415.9	1415.9	1415.9	1415.8
7	2515.7	2515.7		3598.1	2519.0	2516.6	2516.4	2516.3	2515.7	2515.7
8	2741.6	2744.7		4073.5	3584.6	2787	2781.6	2766.7	2747.6	2746.3
9	3183.0	3177.5			4009.7	3689	3295.8	3188	3179.5	3179.3
10	3887.5	3887.6			5334.1	3915.5	3890.4	3888.2	3887.6	3887.6
11	4906.2	4906.6				5034.	5024.4	4976.7	4940.1	4910.6
12	5360.3	5359.8				5815.	5376.6	5372.4	5369.7	5361.2
13	5564.3	5558.4					5815.7	5719.7	5632.6	5569.3
14	6083.2	6081.3					6226.3	6097.9	6086.4	6083.
15	6693.8	6693.8						6701.2	6696.5	6694.1
16	7425.2	7424.9						7444.6	7427.8	7425.8
17	8707.5	8707.3						8114.1	8708.7	8707.7
18	9446.5	9445.6						9480.7	9453.9	9446.9
19	9604.0	9603.5							9609.7	9606.4
20	10478	10478.							10527.1	10482.2
21	10522	10521.								10599.4
22	11303	11302.								11303.5
23	11533	11532.								11553.0
24	11744	11744.								12341.
25	12341	12341								
26	13133	13133								
27	13258	13258								
28	14018	14018								

(1)

* NUMBER OF MODES (INCLUDING 2 RIGID BODY MODES) FOR EACH BEAM

(1) - Modes 1 & 2 represent rigid body motion. All values are substantially zero and therefor show good agreement.

TABLE 11-1

SAMPLE BEAM PROBLEM - COMPARISON OF FREQUENCIES ($K = 10^4$ #/IN)

MODE NO.	CALCULATED FREQ (rad/sec)	RUN 1 12+14	RUN 2 3+3	RUN 3 4+4	RUN 4 5+5	RUN 5 6+6	RUN 6 7+7	RUN 7 9+9	RUN 8 10+10	RUN 9 12+12
1	5.45	3.514	.357	—	—	1.213	—	1.45	—	2.44
2	9.79	5.095	.770	—	.917	1.321	1.34	2.50	2.315	4.03
3	542.19	542.24	542.57	542.54	542.24	542.23	542.23	542.23	542.23	542.21
4	787.27	787.00	857.14	830.89	788.44	788.14	788.13	787.73	787.72	787.06
5	817.24	815.86	977.18	859.35	831.81	818.03	817.97	817.56	816.05	815.98
6	1162.77	1162.58	1196.83	1178.71	1177.75	1177.31	1167.99	1162.69	1162.61	1162.60
7	1418.89	1418.80		1419.90	1419.41	1419.30	1419.00	1418.84	1418.81	1418.81
8	1658.89	1657.45		1680.86	1678.58	1661.03	1660.19	1659.51	1657.73	1657.64
9	2504.04	2503.99			2504.66	2504.17	2504.17	2504.11	2504.09	2503.99
10	2896.02	2895.47			2900.40	2897.57	2897.46	2896.88	2896.87	2895.56
11	3818.63	3819.63				3819.98	3819.98	3819.89	3819.69	3819.63
12	4069.73	4069.55				4070.73	4070.63	4070.38	4069.73	4069.60
13	5314.82	5314.78					5315.06	5314.78	5314.78	5314.78
14	5610.97	5610.79					5611.34	5610.62	5610.83	5610.79
15	6655.91	6655.86						6655.84	6655.86	6655.86
16	7362.54	7362.48						7362.52	7362.48	7362.48
17	8593.70	8593.57						8593.70	8593.63	8593.63
18	9020.42	9020.26						9020.42	9020.35	9020.35
19	9475.63	9475.49							9475.56	9475.56
20	10255.64	10255.46							10255.54	10255.46
21	10461.32	10461.32								10461.32
22	11256.97	11256.97								11256.97
23	11385.56	11385.41								11385.50
24	11631.76	11681.67								12310.94
25	12311.03	12310.94								
26	13126.84	13126.04								
27	13244.34	13244.34								
28	14000.13	14000.13								

TABLE 11-2

SAMPLE BEAM PROBLEM

COMPARISON OF MODE SHAPES FOR ANALYTICAL COUPLING

$K = 10^5$ lbs/in

Mode No.	Freq (RPS)	Mode Shape Calculated with Number of Modes Shown Agrees with that From Full 28 Coordinate Calculations						
		6	8	10	12	14	18	20
3	543	o	o	o	o	o	o	o
4	1087	x	o	o	o	o	o	o
5	1158	x	x	o	o	o	o	o
6	1416	x	x	o	o	o	o	o
7	2516		x	o	o	o	o	o
8	2742		x	x	o	o	o	o
9	3183			x	o	o	o	o
10	3887			x	o	o	o	o
11	4906				o	o	o	o
12	5360				x	o	o	o

$K = 10^4$ lbs/in

3	542	o	o	o	o
4	787	o	o	o	o
5	817	x	o	o	o
6	1163	x	o	o	o
7	1418		o	o	o
8	1658		o	o	o

NOTE: O indicates aggreement

X indicates non-agreement

TABLE 11-3

(1, 1) MATRIX MODEO (23X 4)

	98.8 Hz 1	200.4 Hz 2	R.B. TRANS. 3	R.B. PITCH 4
1	1.200000E 00	2.300000E-02	1.000000E 00	1.442000E 01
2	-4.000000E-01	-1.500000E-01	1.000000E 00	2.787000E 01
3	-1.200000E 00	1.700000E-01	1.000000E 00	4.195000E 01
4	-7.300000E-01	9.700000E-01	1.000000E 00	5.300000E 01
5	4.500000E-01	5.000000E-01	1.000000E 00	6.300000E 01
6	1.950000E 00	-1.500000E-01	1.000000E 00	7.300000E 01
7	3.200000E 00	-5.000000E-01	1.000000E 00	8.079999E 01
8	2.179999E 00	5.599999E-01	1.000000E 00	7.250000E 00
9	2.700000E 00	5.200000E-01	1.000000E 00	8.120000E 00
10	4.500000E-01	0.0	1.000000E 00	2.000000E 01
11	2.500000E-01	-5.999999E-02	1.000000E 00	2.200000E 01
12	-1.500000E-01	-1.400000E-01	1.000000E 00	2.550000E 01
13	-5.100000E-01	-1.500000E-01	1.000000E 00	2.900000E 01
14	-7.750000E-01	-1.400000E-01	1.000000E 00	3.150000E 01
15	-1.000000E 00	-6.999999E-02	1.000000E 00	3.550000E 01
16	-1.200000E 00	1.199999E-01	1.000000E 00	4.079999E 01
17	-1.150000E 00	5.599999E-01	1.000000E 00	4.759999E 01
18	-9.000000E-01	8.700000E-01	1.000000E 00	5.100000E 01
19	-4.500000E-01	1.000000E 00	1.000000E 00	5.600000E 01
20	2.500000E-01	5.500000E-01	1.000000E 00	6.150000E 01
21	1.910000E 00	-1.600000E-01	1.000000E 00	7.320000E 01
22	2.400000E 00	-3.200000E-01	1.000000E 00	7.600000E 01
23	3.599999E 00	-5.000000E-01	1.000000E 00	8.399999E 01

WEIGHTO (

ROW	COLUMN	ELEMENT
1	1.	1.410000E 00
2	2.	2.160000E 00
3	3.	1.690000E 00
4	4.	1.250000E 00
5	5.	1.250000E 00
6	6.	1.250000E 00
7	7.	7.000000E-01
8	8.	5.000000E 00
9	9.	2.800000E-01
10	10.	7.600000E-01
11	11.	1.510000E 01
12	12.	1.510000E 01
13	13.	1.510000E 01
14	14.	1.510000E 01
15	15.	2.799999E 00
16	16.	8.300000E-01
17	17.	1.799999E-01
18	18.	4.950000E 00
19	19.	4.950000E 00
20	20.	1.799999E-01
21	21.	1.899999E 00
22	22.	1.799999E-01
23	23.	4.800000E-01

(1, 1) MATRIX ORTHO (4X 4)

	1	2	3	4
1	9.999996E-01	5.141208E-04	7.145170E-03	6.758729E-03
2	5.141243E-04	9.999985E-01	2.272939E-02	6.729278E-02
3	7.145174E-03	2.272939E-02	1.000000E 00	8.181364E-01
4	6.758712E-03	6.729278E-02	8.181362E-01	9.999999E-01

(1, 1) MATRIX MODES (31, 7)

	38.7 Hz 1	103.2 Hz 2	185.8 Hz 3	277.1 Hz 4	369 Hz 5	R.B. Trans. 6	R.B. Pitch 7
1	9.000000E-01	4.500000E-01	7.200000E-01	4.899999E-01	5.400000E-01	1.000000E 00	2.181000E 01
2	5.250000E-01	1.125000E-01	9.999996E-02	9.999998E-03	-5.000000E-02	1.000000E 00	3.031000E 01
3	7.499999E-02	-2.250000E-01	-4.100000E-01	-2.300000E-01	-9.999998E-03	1.000000E 00	4.079999E 01
4	-2.600000E-01	-2.700000E-01	-2.399999E-01	4.000000E-02	1.300000E-01	1.000000E 00	5.081000E 01
5	-4.725000E-01	-1.462500E-01	2.500000E-01	1.750000E-01	-1.600000E-01	1.000000E 00	6.078999E 01
6	-5.800000E-01	1.199999E-01	4.800000E-01	9.999998E-03	-7.999998E-02	1.000000E 00	6.934000E 01
7	-6.149999E-01	3.600000E-01	5.000000E-01	-3.150000E-01	9.999996E-02	1.000000E 00	7.529999E 01
8	-4.899999E-01	5.549999E-01	1.700000E-01	-3.750000E-01	2.100000E-01	1.000000E 00	8.071999E 01
9	-3.400000E-01	6.250000E-01	-1.250000E-01	-2.500000E-01	2.000000E-01	1.000000E 00	9.916999E 01
10	-1.400000E-01	5.775000E-01	-4.600000E-01	-2.000000E-02	7.499999E-02	1.000000E 00	1.091700E 02
11	1.250000E-01	3.450000E-01	-6.000000E-01	2.000000E-01	-6.500000E-02	1.000000E 00	1.207400E 02
12	4.299999E-01	1.000000E-02	-3.700000E-01	1.400000E-01	-7.999998E-02	1.000000E 00	1.307400E 02
13	7.500000E-01	-4.199999E-01	2.500000E-01	-5.000000E-02	-2.000000E-02	1.000000E 00	1.429100E 02
14	1.192000E 00	-6.300000E-01	1.219999E 00	1.075000E 00	1.160000E 00	1.000000E 00	1.570000E 01
15	1.600000E-01	3.750000E-01	3.500000E-01	1.900000E-01	1.250000E-01	1.000000E 00	2.670000E 01
16	5.400000E-01	1.500000E-01	1.500000E-01	4.000000E-02	-4.500000E-02	1.000000E 00	2.970000E 01
17	2.600000E-01	-8.999997E-02	-2.600000E-01	-2.250000E-01	-1.500000E-01	1.000000E 00	3.600000E 01
18	-1.750000E-01	-2.900000E-01	-3.750000E-01	-7.499999E-02	1.750000E-01	1.000000E 00	4.770000E 01
19	-3.400000E-01	-3.150000E-01	-7.999998E-02	1.199999E-01	3.500000E-02	1.000000E 00	5.350000E 01
20	-4.659999E-01	-1.199999E-01	2.900000E-01	-1.700000E-01	-1.750000E-01	1.000000E 00	6.170000E 01
21	-6.000000E-01	-2.250000E-01	5.200000E-01	-1.300000E-01	-2.500000E-02	1.000000E 00	7.320000E 01
22	-6.199999E-01	-3.400000E-01	5.000000E-01	-2.800000E-01	8.999997E-02	1.000000E 00	7.860000E 01
23	-5.750000E-01	-4.350000E-01	4.000000E-01	-4.000000E-01	1.500000E-01	1.000000E 00	8.379999E 01
24	-3.900000E-01	-6.150000E-01	-4.000000E-02	-3.600000E-01	2.100000E-01	1.000000E 00	9.670000E 01
25	-2.600000E-01	-6.299999E-01	-2.500000E-01	-1.799999E-01	1.600000E-01	1.000000E 00	1.027000E 02
26	-6.000000E-02	-4.299999E-01	-5.000000E-01	1.700000E-01	-4.000000E-02	1.000000E 00	1.173000E 02
27	1.750000E-01	-3.300000E-01	-5.900000E-01	2.000000E-01	-7.499999E-02	1.000000E 00	1.217000E 02
28	6.300000E-01	-2.399999E-01	9.999998E-03	2.500000E-02	-5.000000E-02	1.000000E 00	1.380000E 02
29	6.799999E-01	-3.599999E-01	1.100000E-01	-4.999999E-03	-4.000000E-02	1.000000E 00	1.359000E 02
30	5.500000E-01	-7.200000E-01	6.000000E-01	-1.799999E-01	4.000000E-02	1.000000E 00	1.500000E 02
31	1.000000E 00	-7.900000E-01	7.000000E-01	-2.500000E-01	5.000000E-02	1.000000E 00	1.615000E 02

MATRIX WEIGHTS

ROW	COLUMN	ELEMENT
1	1.	1.448000E 00
2	2.	1.125999E 00
3	3.	1.440000E 00
4	4.	1.625000E 00
5	5.	1.805999E 00
6	6.	1.422000E 00
7	7.	2.639999E 00
8	8.	2.089999E 00
9	9.	1.476999E 00
10	10.	2.900000E 00
11	11.	2.320000E 00
12	12.	2.440000E 00
13	13.	3.679999E 00
14	14.	7.999999E-02
15	15.	8.000000E-01
16	16.	8.099999E 01
17	17.	4.339999E 00
18	18.	4.620000E 01
19	19.	4.620000E 01
20	20.	4.620000E 01
21	21.	3.719999E 00
22	22.	6.959000E 00
23	23.	6.959999E 00
24	24.	1.660000E 01
25	25.	1.719999E 00
26	26.	2.900000E-01
27	27.	2.239999E 01
28	28.	3.200000E-01
29	29.	2.139999E 00
30	30.	5.800000E 00
31	31.	4.000000E 00

(1, 1) MATRIX ORTHO (7, 7)

	1	2	3	4	5	6	7
1	1.000000E 00	5.567487E-03	5.207390E-03	2.553321E-04	2.853026E-03	2.915228E-04	2.684396E-05
2	5.567493E-03	9.999999E-01	1.164059E-04	2.370250E-03	8.780725E-03	5.579181E-03	6.343640E-03
3	5.207382E-03	1.164062E-04	9.999999E-01	2.498389E-02	7.009017E-02	1.718045E-03	1.373054E-04
4	2.553295E-04	2.370262E-03	2.498390E-02	9.999995E-01	2.533821E-01	3.048312E-02	1.112789E-02
5	2.853012E-03	8.780718E-03	7.009023E-02	2.533819E-01	9.999989E-01	6.350501E-05	4.742173E-04
6	2.915210E-04	5.579181E-03	1.718046E-03	3.048319E-02	6.350540E-05	9.999996E-01	7.716175E-01
7	2.684379E-05	6.343640E-03	1.373056E-04	1.112791E-02	4.742197E-04	7.716164E-01	9.999949E-01

TABLE 11-5

(1, 2) MATRIX TGM (11) 11)

	1	2	3	4	5	6
1	1.719904E-01	0.0	0.0	0.0	0.0	0.0
2	0.0	6.492895E-02	0.0	0.0	0.0	0.0
3	0.0	0.0	8.482319E-02	0.0	0.0	0.0
4	0.0	0.0	0.0	1.886551E-02	0.0	0.0
5	0.0	0.0	0.0	0.0	1.161433E-02	0.0
6	0.0	0.0	0.0	0.0	0.0	7.942150E-01
7	0.0	0.0	0.0	0.0	0.0	4.865527E 01
8	0.0	0.0	0.0	0.0	0.0	0.0
9	0.0	0.0	0.0	0.0	0.0	0.0
10	0.0	0.0	0.0	0.0	0.0	0.0
11	0.0	0.0	0.0	0.0	0.0	0.0

	7	8	9	10	11
1	0.0	0.0	0.0	0.0	0.0
2	0.0	0.0	0.0	0.0	0.0
3	0.0	0.0	0.0	0.0	0.0
4	0.0	0.0	0.0	0.0	0.0
5	0.0	0.0	0.0	0.0	0.0
6	4.865529E 01	0.0	0.0	0.0	0.0
7	3.862956E 03	0.0	0.0	0.0	0.0
8	0.0	2.069213E-01	0.0	0.0	0.0
9	0.0	0.0	3.416061E-02	0.0	0.0
10	0.0	0.0	0.0	2.387462E-01	7.741657E 00
11	0.0	0.0	0.0	7.741656E 00	3.068354E 02

TABLE 11-6

(1, 2) MATRIX PLOTALL (58) 111

	29.4 Hz 8	10.4 Hz 9	.19Hz 10	.15 Hz 11	
1	-1.446E-01	3.502E-01	1.069E-01	-8.941E-01	BOOSTER
2	-1.212E-01	3.226E-01	1.471E-01	-3.038E-01	
3	-9.642E-02	3.126E-01	1.793E-01	-7.347E-01	
4	-8.584E-02	2.956E-01	1.990E-01	-6.031E-01	
5	-8.766E-02	2.867E-01	2.026E-01	-5.841E-01	
6	-8.414E-02	2.837E-01	2.048E-01	-5.671E-01	
7	-8.067E-02	2.844E-01	2.720E-01	-5.410E-01	
8	-2.537E-02	2.175E-01	3.174E-01	-4.475E-01	
9	-1.715E-02	2.068E-01	3.378E-01	-4.057E-01	
10	-9.349E-03	1.943E-01	3.555E-01	-3.683E-01	
11	4.566E-03	1.825E-01	4.034E-01	-2.688E-01	
12	6.675E-03	1.567E-01	4.094E-01	-2.564E-01	
13	1.725E-02	1.241E-01	4.597E-01	-1.522E-01	
14	2.000E-02	1.068E-01	4.850E-01	-9.955E-02	
15	2.251E-02	9.185E-02	5.177E-01	-3.269E-02	
16	2.213E-02	7.669E-02	5.252E-01	-1.633E-02	
17	1.931E-02	5.194E-02	5.549E-01	4.513E-02	
18	9.287E-03	1.477E-02	6.003E-01	1.395E-01	
19	-1.513E-03	-1.926E-02	6.396E-01	2.211E-01	
20	-6.891E-03	-3.162E-02	6.554E-01	2.533E-01	
21	-1.359E-02	-5.181E-02	6.790E-01	3.029E-01	
22	-2.911E-02	-8.981E-02	7.216E-01	3.912E-01	
23	-5.194E-02	-1.760E-01	7.761E-01	5.219E-01	
24	-8.664E-02	-1.562E-01	7.977E-01	5.491E-01	
25	-8.331E-02	-1.618E-01	8.240E-01	5.623E-01	
26	-2.955E-02	-2.183E-01	8.534E-01	6.855E-01	
27	-1.999E-01	-2.581E-01	9.112E-01	7.846E-01	
28	-1.160E-01	-2.695E-01	9.237E-01	8.156E-01	
29	-1.282E-01	-2.868E-01	9.475E-01	8.516E-01	
30	-1.437E-01	-3.056E-01	9.901E-01	9.423E-01	
31	-1.476E-01	-3.277E-01	9.991E-01	9.634E-01	
32	-3.561E-01	-9.999E-02	5.164E-02	-9.999E-01	ORBITER
33	-3.396E-01	-9.817E-01	5.735E-02	-9.831E-01	
34	-2.111E-01	-9.499E-01	9.875E-02	-9.952E-01	
35	-9.726E-02	-7.317E-01	1.354E-01	-8.259E-01	
36	-5.784E-02	-6.064E-01	1.495E-01	-7.985E-01	
37	1.216E-02	-6.177E-01	1.715E-01	-7.517E-01	
38	5.933E-02	-5.699E-01	1.871E-01	-7.134E-01	
39	8.149E-02	-5.456E-01	1.945E-01	-7.003E-01	
40	1.314E-01	-4.942E-01	2.110E-01	-6.837E-01	
41	2.078E-01	-4.141E-01	2.372E-01	-6.143E-01	
42	2.674E-01	-3.656E-01	2.721E-01	-5.413E-01	
43	3.286E-01	-3.071E-01	2.796E-01	-5.261E-01	
44	4.315E-01	-1.789E-01	3.168E-01	-4.490E-01	
45	4.887E-01	-1.164E-01	3.301E-01	-4.026E-01	
46	5.223E-01	-7.399E-02	3.523E-01	-3.753E-01	
47	5.717E-01	-2.582E-02	3.721E-01	-3.243E-01	
48	6.577E-01	7.196E-02	4.051E-01	-2.592E-01	
49	6.991E-01	9.833E-02	4.103E-01	-2.397E-01	
50	8.333E-01	2.729E-01	4.837E-01	-1.022E-01	
51	8.376E-01	2.771E-01	4.956E-01	-4.953E-02	
52	8.791E-01	3.201E-01	5.074E-01	-6.127E-02	
53	9.512E-01	4.007E-01	5.355E-01	-1.261E-02	
54	9.699E-01	4.628E-01	5.553E-01	4.636E-02	
55	9.169E-01	-4.065E-01	2.410E-01	-5.074E-01	SPRINGS (41+)
56	8.377E-01	2.777E-01	4.350E-01	-3.993E-02	(61)
57	-6.416E-02	9.637E-01	2.404E-01	-5.071E-01	(6)
58	2.000E-02	1.056E+00	4.850E-01	-9.955E-02	(14)

TABLE II-7-1

MATRIX PLOTALL

103.5 Hz 2	101.5 Hz 6	40.0 Hz 7
7.719703E-01	1.151462E-01	9.999999E-01
5.642506E-01	8.370417E-02	7.782184E-01
3.367619E-01	5.046317E-02	5.664779E-01
1.323074E-01	2.850259E-02	4.597536E-01
1.513334E-01	2.413613E-02	4.461936E-01
-1.137106E-01	-1.401189E-02	2.114721E-01
-2.804287E-01	-3.777243E-02	4.771160E-02
-3.596649E-01	-4.991912E-02	-1.716452E-01
-3.343912E-01	-4.683216E-02	-2.454817E-01
-3.093345E-01	-4.355079E-02	-3.146695E-01
-1.716100E-01	-2.550549E-02	-4.265367E-01
-1.464512E-01	-2.229739E-02	-4.437416E-01
1.547431E-01	1.671643E-02	-5.199656E-01
2.866220E-01	3.371659E-02	-5.367407E-01
4.314539E-01	5.208833E-02	-5.539675E-01
4.565604E-01	5.533579E-02	-5.496621E-01
5.700018E-01	6.967270E-02	-5.155325E-01
7.091408E-01	8.695045E-02	-4.436640E-01
7.726783E-01	9.457582E-02	-3.591514E-01
7.917454E-01	9.688008E-02	-3.167743E-01
7.922210E-01	9.659499E-02	-2.664091E-01
7.299246E-01	8.821058E-02	-1.485076E-01
5.474492E-01	6.498206E-02	2.032706E-02
4.463613E-01	5.241761E-02	9.662771E-02
4.084483E-01	4.770574E-02	1.178695E-01
4.052256E-02	3.070653E-03	3.352498E-01
-3.020449E-01	-3.849031E-02	5.058565E-01
-3.909568E-01	-4.919777E-02	5.485746E-01
-5.242339E-01	-6.653937E-02	6.062259E-01
-9.110385E-01	-1.133944E-01	7.787419E-01
-9.999999E-01	-1.230794E-01	8.216429E-01
-4.957345E-01	5.590774E-01	-2.947108E-01
-4.703796E-01	5.306348E-01	-2.814077E-01
-2.685650E-01	3.048587E-01	-1.635288E-01
-9.592426E-02	1.110514E-01	-9.611470E-02
-5.038824E-02	5.970597E-02	-6.705478E-02
4.115210E-02	-4.331042E-02	-1.452519E-02
9.802723E-02	-1.074623E-01	2.053677E-02
1.208239E-01	-1.329618E-01	3.669123E-02
1.831699E-01	-2.035967E-01	7.402495E-02
2.316523E-01	-2.595791E-01	1.278062E-01
2.720683E-01	-3.076066E-01	1.958818E-01
2.703981E-01	-3.065122E-01	2.094176E-01
2.497872E-01	-2.876742E-01	2.748767E-01
1.845067E-01	-2.180353E-01	3.677577E-01
1.406536E-01	-1.710277E-01	3.263480E-01
6.937963E-02	-9.420484E-02	3.529018E-01
-1.049504E-01	9.537582E-02	3.946594E-01
-1.545236E-01	1.493970E-01	4.055987E-01
-5.259933E-01	5.542622E-01	4.746329E-01
-5.166318E-01	5.429287E-01	4.781314E-01
-6.378053E-01	6.757649E-01	4.954234E-01
-8.358819E-01	8.915146E-01	5.265740E-01
-9.352512E-01	9.999999E-01	5.502910E-01
2.309872E-01	-2.591431E-01	1.334213E-01
-5.142038E-01	5.411600E-01	4.784005E-01
-1.200477E-01	-1.477960E-02	2.111466E-01
2.866220E-01	-3.371659E-02	-5.367407E-01

TABLE 11-7-2

(1, 1) MATRIX PLOTALL (59× 11)

		368.9 Hz 1	277.2 Hz 2	200.4 Hz 3	186.0 Hz 4
BOOSTER2	1	9.999957E-01	-9.999999E-01	6.849729E-03	-9.999993E-01
	2	4.654957E-01	-4.656691E-01	3.831733E-03	-5.000044E-01
	3	1.777671E-01	-1.776663E-01	1.793711E-03	-2.500 [illegible]E-01
	4	-3.876021E-03	-3.719287E-03	7.133975E-04	-1.225249E-01
	5	-4.311947E-03	-9.210588E-03	4.623604E-04	-8.148277E-02
	6	-1.894385E-01	2.096134E-01	-1.347073E-03	2.138334E-01
	7	-9.945102E-02	2.144214E-01	-1.904939E-03	3.366811E-01
	8	1.506366E-01	7.021433E-02	-1.427251E-03	3.078993E-01
	9	1.113612E-01	-3.658459E-02	-6.995772E-04	1.969226E-01
	10	3.019120E-02	-1.116286E-01	6.052740E-05	5.544292E-02
	11	-1.777249E-01	-1.633183E-01	1.491486E-03	-2.057940E-01
	12	-1.506469E-01	-1.584399E-01	1.615559E-03	-2.304819E-01
	13	-6.893620E-02	-9.219636E-03	2.358415E-03	-3.951119E-01
	14	-2.160513E-02	1.213305E-01	2.391850E-03	-4.231097E-01
	15	7.736319E-02	2.612042E-01	2.195081E-03	-4.119052E-01
	16	8.595484E-02	2.939280E-01	2.156118E-03	-4.119319E-01
	17	1.289673E-01	3.730781E-01	1.679199E-03	-3.300182E-01
	18	1.506626E-01	3.498281E-01	8.360748E-04	-1.641504E-01
	19	1.517044E-01	2.799162E-01	9.263658E-05	3.071034E-02
	20	1.721199E-01	2.333031E-01	-1.591622E-04	1.004297E-01
	21	1.377038E-01	1.680120E-01	-6.218962E-04	2.029731E-01
	22	6.457829E-02	1.978942E-02	-1.329846E-03	3.753745E-01
	23	-3.436837E-02	-1.584260E-01	-1.787135E-03	4.905953E-01
	24	-5.598545E-02	-1.364218E-01	-1.817854E-03	4.909307E-01
	25	-6.449389E-02	-1.364366E-01	-1.802674E-03	4.827107E-01
	26	-6.883740E-02	-1.305472E-01	-9.421832E-04	2.457172E-01
	27	-4.326033E-02	-2.336011E-02	-4.347668E-05	-7.751519E-03
	28	-3.446205E-02	4.660012E-03	2.503736E-04	-8.956701E-02
	29	-1.725773E-02	4.688031E-02	7.220077E-04	-2.044963E-01
	30	3.433377E-02	1.677620E-01	1.734350E-03	-4.902861E-01
	31	4.292464E-02	2.330005E-01	1.992264E-03	-5.720654E-01
ORBITER2	32	-2.202542E-04	7.055855E-04	5.503262E-01	1.091869E-02
	33	-2.641858E-04	6.523344E-04	5.202855E-01	1.021630E-02
	34	-6.268731E-05	1.176512E-04	2.261988E-02	3.047273E-03
	35	2.186625E-05	-5.618620E-05	-8.654247E-05	2.265756E-04
	36	5.266530E-05	-1.668399E-04	-7.019049E-02	-9.322281E-04
	37	1.054987E-04	-3.182797E-04	-1.402139E-01	-2.790167E-03
	38	1.351361E-04	-3.952710E-04	-1.501545E-01	-3.632785E-03
	39	1.488201E-04	-4.294121E-04	-1.501416E-01	-3.895357E-03
	40	1.500895E-04	-4.953621E-04	-1.400326E-01	-4.674487E-03
	41	2.084651E-04	-5.714733E-04	-6.997579E-02	-4.357468E-03
	42	2.293609E-04	-6.065769E-04	1.202034E-01	-2.628231E-03
	43	2.097239E-04	-6.079704E-04	1.702139E-01	-1.954918E-03
	44	2.140984E-04	-5.237651E-04	5.565246E-01	2.797948E-03
	45	1.844060E-04	-4.562754E-04	3.365480E-01	7.074018E-03
	46	1.669460E-04	-4.311546E-04	9.704959E-01	9.586312E-03
	47	1.557314E-04	-5.242027E-04	9.999998E-01	1.197377E-02
	48	1.589157E-04	-8.951571E-04	6.480669E-01	1.401507E-02
	49	1.640791E-04	-1.163284E-03	4.977353E-01	1.417171E-02
	50	1.574391E-04	-2.032975E-03	-1.565555E-01	1.894382E-02
	51	1.583433E-04	-2.051538E-03	-1.665605E-01	1.870407E-02
	52	1.479899E-04	-2.284057E-03	-3.276814E-01	2.058699E-02
	53	1.242230E-04	-2.612946E-03	-5.093547E-01	2.437967E-02
	54	1.156647E-04	-2.911279E-03	-6.012509E-01	2.643627E-02
SPRINGS (114)	55	2.196643E-04	-5.883363E-04	-7.011541E-02	-4.243001E-03
(51)	56	1.600538E-04	-2.058302E-03	-1.765713E-01	1.855993E-02
(6)	57	-1.240249E-01	2.669261E-01	-1.361610E-03	2.956443E-01
(14)	58	-2.160513E-02	1.213305E-01	2.391850E-03	-4.231097E-01

TABLE II-7-3

(1, 1) MATRIX NASAO (7, 7)

	1	2	3	4
1	9.999999E-01	8.688779E-02	1.064282E-01	3.415843E-02
2	8.688761E-02	9.899994E-01	8.654010E-02	8.482938E-01
3	1.064282E-01	8.654004E-02	1.000001E 00	5.684620E-02
4	3.415846E-02	8.482940E-01	5.684621E-02	1.000000E 00
5	1.327043E-03	6.354020E-04	1.994901E-03	8.761680E-02
6	1.167057E-01	1.197767E-02	6.114777E-03	2.175474E-02
7	1.518517E-01	3.223889E-02	2.165090E-01	2.185233E-02

5	6	7
1.327045E-03	1.167058E-01	1.518517E-01
6.354020E-04	1.197769E-02	3.223889E-02
1.994901E-03	6.114777E-03	2.166090E-01
8.761680E-02	2.175474E-02	2.185229E-02
1.000000E 00	6.277204E-02	8.014855E-04
6.277188E-02	9.999996E-01	3.729792E-03
8.014899E-04	3.729792E-03	9.999988E-01

TABLE 11-8

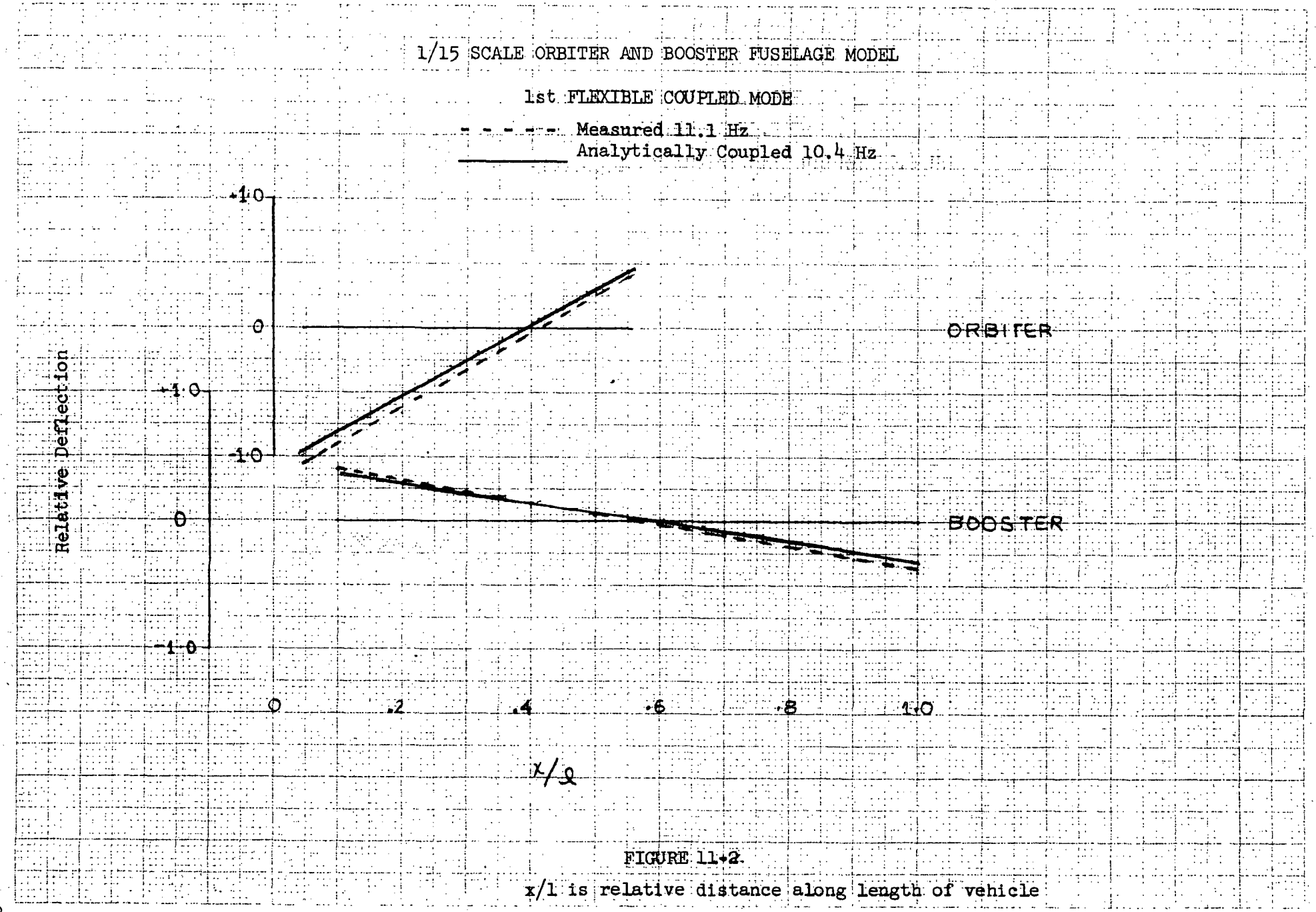

FIGURE 11-2.

x/l is relative distance along length of vehicle

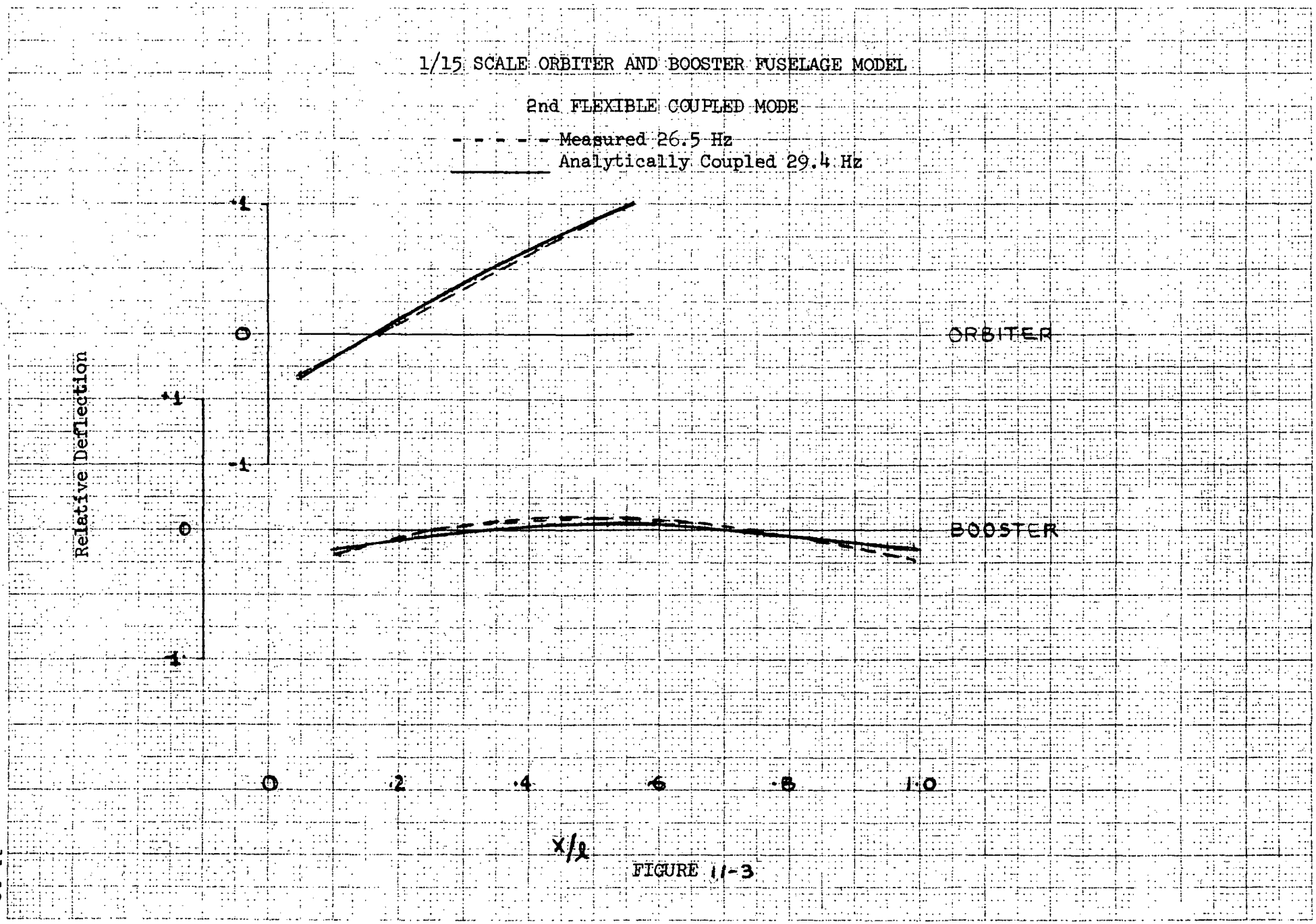
1/15 SCALE ORBITER AND BOOSTER FUSELAGE MODEL
2nd FLEXIBLE COUPLED MODE
Measured 26.5 Hz
Analytically Coupled 29.4 Hz
ORBITER
BOOSTER
Relative Deflection
+1
0
-1
+1
0
-1
0
.2
.4
.6
.8
1.0
X/ℓ

FIGURE 11-3

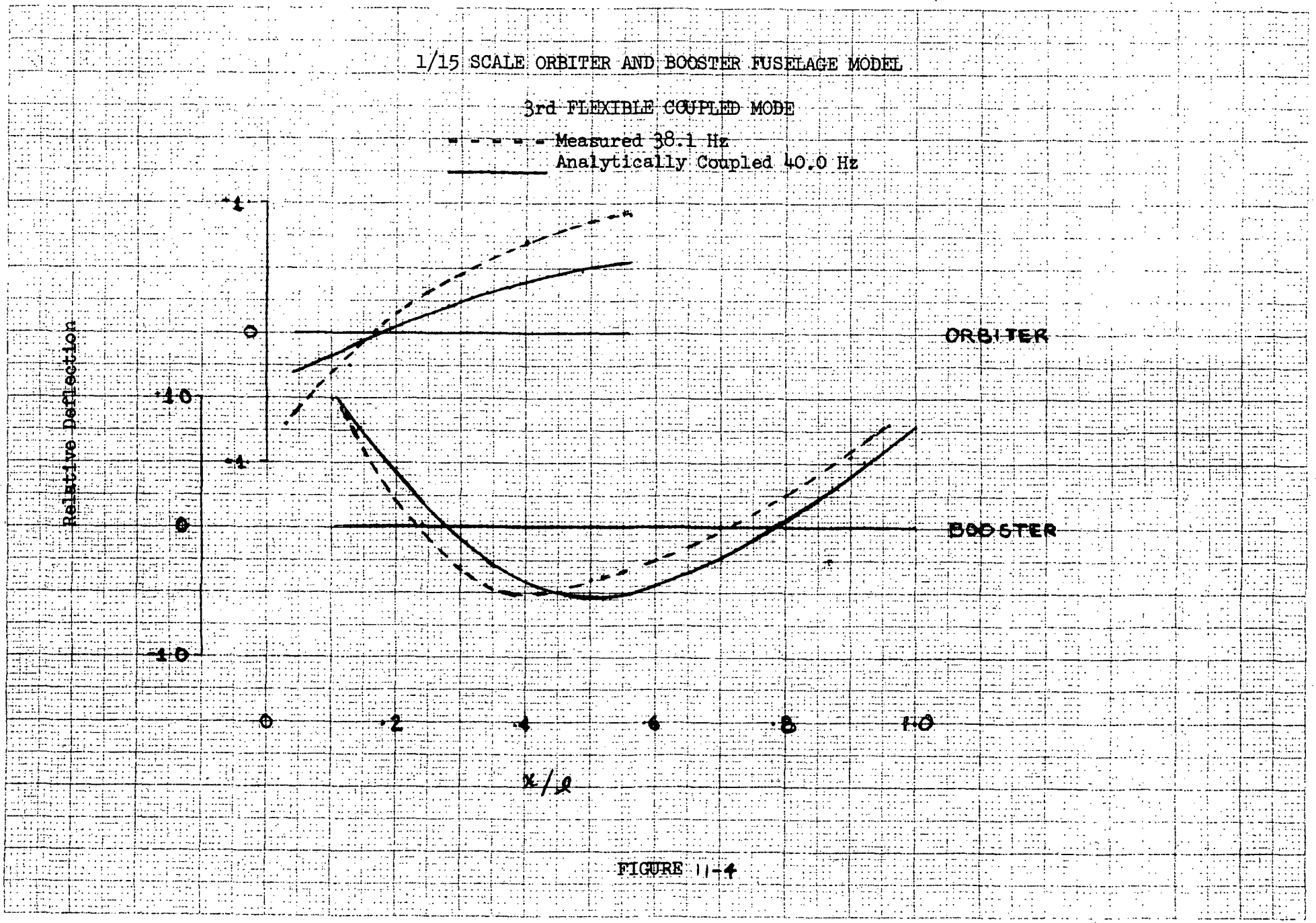
1/15 SCALE ORBITER AND BOOSTER FUSELAGE MODEL
3rd FLEXIBLE COUPLED MODE
- - - - - Measured 38.1 Hz
Analytically Coupled 40.0 Hz
Relative Deflection
.1
0
-.1
.1
0
-.1
ORBITER
BOOSTER
0
.2
.4
.6
.8
1.0
x/ℓ

FIGURE 11-4

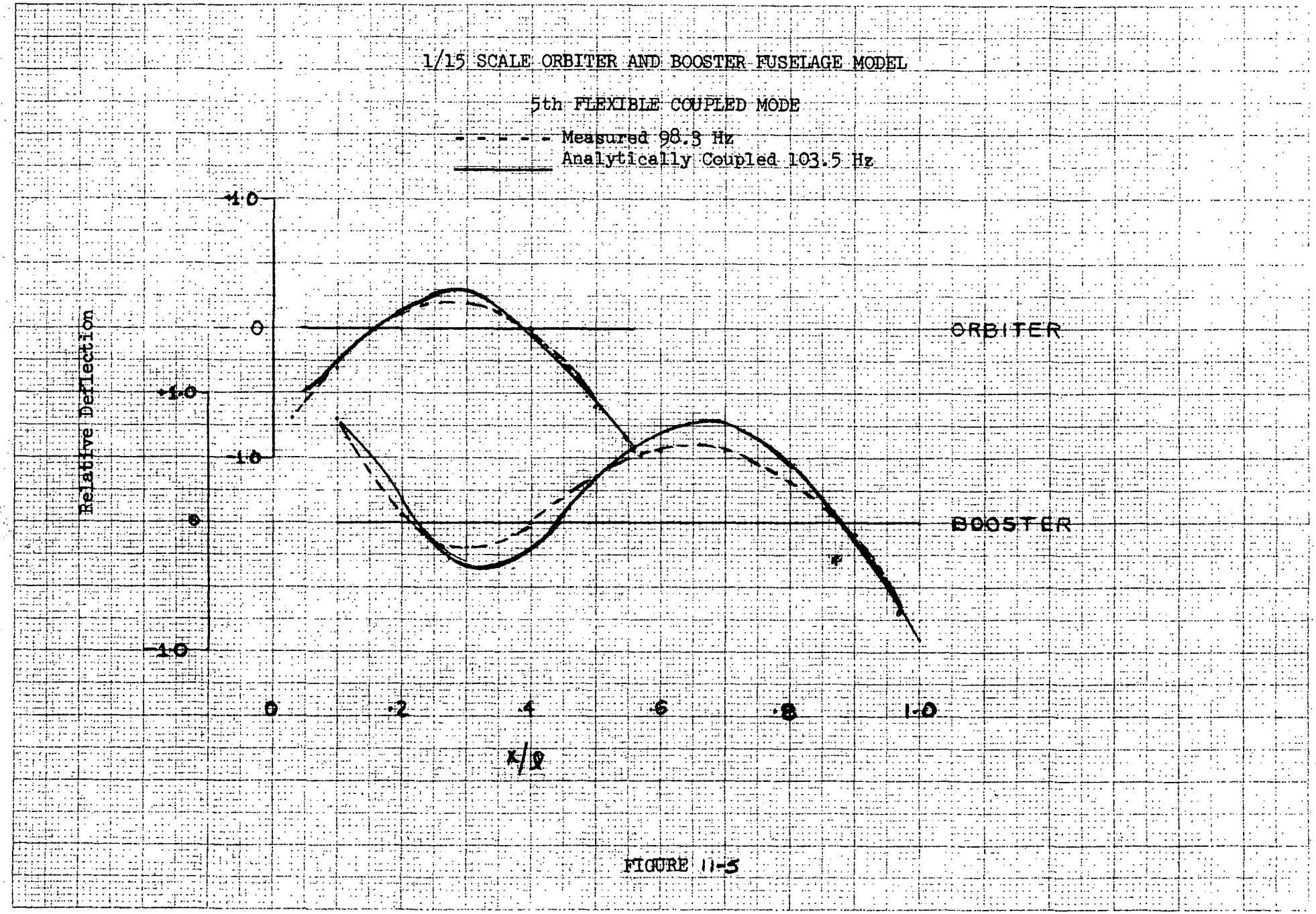
1/15 SCALE ORBITER AND BOOSTER FUSELAGE MODEL
5th FLEXIBLE COUPLED MODE
- - - - - Measured 98.3 Hz
Analytically Coupled 103.5 Hz
Relative Deflection
1.0
0
-1.0
ORBITER
BOOSTER
0
.2
.4
.6
.8
1.0
x/ℓ

FIGURE 11-5

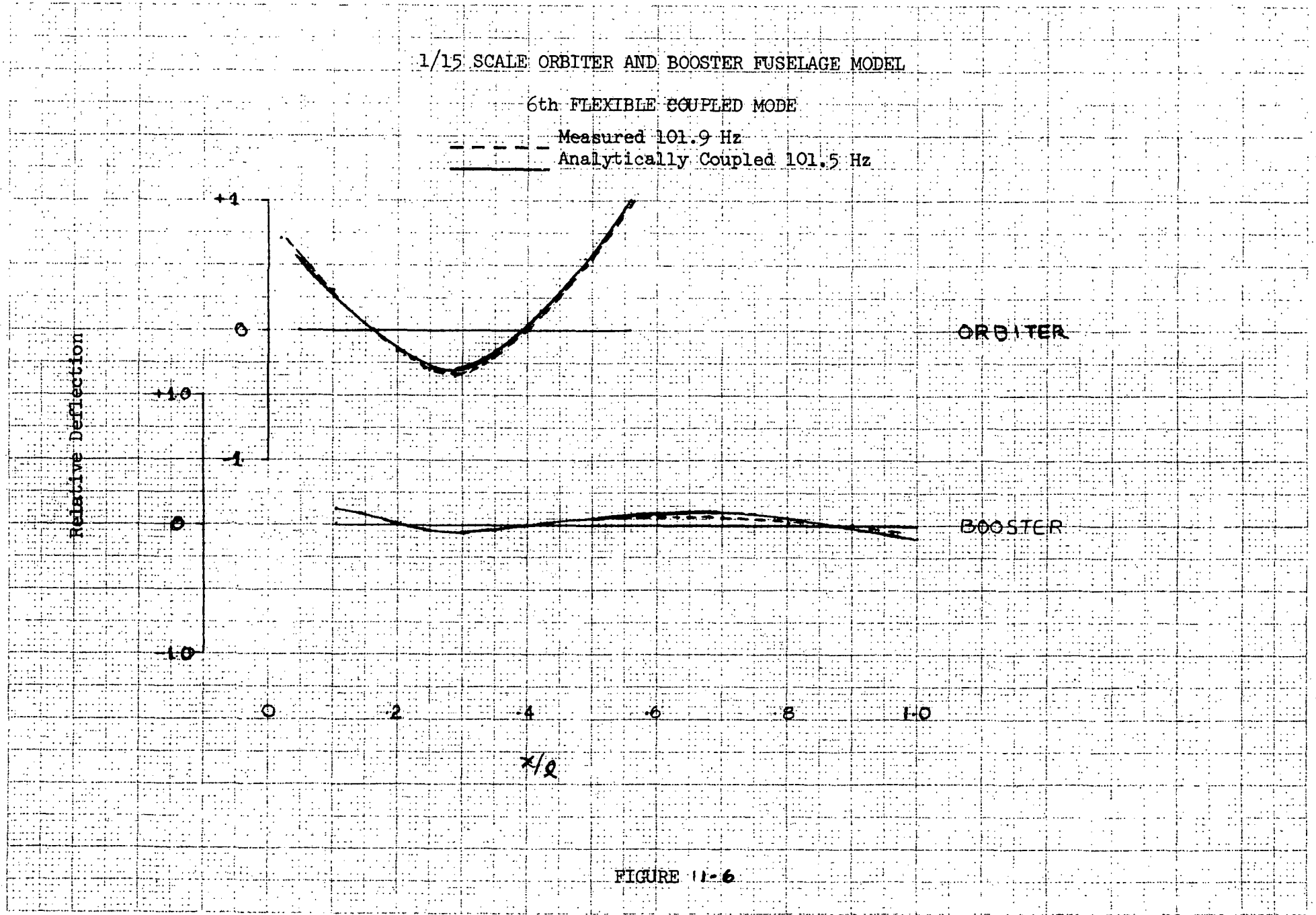
1/15 SCALE ORBITER AND BOOSTER FUSELAGE MODEL
6th FLEXIBLE COUPLED MODE
Measured 101.9 Hz
Analytically Coupled 101.5 Hz
Relative Deflection
+1
0
-1
+1.0
0
-1.0
ORBITER
BOOSTER
0
.2
.4
.6
.8
1.0
x/ℓ

FIGURE 11-6

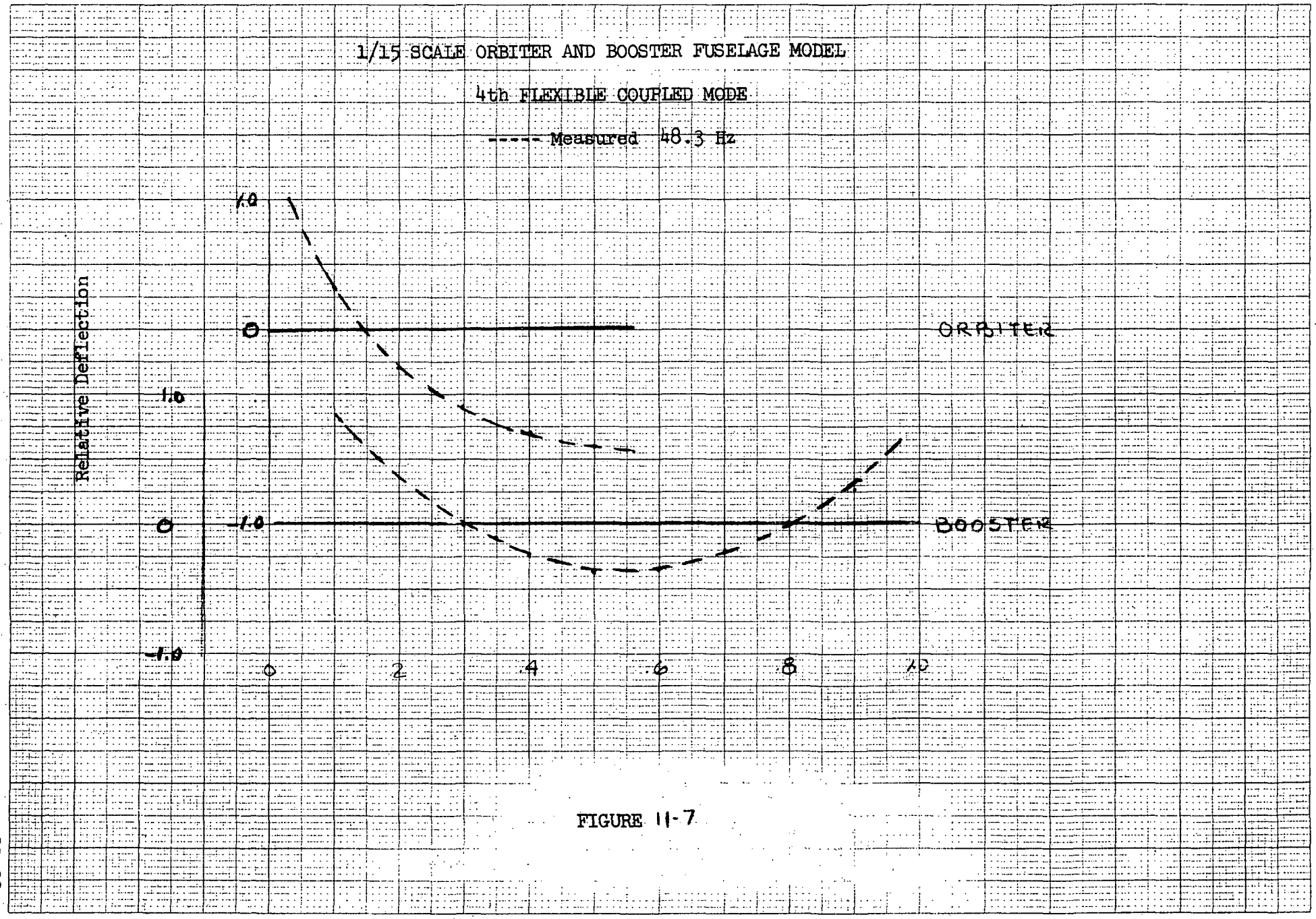

FIGURE 11-7

12. DESIGN OF 1/10 SCALE PRELIMINARY STRUCTURAL DYNAMICS MODEL OF SERIES-BURN SHUTTLE CONFIGURATION

12. DESIGN OF 1/10 SCALE PRELIMINARY MODEL OF SERIES - BURN SHUTTLE CONFIGURATION

12.1 External Configuration and General Arrangement

After the series-burn configuration had been selected as the baseline, Modification 3 to this Task Order was issued to change the remainder of the effort at GAC to study the design of an appropriate structural dynamics model. In particular, fabrication costs and time were to be determined and the details of the propellant storage system were to be studied.

The external configuration of the model is shown schematically on Figure 12-1. The design details studied for the various parts are shown on the drawing numbers called out near each part. These drawings have been previously submitted for NASA review. Reproducible copies of these drawings have been sent to the NASA Langley Research Center Technical Monitor for this task.

A general description of the model construction for the Orbiter, Booster, and HO tank assembly is given in the Stress Analysis Report in Appendix B.

12.2 Details of the Propellant Storage System

The LO_2 tanks were of welded aluminum monocoque design. The HO tank was .032" thick within 1/2" of the welds and chem milled to .016" over the remainder of the surface. The dome was elliptical of .016" thick aluminum. The Y ring was designed as a stepped element with provisions for welding the dome and the cylindrical portion of the tank. The booster LO_2 tank was heavy walled (.1" dome, .167" cylindrical section) aluminum. Simple flat cover plates were used in place of upper domes on both tanks.

The LH_2 tank was a thin walled riveted tank with a .008" thick aft dome and a cylindrical section which was .002" thick for the 120 degree segment nearest the orbiter and .016" elsewhere. In order to stabilize this structure against 1.5 g limit handling loads, rings were added at about 2 1/2" pitch. The Y ring was machined in a stepped section.

The RP-1 tank at the base of the booster consisted of an aft elliptical end dome of .113" thickness, a machined Y ring, a cylindrical section of .139" thickness, a forward machined Y ring, and a forward dome with access through an elliptical cover plate. This tank was also seam welded of aluminum.

12.3 Intertank Structure

The skirt between the LO_2 and LH_2 HO tanks was .15" thick skin stiffened by angle rings. At the center of the skirt two back-to-back channels formed a heavy frame with the fittings for the orbiter attachment fastened between them. A similar arrangement was used inside the LH_2 tank as a support for the aft fitting from the orbiter. The members between orbiter and HO tank were simple tubular elements. The skirt between the HO tank and the booster was of similar ring stiffened .015" thick skin. The aft thrust structure on the booster was a conical element with 12 radial bulkheads meeting in a hexagonal shaped cylinder in the center.

12.4 Orbiter

The orbiter mid fuselage was basically series of U shaped frames with corner longerons along the top and bottom covered by aluminum skin. The skins were stiffened by intermediate frames every 2" to prevent buckling. The orbiter engine support structure consisted of full bulkheads connected by longerons. The wings consisted of four beams carried through the fuselage covered by flat skins.

12.5 Budgetary Cost

A budgetary cost estimate was performed by a member of the manufacturing group normally making shop estimates at Grumman. Preliminary drawings AD604 through 611 defining the HO tank and booster were used. The 1970 rates were applied including G&A costs but not including profit. Results were $55,380 for the HO tank and $64,200 for the booster. The cost of the orbiter was not estimated. Fabrication time was estimated as 4 months from go-ahead.

12.6 Utilization of Designs

The design work on the orbiter and the external tanks completed in this contract was used subsequently as the basis for the design of a 1/8 scale structural dynamics model of the parallel burn shuttle using solid rocket boosters.

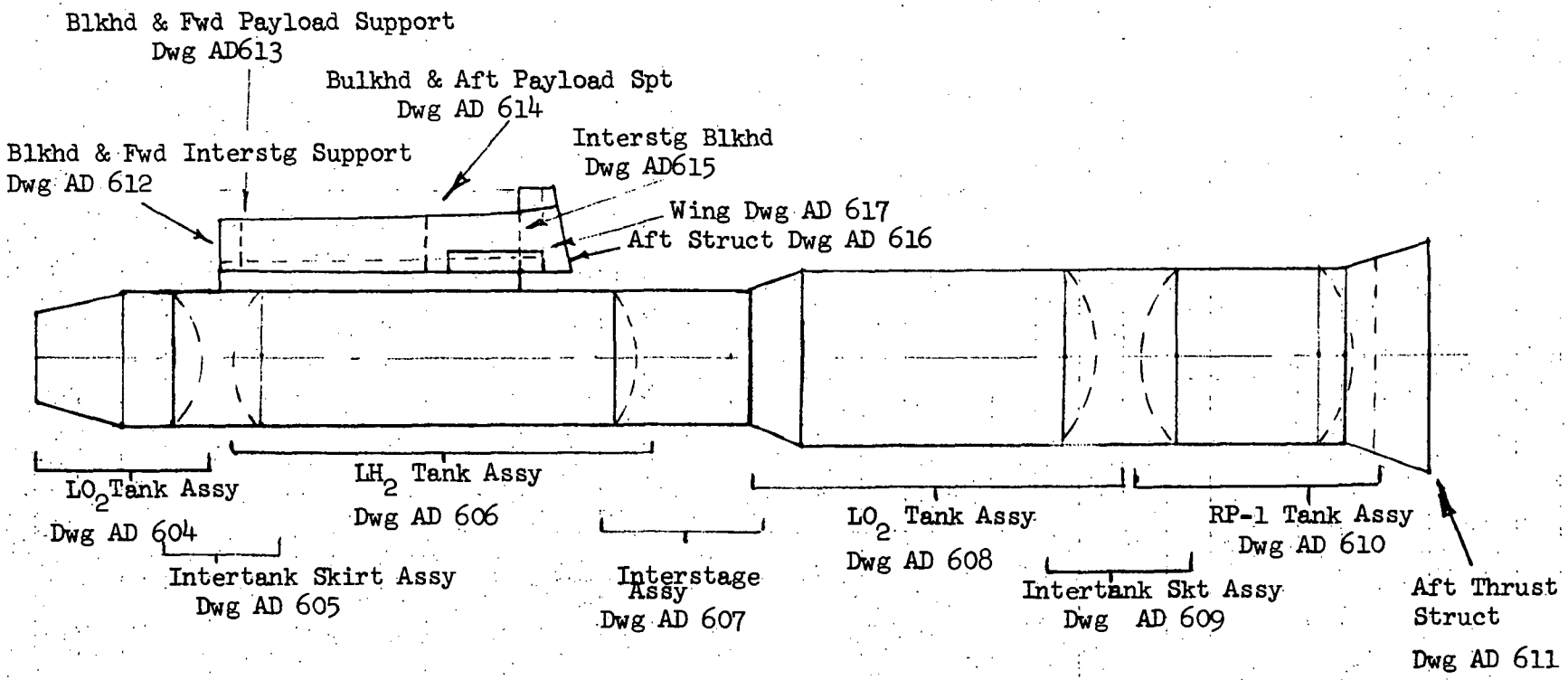

SCHEMATIC OF PRELIMINARY MODEL OF SERIES-BURN SHUTTLE CONFIGURATION

Figure 12-1

REFERENCES

REFERENCES

2-1 Grumman Aerospace Corporation letter 552-55L-214, 30 June 1972, M. Bernstein to D. H. Mitchell (including 7 unnumbered drawings).

2-2 Rubin, S., "Suppression of POGO Instabilities on Space Shuttle," Aerospace Corporation, Space Shuttle Dynamics and Aeroelasticity Working Group, NASA Ames Research Center, November 1971.

2-3 Palmer, J. H. and Asher, G. W., "Calculation of Axisymmetric Longitudinal Modes for Fluid-Elastic Tank-Ullage Gas Systems and Comparison with Model Test Results," Boeing Company, AIAA Symposium on Structural Dynamics and Aeroelasticity, Boston, Massachusetts, September 1965.

2-4 Grimes, P. J., McTigue, L. D. and Riley, G. F., "Advancements in Structural Dynamic Technology Resulting from Saturn V Programs," Boeing Company NASA CR-1540, June 1970.

2-5 Ujihara, B. H. and Guyan, R. J., "Hydroelastic Properties of a Full Scale SII LOX Tank," NAR, AIAA Paper 72-173, presented at AIAA 10th Aerospace Sciences Meeting, January 1972, San Diego, California.

2-6 Jaszlics, I. J. and Morosow, G., "Dynamic Testing of a 20% Scale Model of the Titan III," AIAA Symposium on Structural Dynamics and Aeroelasticity, Boston, Massachusetts, September 1965.

2-7 Leadbetter, S. A., Leonard, H. W. and Brock, Jr., E. J., "Design and Fabrication Considerations for a 1/10 Scale Replica Model of the Apollo/Saturn V," NASA TN D-4138, October 1967.

2-8 Guyan, R. J., Ujihara, B. H., Welch, P. W., "Hydroelastic Analysis of Axisymmetric Systems by a Finite Element Method." AFFDL TR-68-150 WPAFB, October 1968.

2-9 Winje, R. A., Galef, A. E., "Guidelines for POGO Avoidance Based on Titan and Saturn Experience," TRW Report 17618-6001-RO-00, 24 December 1970. Prepared for NASA MSC under NAS 9-8166.

4-1 Daniels, G. E., "Terrestrial Environment (Climatic) Criteria Guidelines for Use in Space Vehicles, 1969 Revision, "NASA MSFC Report TMX 53872, 8 September 1969.

4-2 Houbolt, J. C., Steiner, R., and Pratt, K. G., "Dynamic Response of Airplanes to Atmospheric Turbulence Including Flight Data on Input and Response," NASA TR R-199, June 1964, pp. 20, 21.

4-3 Templin, R. J., Wind Tunnel Simulation of Ground Wind Shear and Turbulence Spectra with Possible Application to Space Shuttle Launch Problems, Space Transportation System Technology Symposium NASA TMX 52876, Vol. II 1970, pp. 161-175.

5-1 Holblit, F. M., et al., "Development of a Power-Spectral Gust Design Procedure for Civil Aircraft," Federal Aviation Agency Report No. FAA-ADS-53, January 1966.

5-2 "Alternate Space Shuttle Concepts Study, H3T Orbiter, Preliminary Assessment of Structure and Structural Dynamics, Appendix D, Dynamic Analysis, Modal and Response Results," Grumman Report B26100RP105 July 1971.

5-3 "Alternate Space Shuttle Concepts Midterm Report," Appendix A, Structural Descriptions, Loads, and Analysis, Grumman Report B35-43RP-5, 31 December 1970.

11-1 Leadbetter, S. A., and Kiefling, L. A., "Recent Studies of Space Shuttle Multibody Dynamics," NASA Space Shuttle Technology Conference NASA TMX-2274 Vol. III, April 1971.

11-2 Thornton, E. A., "Vibration Analysis of a 1/15 Scale Dynamic Model of a Space Shuttle Configuration," NASA CR111984, 1971.

11-3 Fralich, R. W., Green, C. E., Rheinfurth, M. H. "Dynamic Analysis for Shuttle Design Verification," NASA TMX 2570, July 1972.

A-1 George, D., Kellar, V., Smedfjeld, J. B., Schriro, G. R., "An Engineering Evaluation of Airplane Gust Load Analysis Methods Volume II - Calculation Procedure," Grumman Report ADR 06-14-63.2, November 1963.

APPENDIX A

A. GUST RESPONSE ANALYSIS

A.1 Description

In order to provide representative quantitative data on the response of a shuttle type of vehicle to gusts, an extended and improved version of the aircraft program described in Reference (A-1) was utilized. In this program, vehicle motion is described by a linear, multi-degree-of-freedom system of forced response equations in terms of rigid and flexible normal modes. The effect of control laws in deflecting the engine due to rotation and rotation rate is included in the two rigid-mode equations. Additional differential equations, derived from an indicial formulation of the unsteady aerodynamics, are used to define the generalized aerodynamic forces due to motion and gust. The program can consider two symmetric rigid-body modes (vertical translation and pitch) and up to 8 symmetric vibration modes of the wings and fuselages. In order to accommodate the 22 flexible modes which appeared significant, the program was run three times, with the first flexible mode appearing in all three runs. Although this is not rigorously correct due to the elimination of the aerodynamic coupling between many of the modes, it is considered acceptable for this application. The modes used in each case are as follows:

Run 1 (15 July 1971)		Run 2 (23 July 1971)		Run 3 (29 July 1971)	
Mode No.	Freq. (Rad/Sec)	Mode No.	Freq. (Rad/Sec)	Mode No.	Freq. (Rad/Sec)
1	9.23	1	9.23	1	9.23
2	9.84	6	15.77	3	13.54
9	18.78	7	17.14	4	14.52
11	20.25	10	19.26	5	14.89
12	20.59	21	34.99	8	18.25
17	27.46	23	39.12	13	22.28
22	38.52	29	48.78	14	23.81
24	40.51	30	50.23	18	29.07

In formulating the generalized forces, strip theory, appropriately modified to yield experimental complete-vehicle steady-state stability derivatives, was used. The orbiter wing and booster wing were each represented by 6 panels per side, with the aerodynamic loading on the remainder of the two vehicles being assumed to act on center section panels of each of the two wings. Values of the coefficients used are shown on Table A-1.

The shuttle configuration used in the analysis was an external hydrogen tank orbiter on a heat sink booster designated H3T, as described in Reference (5-2). The vehicle was assumed in steady flight at Mach 1.05 at 25,000 feet.

The lowest 30 symmetric modes for the ascent configuration corresponding to maximum $q\alpha$ were calculated, and the 22 of these which came closest to satisfying the criteria of Section 6.2 were used in the gust response analysis. The general characteristics of these modes are described in Table A-2. Structural damping was assumed as 2 percent in each mode, after initial analyses showed that the aerodynamic damping in some modes could be significantly lower.

The turbulence was represented by the boost spectrum shown in NASA TM X-53973, Section 1.3.2.

A.2 Results

The analysis proceeds by calculating the response to a 1 ft/sec sinusoidal gust velocity applied at various frequencies in the range of interest. The transfer function obtained is then used in calculating the response to the spectrum representing the turbulence. For each mode and coordinate therefore both a frequency response to a sinusoidal input and a power spectral density response is determined.

The generalized force frequency response illustrates the effects of unsteady aerodynamics including wing sweep and transport time delays between the two surfaces. The power spectrum of the generalized force exhibits a single low frequency peak at about 1 1/2 radians per second, reflecting the nature of the turbulence which peaks at about 2 radians per second and then drops off at about 20 db per decade. These characteristics are shown typically on Figures A-1 to A-4.

The modal accelerations in most flexible modes (Figures A-6 and A-8) show responses typical of uncoupled single degree of freedom systems; however, some coupling between modes is evident in the rigid body translation plots in Figure A-5 and in one higher flexible mode shown in Figure A-7. The integrated response to the applied turbulent spectrum yields the rms values shown in Table A-3. It may be noted that both the force and acceleration values remain significantly high even among the higher modes.

The important feature in determining the significance of the higher modes is the contribution of such modes to the rms response at various locations. Responses were calculated for 5 locations in the orbiter and 5 in the booster. These are summarized in Table A-4. An estimate of the peak acceleration may be obtained by multiplying the rms values shown by 3. The largest acceleration in the orbiter coordinates other than the wing tip, occurs at the LH_2 tank and is equivalent to 0.45g. The crew compartment response is somewhat lower (0.4g). Responses in the booster are all lower. The contribution of each mode to this rms response may be determined by comparing the energy for the various modes in the power spectrum response at each coordinate. As an example Figures A-9 through A-11 are the accelerations at coordinate 60, the orbiter payload. Figure A-9 includes the 8 flexible modes used for Run 1 on 15 July, whereas the next two figures include the flexible modes used in Runs 2 and 3 on 23 and 29 July, respectively. The largest portion of the energy under the power spectrum curve in Figure A-9 is at 2 1/2 radians/sec., the rigid body (RB) mode. The energy near 38 radians/sec, the 22nd mode, is almost as high, and the mode at 20 radians/second, the 12th mode, also contributes significantly. Figure A-10 indicates that the flexible modes selected for the 23 July run were more significant, in particular, both the 21st and 23rd modes near 35 radians/sec encompassed much more energy than the rigid body mode, and the 10th and 17 radians/sec and the 29th at 49 radians/sec are both marginally significant. The power spectrum curve on Figure A-11 indicates that none of the flexible body modes used in the 29 July run were as significant as the rigid body (RB) mode.

Reviewing the power spectrum curves at other coordinates, it can be noted that the first flexible mode at 9 radians/sec is most significant for the remainder of the orbiter locations, except for the crew compartment (57) as shown in Figure A-16, where the 21st mode contains more energy. Coordinate 126, the booster crew compartment, responded in the 18 mode at 29 radians/second to a greater extent than in the RB mode.

Response at each coordinate were reviewed in a similar manner and the results summarized as shown on Table 6-2 on page 6-5.

Table A-1

Distribution of Lift Curve Slope Coefficients

Panel No.	Orbiter		Booster	
	Width (in.)	C_{L_α}	Width (in.)	C_{L_α}
1	185	1.83	190	4.09
2	80	2.43	200	4.35
3	90	2.61	200	4.51
4	80	2.80	180	4.83
5	80	3.00	200	5.10
6	130	2.58	200	3.43

NOTE: 1. The panel 1 values represent the orbiter fuselage and the booster fuselage and horizontal tail.

2. The integrated lift and moment curve slopes of the combined orbiter and booster are $C_{L_\alpha} = 6.55$ and $C_{M_\alpha} = 1.49$ compared with 6.65 and 1.77 estimated from wind tunnel model data on somewhat similar models.

Table A-2

Summary of H3T Max Qα Mode Patterns

Mode No.	Freq. Hz	Fuselage		Wing		Hor. Tail Booster
		Booster	Orbiter	Booster	Orbiter	
1	1.48		1st Bending	1st Bending	Pitch	
2	1.57			1st Bending		
3	2.16	Pitch, Fwd	1st Bending, Fwd	1st Bending, Fwd	Down	
4	2.31	Pitch				
5	2.37	Fwd & Pitch	1st Bending & Pitch			
6	2.51	Pitch	1st Bending	1st Bending	1st Bending	1st Bending
7	2.73	1st Bending	1st Bending		1st Bending	1st Bending
8	2.90	Pitch	1st Bending			1st Bending
9	2.99				1st Bending	1st Bending
10	3.06				1st Bending & Pitch	1st Bending
11	3.22		1st Bending	1st Fore & Aft	1st Bending & Pitch	1st Bending
12	3.28			1st Fore & Aft	1st Bending & Pitch	1st Bending
13	3.55		1st Bending		1st Bending & Pitch	1st Bending
14	3.79		2nd Bending		1st Torsion & Bending	
15	3.92			1st Fore & Aft		
16	4.13					
17	4.37	1st Bending	1st F & A, 2nd Bending	2nd Bending, 1st F & A	2nd Torsion, 1st Bending	1st F & A, 2nd Bending
18	4.63	1st Bending	2nd Bending	2nd Bending	2nd Torsion	1st F & A, 2nd Bending

TABLE A-2

CONTINUED

MODE NO.	FREQ. HZ	FUSELAGE		WING		HOR. TAIL
		BOOSTER	ORBITER	BOOSTER	ORBITER	BOOSTER
19	4.99	Rigid F & A	1st F & A	2nd F & A	2nd Bending, 1st Torsion	1st F & A
20	5.42		1st F & A			1st F & A
21	5.57	1st Bending	1st F & A, 2nd Bending	2nd Bending	2nd Bending, 1st Torsion	1st F & A, 2nd Bending
22	6.13	Rigid F & A	2nd Bending	2nd Bending	2nd Bending, 1st Torsion	1st F & A
23	6.22	1st Axial, 1st Bending	1st F & A, 1st Bending	2nd Bending	2nd Bending, 1st Torsion	1st F & A
24	6.45	Rigid F & A	1st F & A, 1st Bending	2nd Bending	2nd Bending, 2nd Torsion	1st F & A
25	7.07					
26	7.33		1st F & A		2nd Bending, 2nd Torsion	

TABLE A-2 (CONT'D)

SUMMARY OF H3T MAX Qα MODE PATTERNS

MODE NO.	FIN		BOOST FLUID		ORB FLUID		ORBITER TANKS	
	BOOSTER	ORBITER	LO_2	LH_2	LO_2	LH_2	LO_2	LH_2
1		Pitch				Fwd		Fwd & Pitch
2								
3	Pitch	Pitch	Aft	Fwd	Fwd	Fwd	Fwd, Up, 1st Bending	Fwd & Down
4		Pitch					1st Bending Sideward	Fwd & Pitch
5		Pitch	Aft	Fwd	Fwd		Fwd & Pitch	Pitch
6	Pitch	Pitch		Fwd	Fwd	Aft	Fwd & 1st Bending	Pitch & 1st Bending, Sideward
7	Pitch	Pitch				Fwd	Fwd & 1st Bending	Pitch
8		Pitch				Aft		Aft & 1st Bending
9		Pitch						
10		Pitch						
11		Pitch		Aft			Pitch	1st Bending
12	Pitch	Pitch		Fwd	Aft			1st Bending
13	Pitch	Pitch			Fwd	Fwd		Fwd & Pitch & 1st Bending Sideward
14	Pitch	Pitch		Fwd	Aft	Aft		1st Bending
15				Fwd				
16								
17	Pitch	1st Fore & Aft			Aft	Aft	1st Bending	1st Bending & Pitch
18				Aft			1st Bending & Pitch	1st Bending & Pitch
19	Pitch & 1st F & A	1st F & A		Aft	Aft	Aft		1st Bending

TABLE A-2

CONTINUED

MODE NO.	FIN		BOOST FLUID		ORB FLUID		ORBITER TANKS	
	BOOSTER	ORBITER	LO_2	LH_2	LO_2	LH_2	LO_2	LH_2
20								
21	Pitch & 1st F & A	Pitch				Fwd	1st Bending & Pitch	1st Bending & Pitch
22		1st F & A						1st Bending & Pitch
23		1st F & A		Aft				
24		Plunge						2nd Bending
25							1st Bending & Yaw	2nd Bending
26		Pitch						1st Bending & Pitch

Table A-3

Mode	Generalized Force RMS lbs.	Generalized Acceleration RMS ft/sec^2
Rigid Translation	69,430	1.09
Rigid Rotation	9,186	.52
1 (1.47 Hz)	9,288	24.23
2 (1.57 Hz)	11,370	21.96
3 (2.16 Hz)	12,080	1.15
4 (2.31 Hz)	119	.12
5 (2.37 Hz)	1,371	1.49
6 (2.51 Hz)	8,584	3.39
7 (2.73 Hz)	5,335	6.75
8 (2.90 Hz)	517	2.06
9 (2.99 Hz)	3,003	17.13
10 (3.06 Hz)	1,375	8.34
11 (3.22 Hz)	4,674	8.42
12 (3.28 Hz)	1,350	2.43
13 (3.54 Hz)	780	.51
14 (3.79 Hz)	248	1.47
17 (4.37 Hz)	5,153	1.36
18 (4.63 Hz)	4,460	3.87
21 (5.57 Hz)	8,661	6.97
22 (6.13 Hz)	10,680	8.63
23 (6.22 Hz)	11,430	4.58
24 (6.45 Hz)	2,350	3.05
29 (7.76 Hz)	734	2.95
30 (7.99 Hz)	4,013	12.18

TABLE A-4

RESPONSE OF H3T TO BOOST TURBULENCE

Location		RMS Response (ft/sec^2)		
Description	Coord.	Run 1 (15 July)	Run 2 (23 July)	Run 3 (29 July)
Orbiter:				
LO_2 Tank Z	39	2.00	2.67	3.05
Crew Compt Z	57	2.95	4.27	3.22
Payload Z	60	2.61	2.69	1.35
LH_2 Tank Z	84	3.37	4.71	3.71
Wing Tip Z	110	21.12	13.58	11.20
Booster:				
Crew Compt Z	126	2.19	2.72	2.99
LH_2 Tank Z	136	1.62	1.90	1.81
LO_2 Tank Z	150	1.06	.95	.94
Wing Tip Z	173	2.51	6.61	4.49
Engine Z	196	1.89	2.23	2.03

JUDSON BIGELOW INC. CHART NO. 02 CA

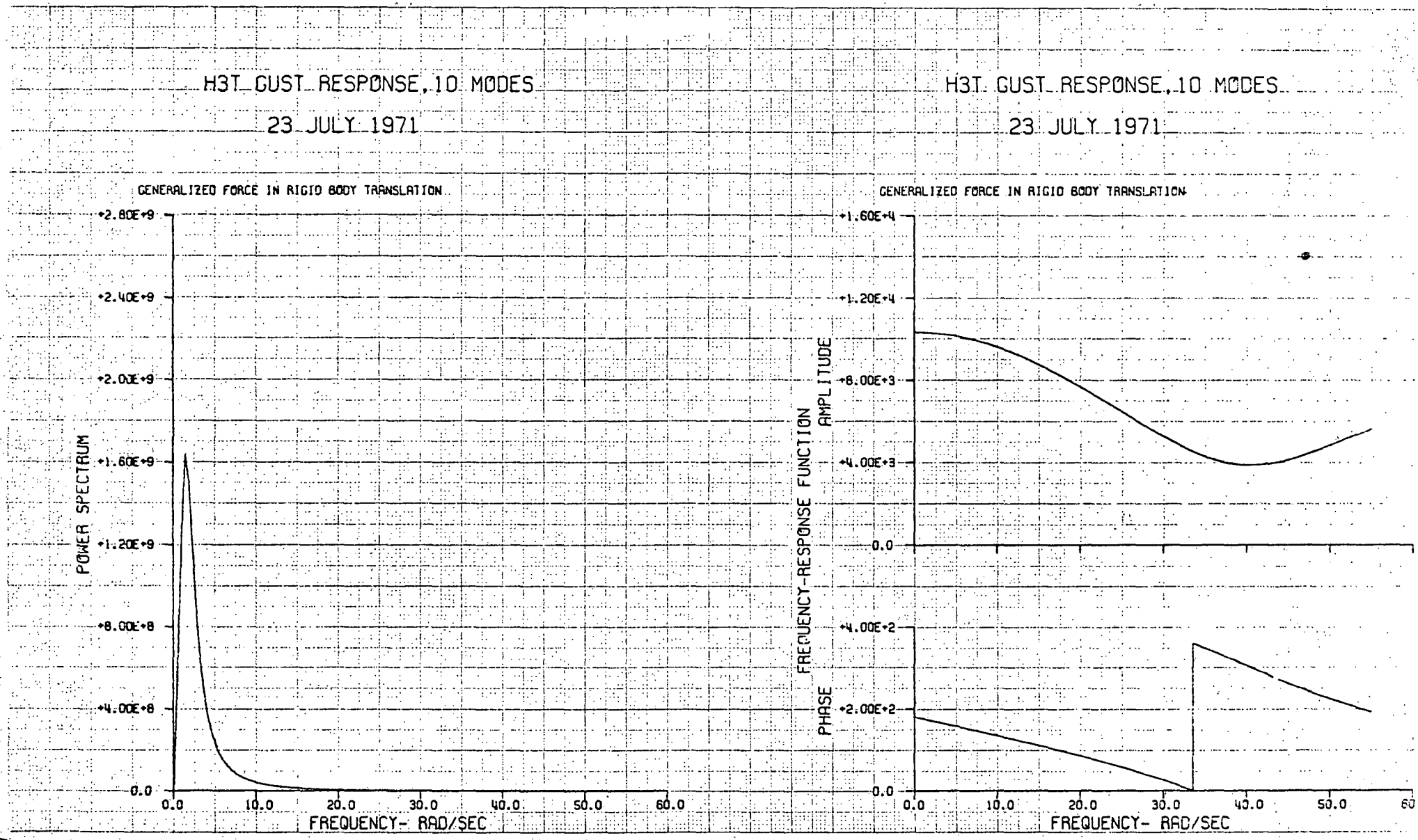

FIGURE A-1

JUDSON BIGELOW INC. - CHART NO. 02 CA

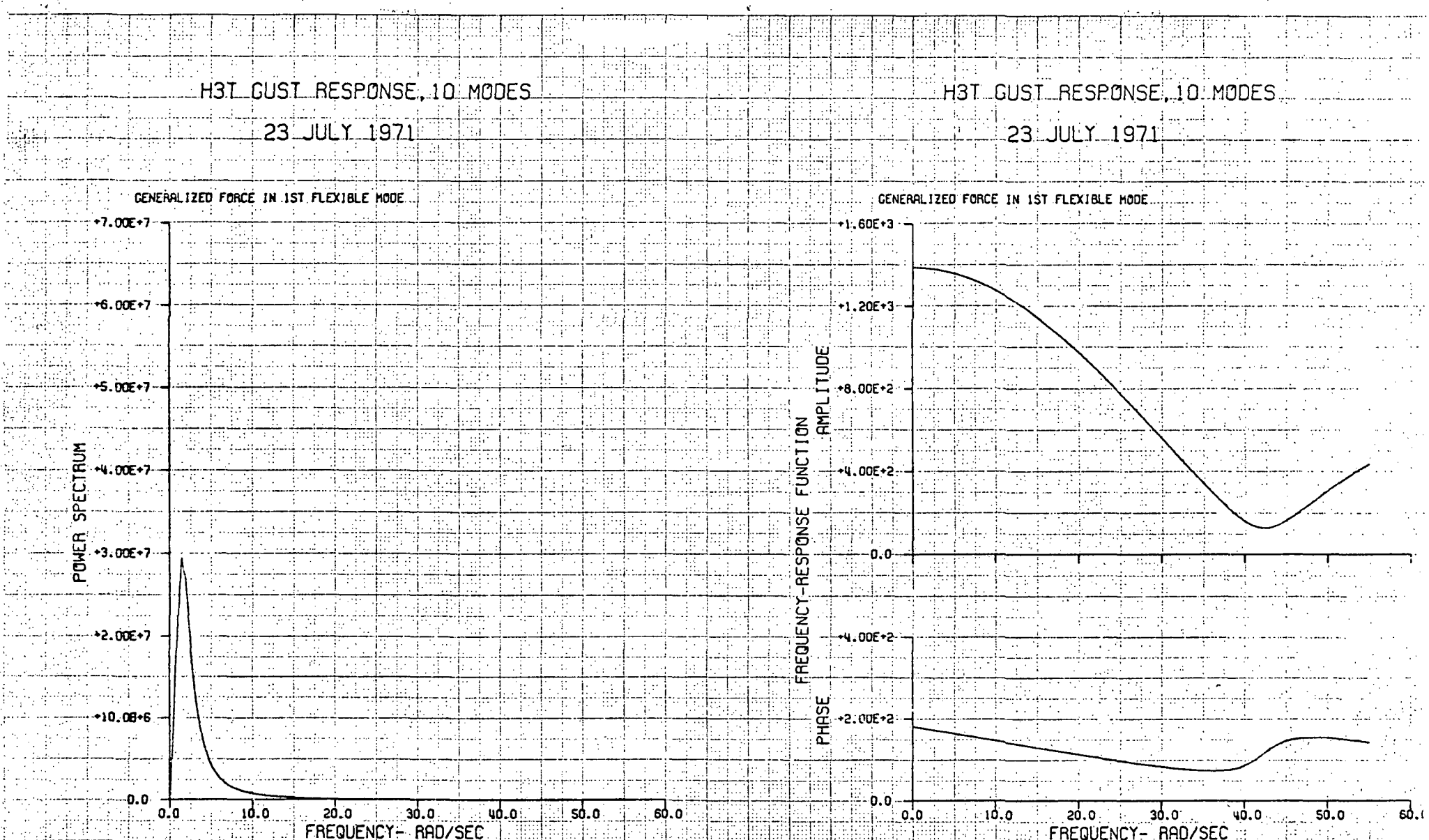

FIGURE A-2

JUDSON BIGELOW INC. CHART NO. 02 CA

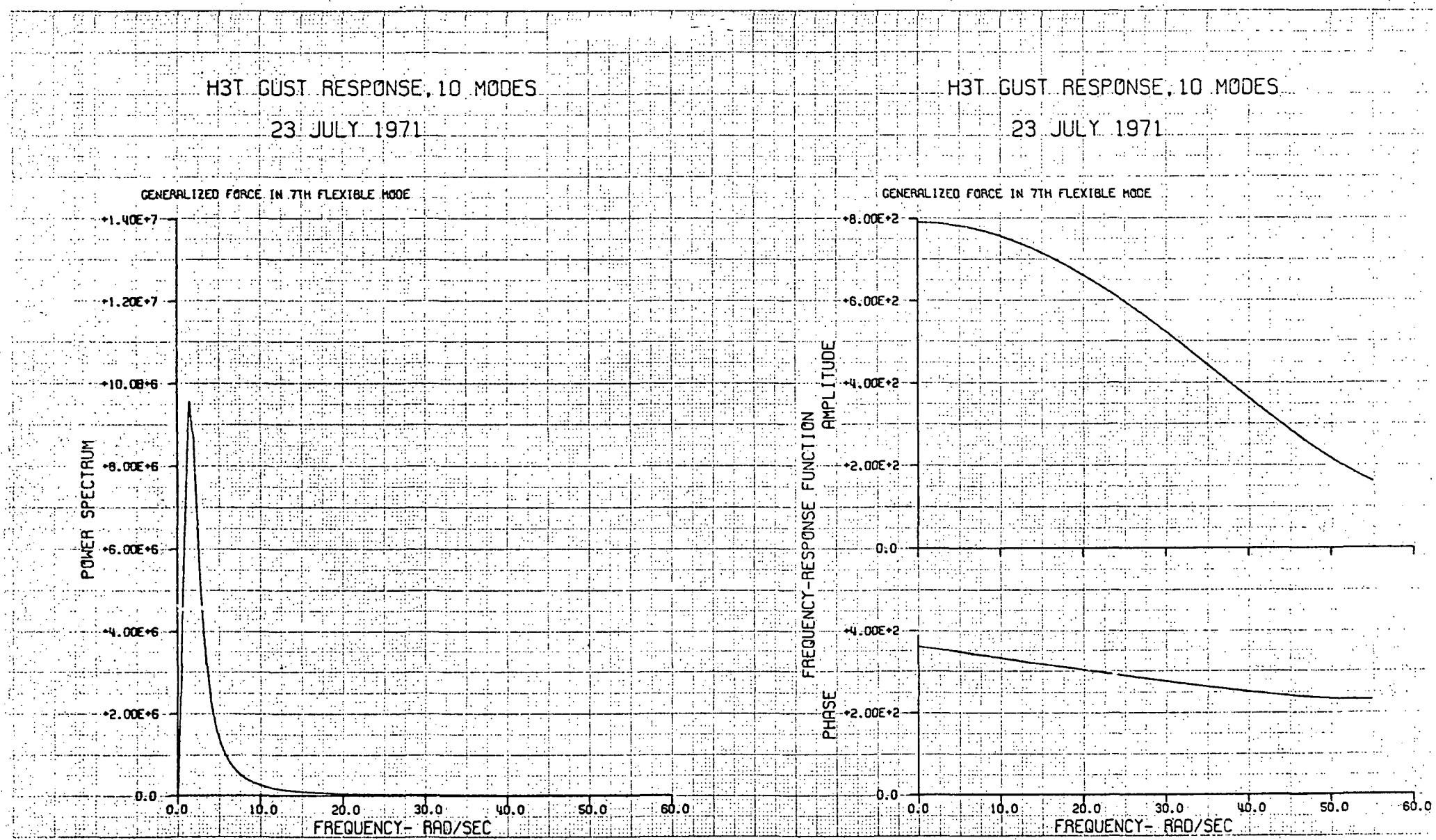

FIGURE A-3

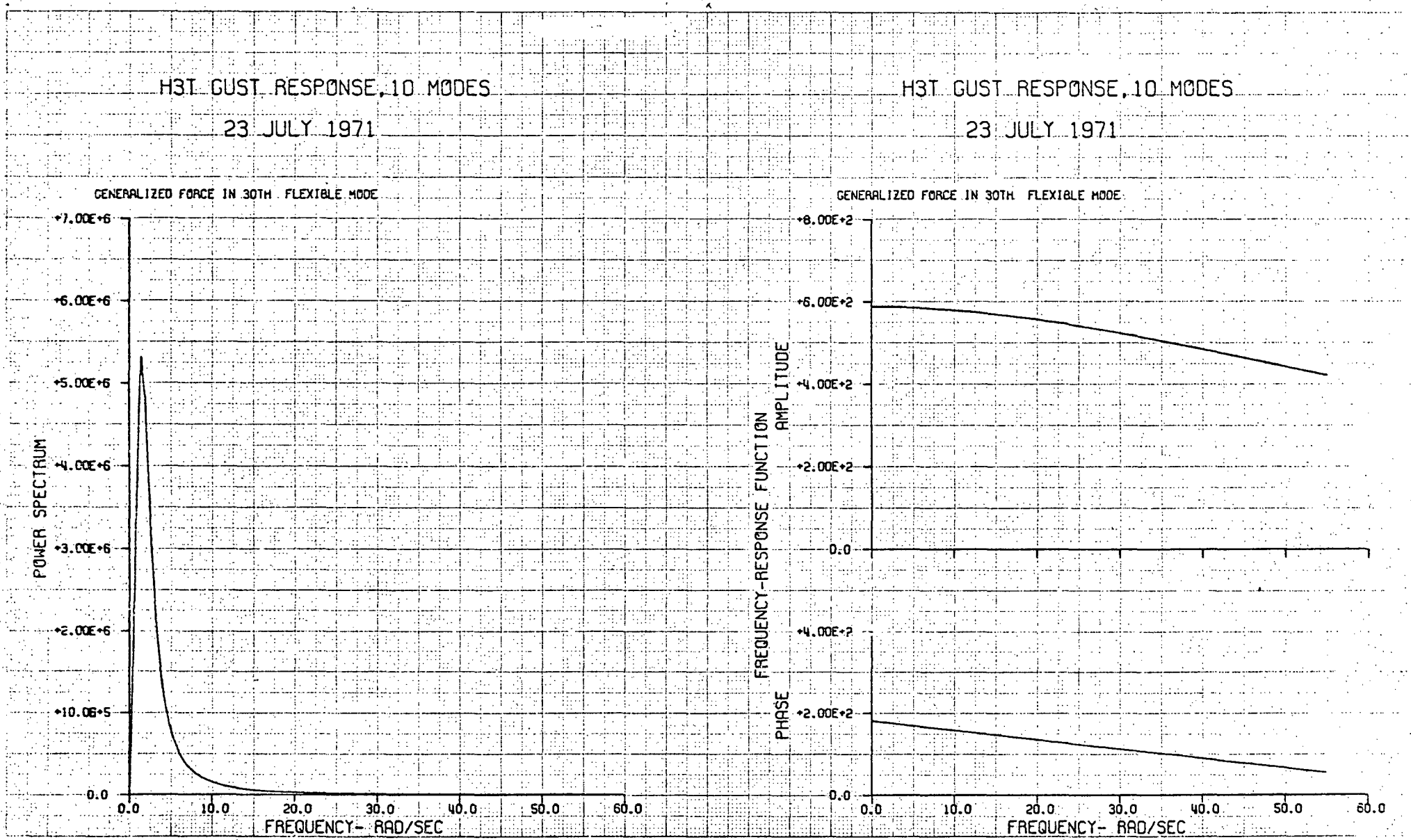
H3T GUST RESPONSE, 10 MODES
23 JULY 1971
GENERALIZED FORCE IN 30TH FLEXIBLE MODE
POWER SPECTRUM
+7.00E+6
+6.00E+6
+5.00E+6
+4.00E+6
+3.00E+6
+2.00E+6
+10.0E+5
0.0
0.0
10.0
20.0
30.0
40.0
50.0
60.0
FREQUENCY- RAD/SEC
H3T GUST RESPONSE, 10 MODES
23 JULY 1971
GENERALIZED FORCE IN 30TH FLEXIBLE MODE
FREQUENCY-RESPONSE FUNCTION
AMPLITUDE
+8.00E+2
+6.00E+2
+4.00E+2
+2.00E+2
0.0
PHASE
+4.00E+2
+2.00E+2
0.0
0.0
10.0
20.0
30.0
40.0
50.0
60.0
FREQUENCY- RAD/SEC

FIGURE A-4

JUDSON BIGELOW INC. CHART NO. 02 CA

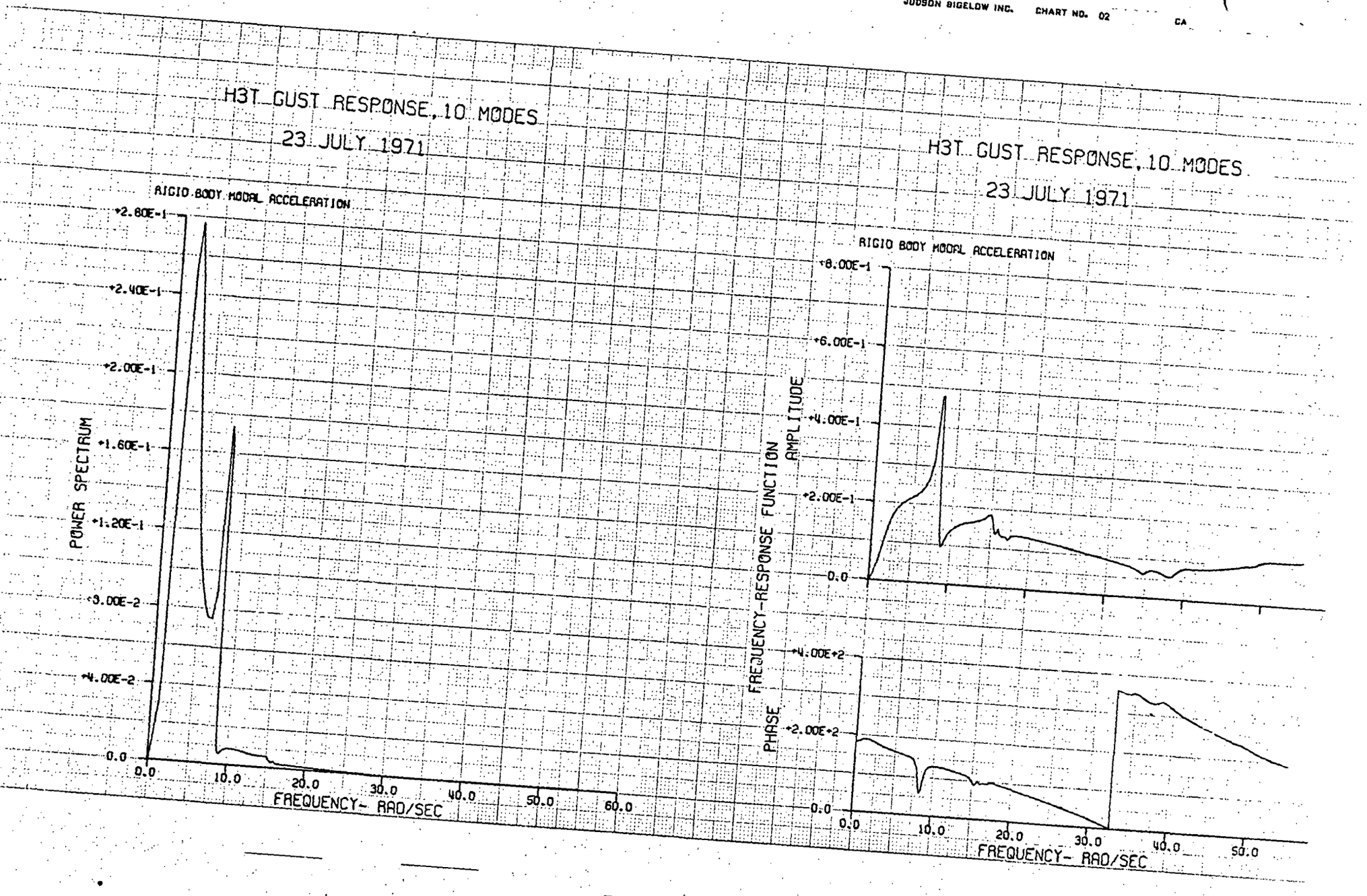

FIGURE A-5

JUDSON BIGELOW INC. CHART NO. 02 CA

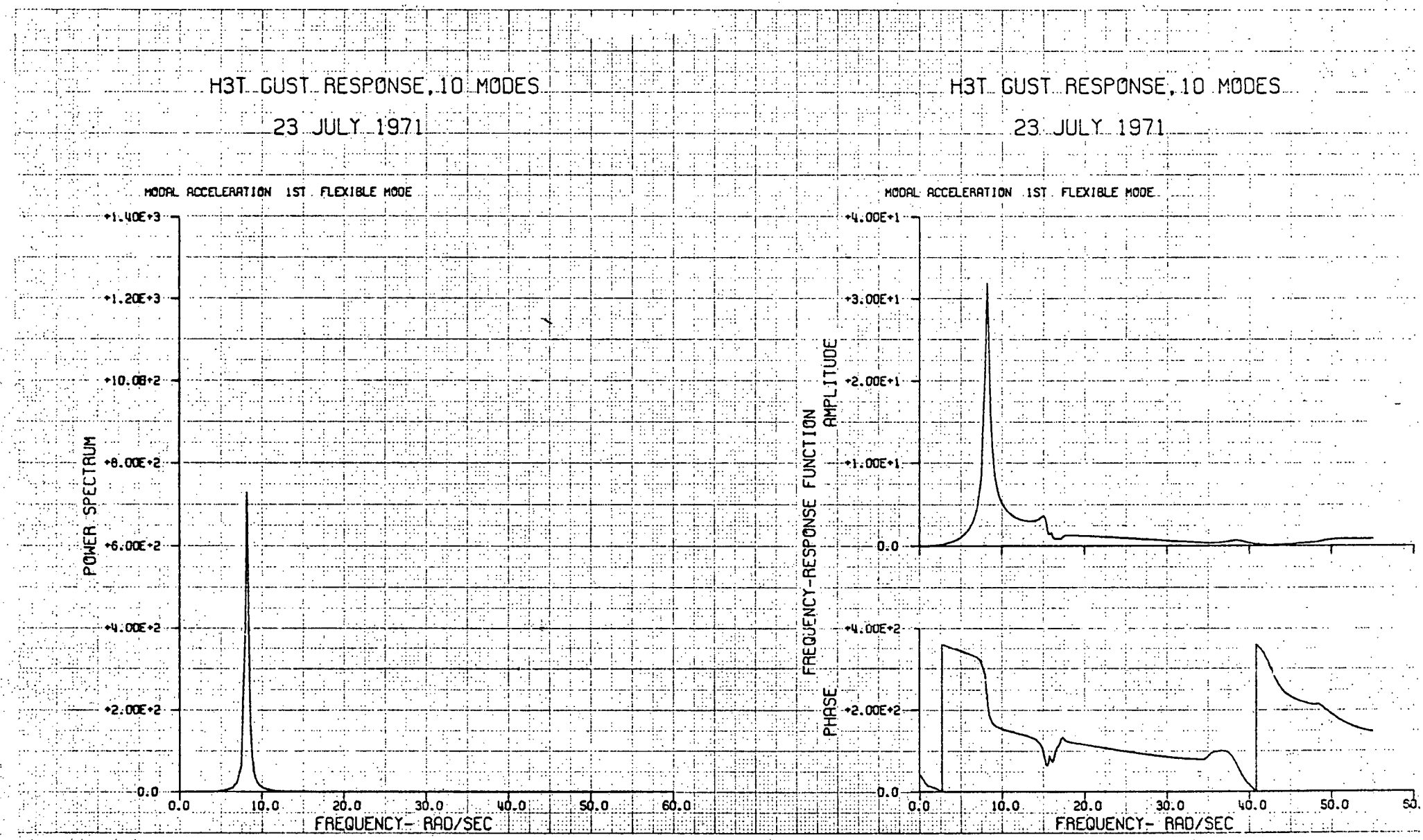

FIGURE A-6

JUDSON BIGELOW INC. CHART NO. 02 CA

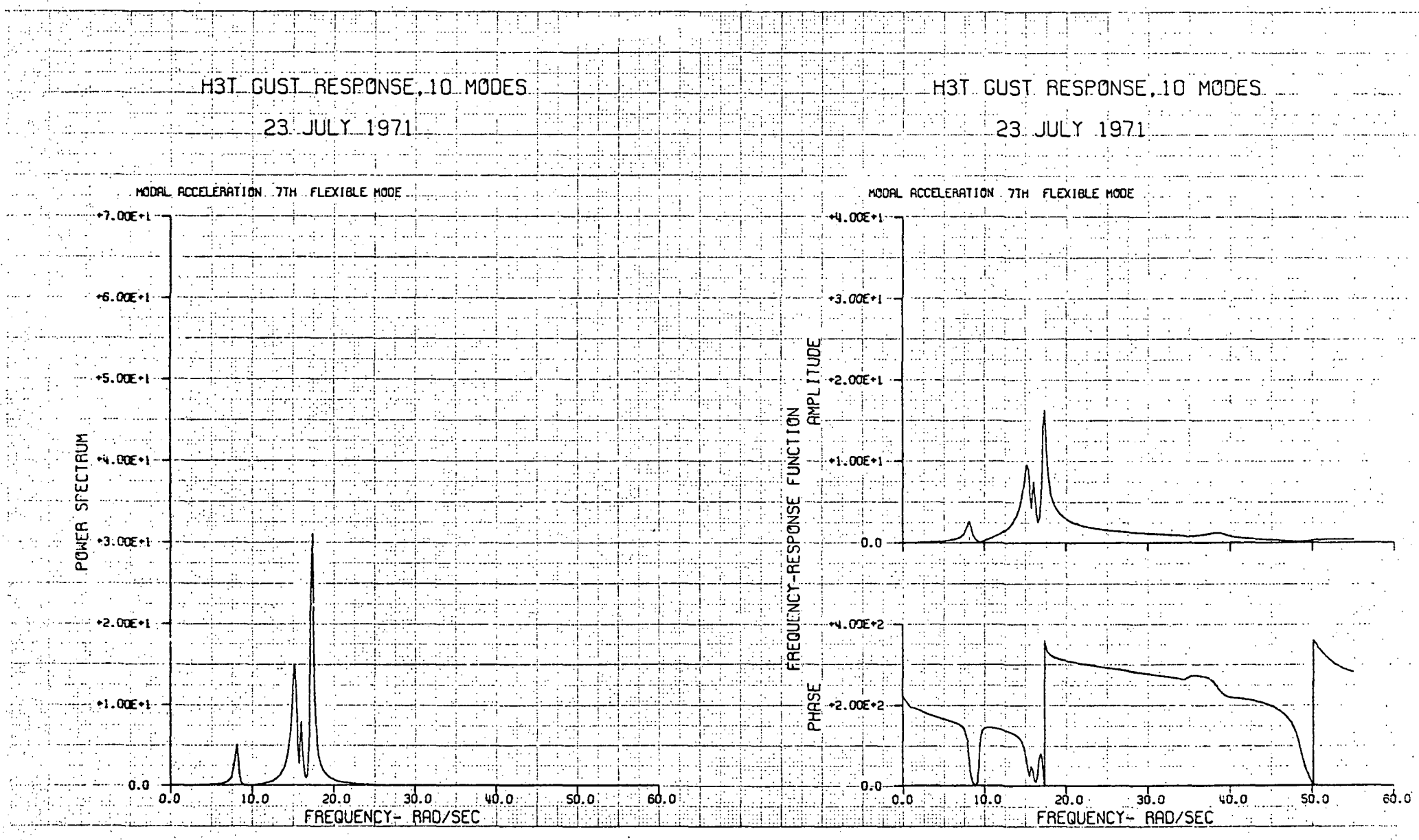

FIGURE A-7

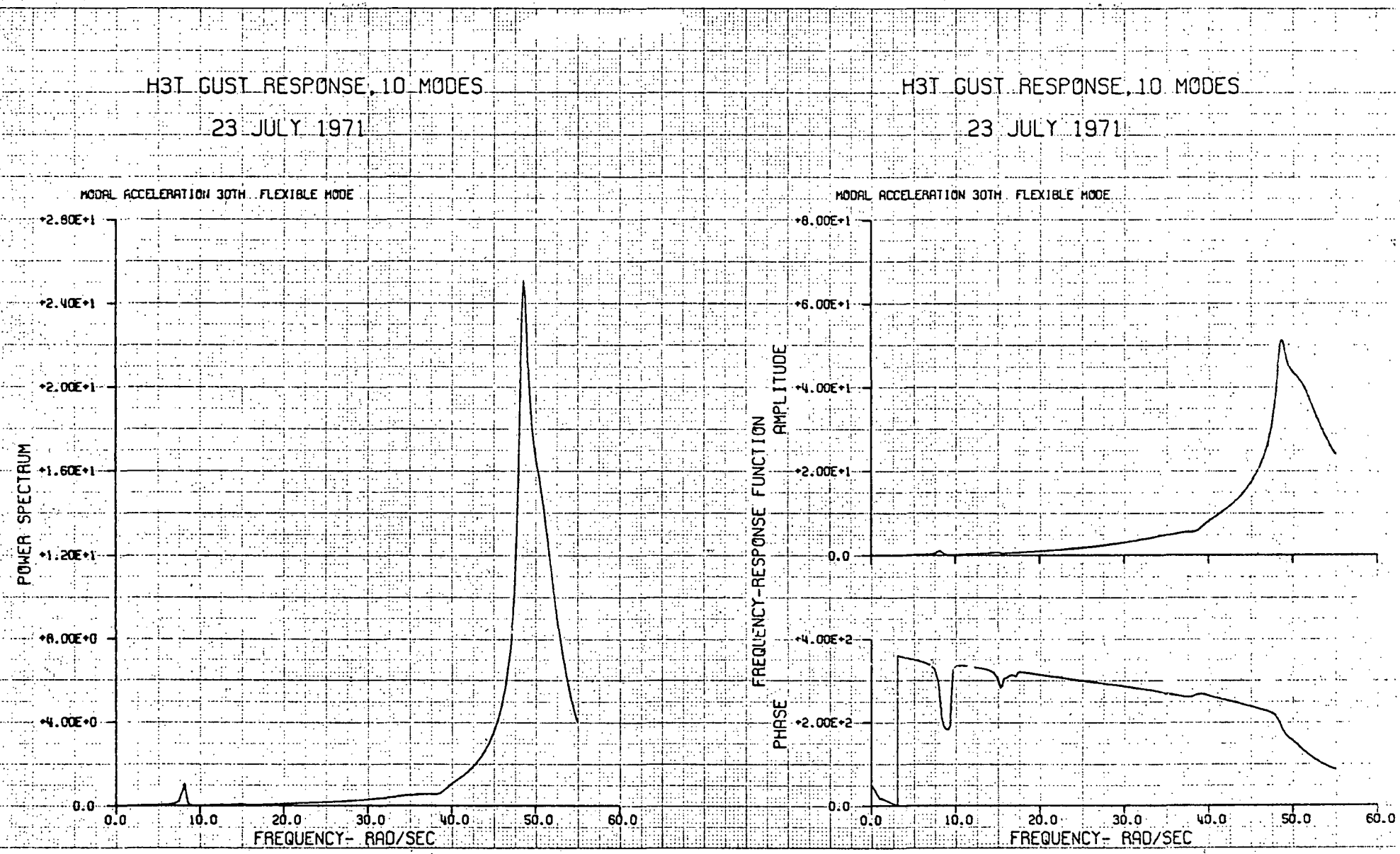
H3T GUST RESPONSE, 10 MODES
23 JULY 1971
MODAL ACCELERATION 30TH FLEXIBLE MODE
POWER SPECTRUM
+2.80E+1
+2.40E+1
+2.00E+1
+1.60E+1
+1.20E+1
+8.00E+0
+4.00E+0
0.0
0.0
10.0
20.0
30.0
40.0
50.0
60.0
FREQUENCY- RAD/SEC
H3T GUST RESPONSE, 10 MODES
23 JULY 1971
MODAL ACCELERATION 30TH FLEXIBLE MODE
FREQUENCY-RESPONSE FUNCTION
AMPLITUDE
+8.00E+1
+6.00E+1
+4.00E+1
+2.00E+1
0.0
PHASE
+4.00E+2
+2.00E+2
0.0
0.0
10.0
20.0
30.0
40.0
50.0
60.0
FREQUENCY- RAD/SEC

FIGURE A-8

JUDSON BIGELOW INC. CHART NO. 02 CA

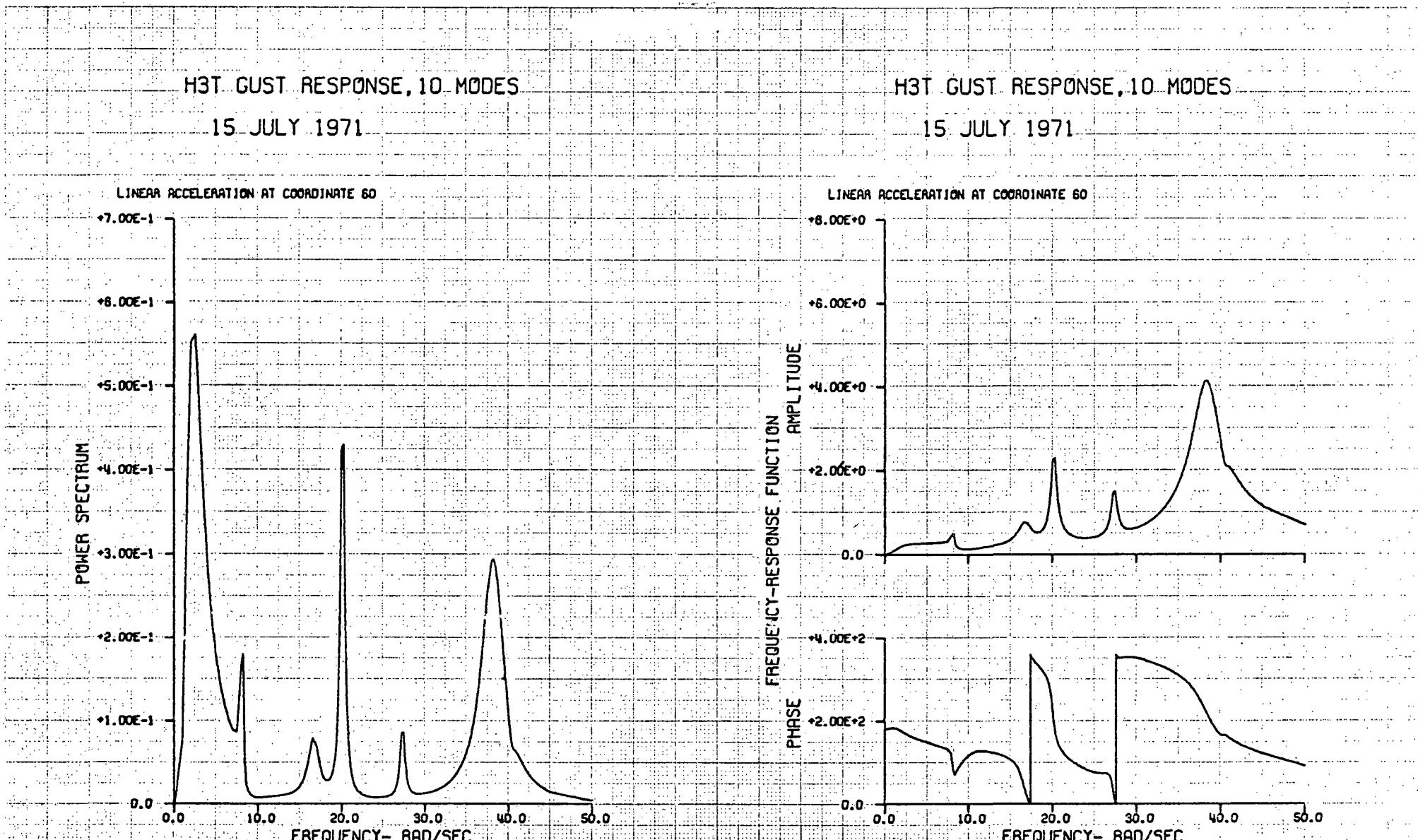

FIGURE A-9

JUDSON BIGELOW INC. CHART NO. 02 CA

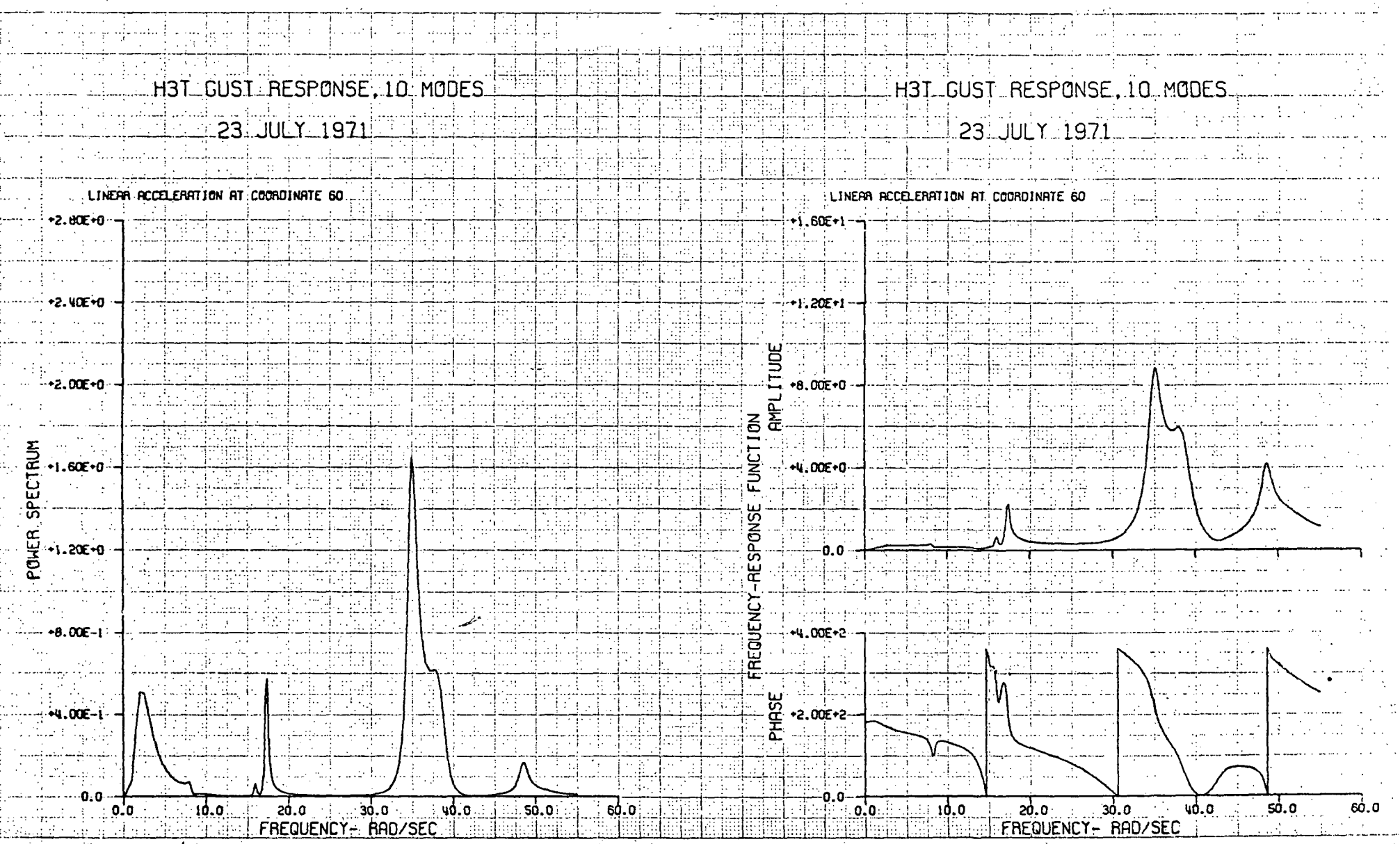

FIGURE A-10

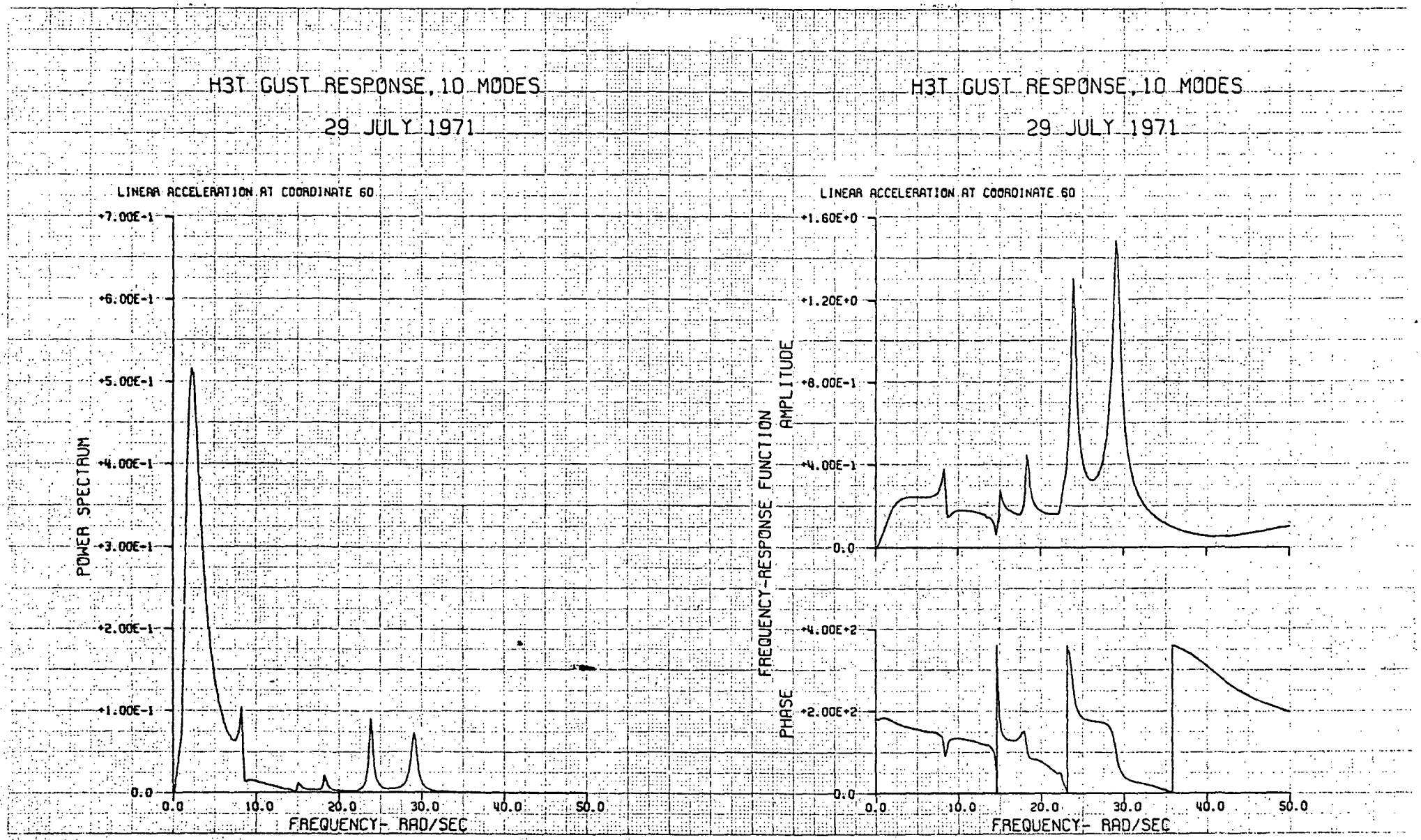
H3T GUST RESPONSE, 10 MODES
29 JULY 1971
LINEAR ACCELERATION AT COORDINATE 60
POWER SPECTRUM
+7.00E-1
+6.00E-1
+5.00E-1
+4.00E-1
+3.00E-1
+2.00E-1
+1.00E-1
0.0
0.0
10.0
20.0
30.0
40.0
50.0
FREQUENCY- RAD/SEC
H3T GUST RESPONSE, 10 MODES
29 JULY 1971
LINEAR ACCELERATION AT COORDINATE 60
FREQUENCY-RESPONSE FUNCTION
AMPLITUDE
+1.60E+0
+1.20E+0
+8.00E-1
+4.00E-1
0.0
PHASE
+4.00E+2
+2.00E+2
0.0
0.0
10.0
20.0
30.0
40.0
50.0
FREQUENCY- RAD/SEC

FIGURE A-11

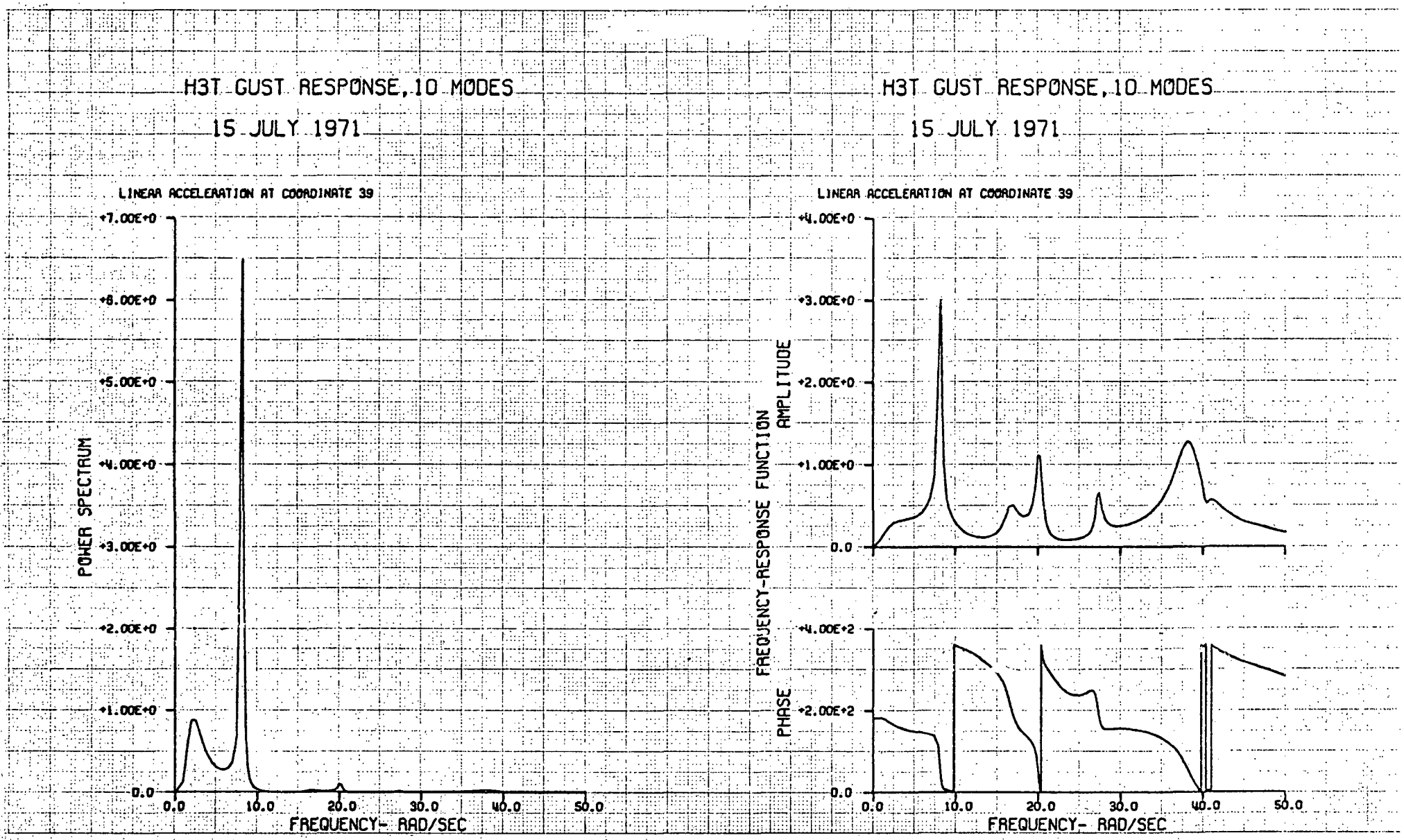
H3T GUST RESPONSE, 10 MODES
15 JULY 1971
LINEAR ACCELERATION AT COORDINATE 39
POWER SPECTRUM
+7.00E+0
+6.00E+0
+5.00E+0
+4.00E+0
+3.00E+0
+2.00E+0
+1.00E+0
0.0
0.0
10.0
20.0
30.0
40.0
50.0
FREQUENCY- RAD/SEC
H3T GUST RESPONSE, 10 MODES
15 JULY 1971
LINEAR ACCELERATION AT COORDINATE 39
FREQUENCY-RESPONSE FUNCTION
AMPLITUDE
+4.00E+0
+3.00E+0
+2.00E+0
+1.00E+0
0.0
PHASE
+4.00E+2
+2.00E+2
0.0
0.0
10.0
20.0
30.0
40.0
50.0
FREQUENCY- RAD/SEC

FIGURE A-12

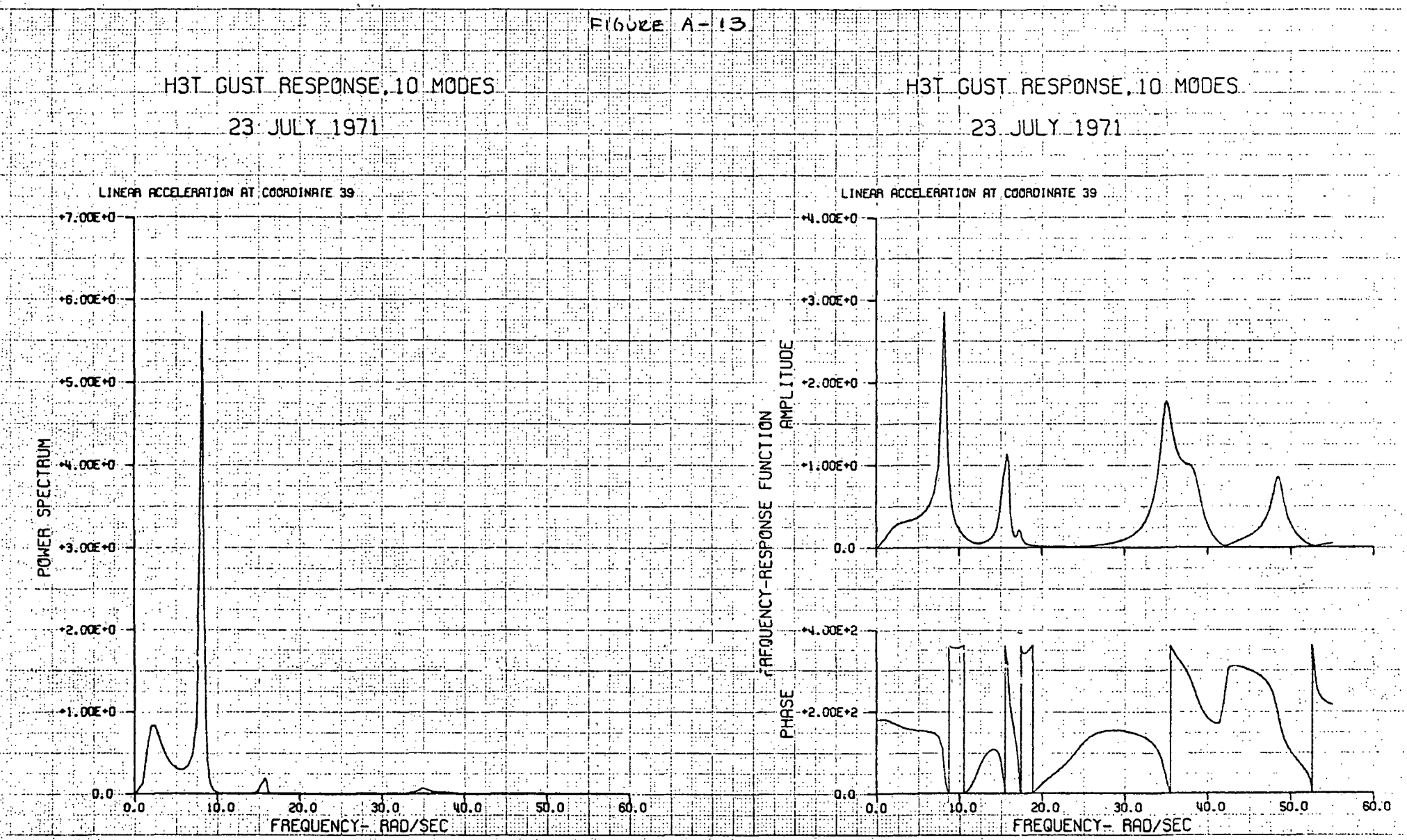
FIGURE A-13
H3T GUST RESPONSE, 10 MODES
23 JULY 1971
LINEAR ACCELERATION AT COORDINATE 39
POWER SPECTRUM
+7.00E+0
+6.00E+0
+5.00E+0
+4.00E+0
+3.00E+0
+2.00E+0
+1.00E+0
0.0
0.0
10.0
20.0
30.0
40.0
50.0
60.0
FREQUENCY- RAD/SEC
H3T GUST RESPONSE, 10 MODES
23 JULY 1971
LINEAR ACCELERATION AT COORDINATE 39
FREQUENCY-RESPONSE FUNCTION AMPLITUDE
+4.00E+0
+3.00E+0
+2.00E+0
+1.00E+0
0.0
PHASE
+4.00E+2
+2.00E+2
0.0
0.0
10.0
20.0
30.0
40.0
50.0
60.0
FREQUENCY- RAD/SEC

FIGURE A-13

FIGURE A-14

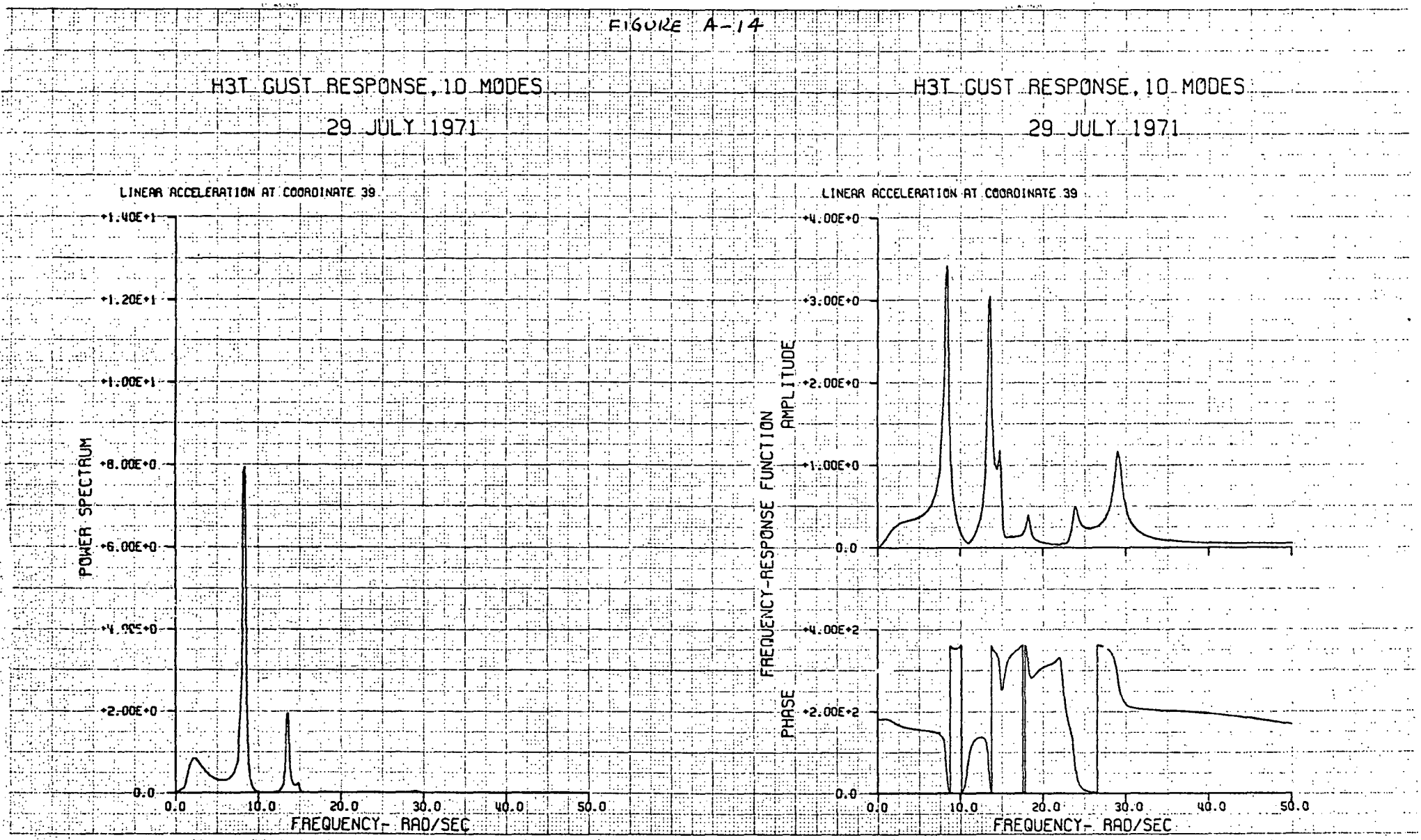

FIGURE A-14

JUDSON BIGELOW INC. CHART NO. 02 C.

FIGURE A-15

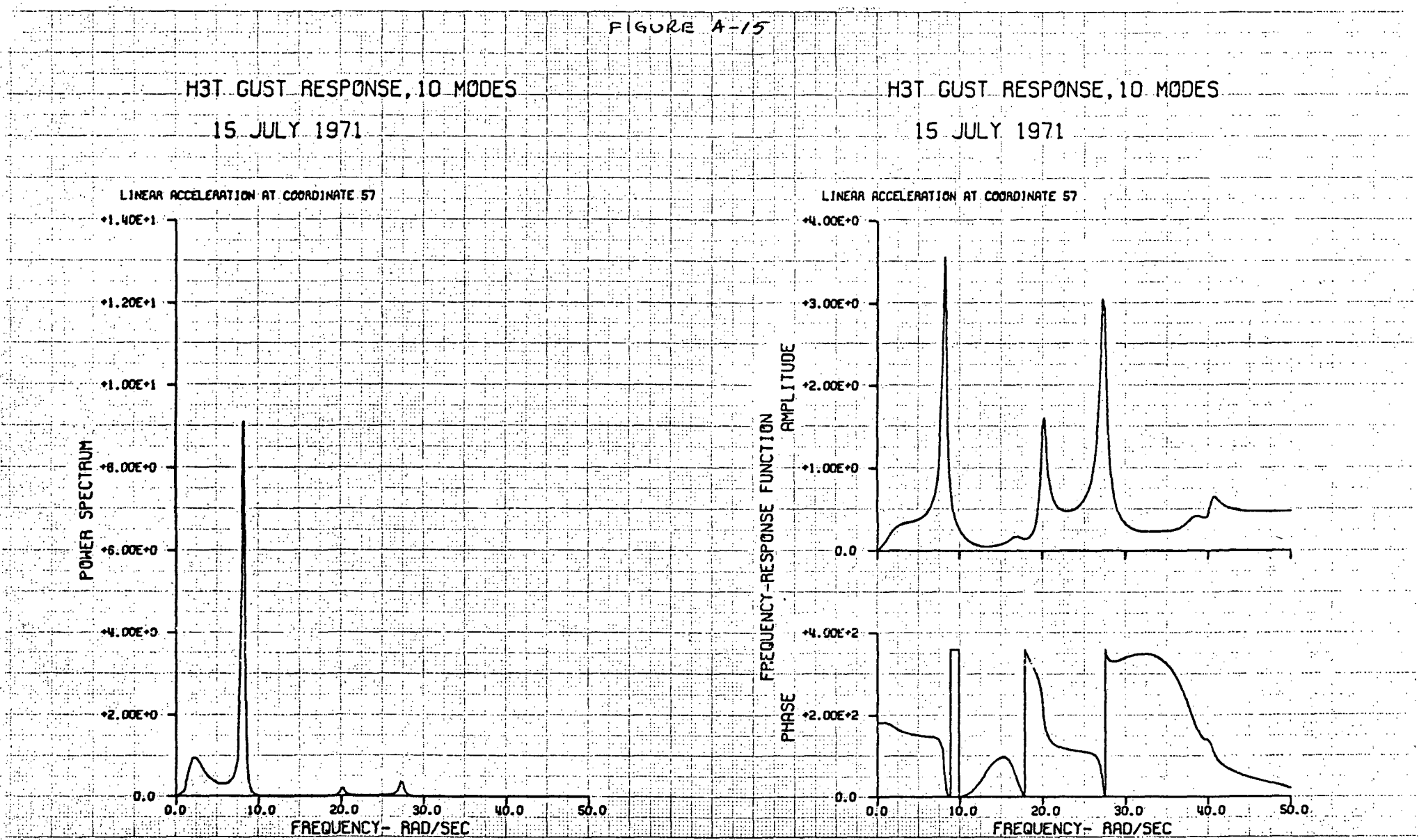

FIGURE A-15

JUDSON BIGELOW INC. CHART NO. 02 CA

FIGURE A-16

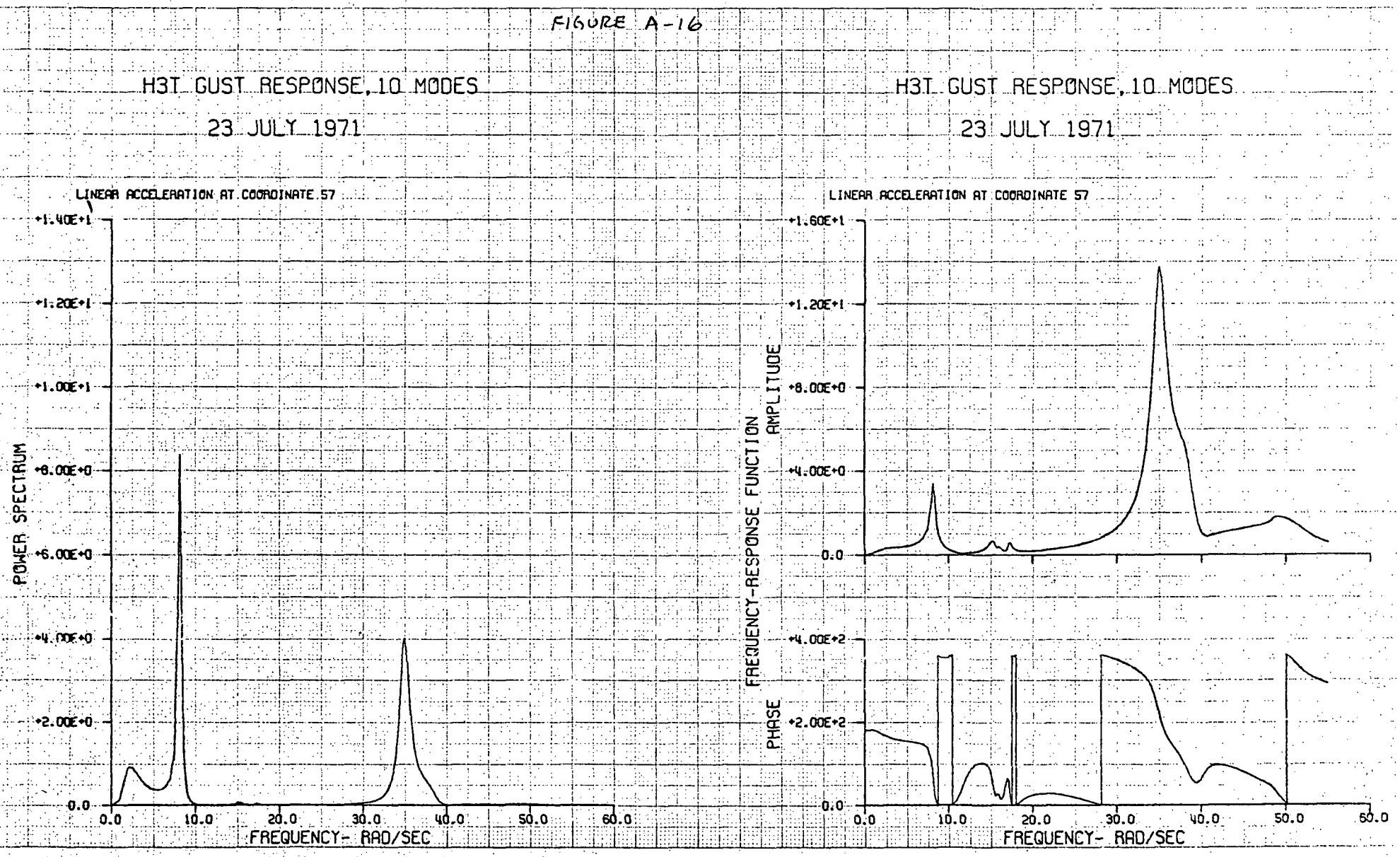

FIGURE A-16

FIGURE A-17

H3T GUST RESPONSE, 10 MODES
29 JULY 1971

LINEAR ACCELERATION AT COORDINATE 57

POWER SPECTRUM

+1.40E+1
+1.20E+1
+1.00E+1
+8.00E+0
+6.00E+0
+4.00E+0
+2.00E+0
0.0

0.0 10.0 20.0 30.0 40.0 50.0

FREQUENCY- RAD/SEC

H3T GUST RESPONSE, 10 MODES
29 JULY 1971

LINEAR ACCELERATION AT COORDINATE 57

FREQUENCY-RESPONSE FUNCTION AMPLITUDE

+8.00E+0
+6.00E+0
+4.00E+0
+2.00E+0
0.0

PHASE

+4.00E+2
+2.00E+2
0.0

0.0 10.0 20.0 30.0 40.0 50.0

FREQUENCY- RAD/SEC

FIGURE A-17

FIGURE A-18

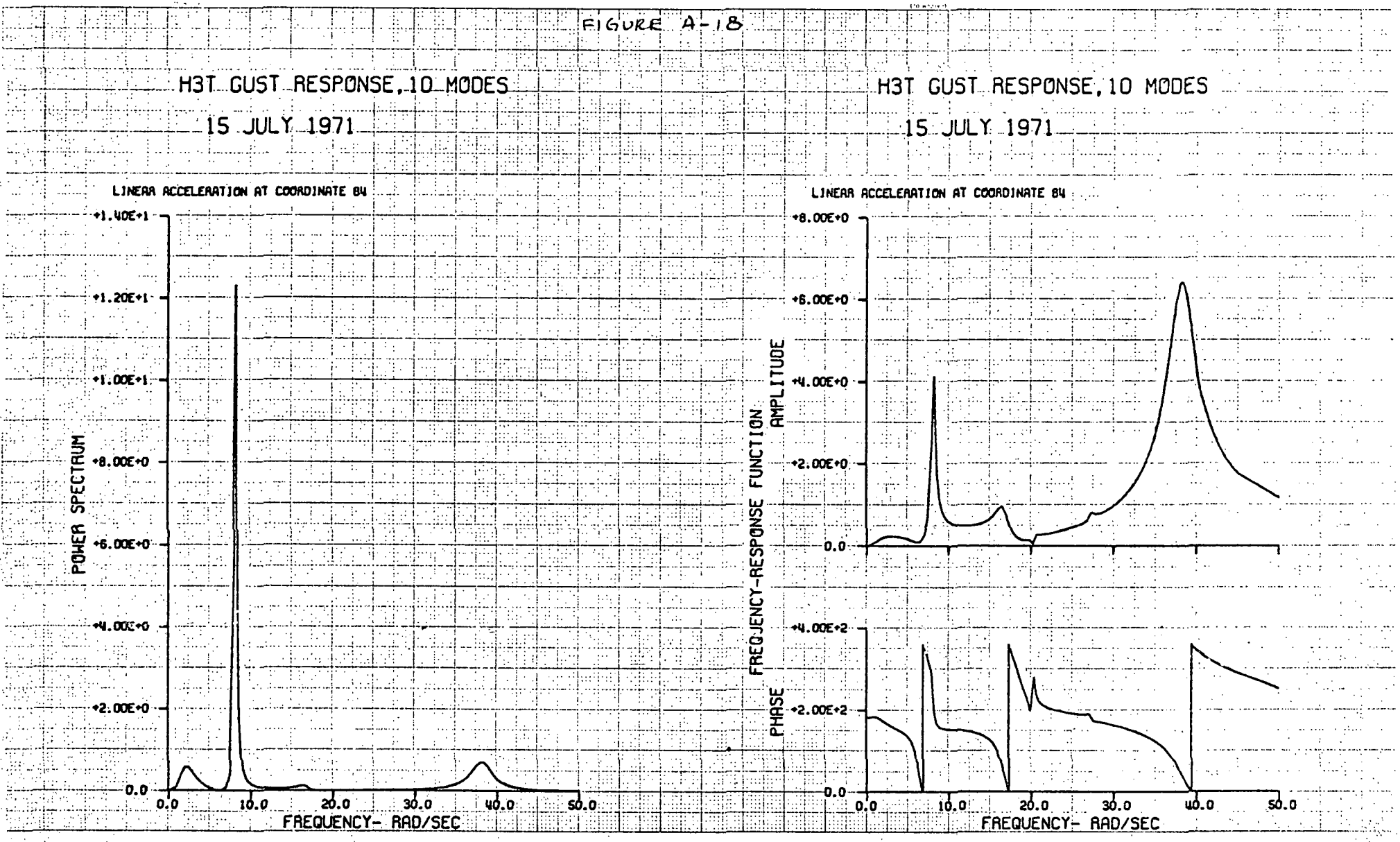

FIGURE A-18

FIGURE A-19

H3T GUST RESPONSE, 10 MODES

23 JULY 1971

LINEAR ACCELERATION AT COORDINATE 84

POWER SPECTRUM

+1.40E+1
+1.20E+1
+1.00E+1
+8.00E+0
+6.00E+0
+4.00E+0
+2.00E+0
0.0

0.0 10.0 20.0 30.0 40.0 50.0 60.0

FREQUENCY- RAD/SEC

H3T GUST RESPONSE, 10 MODES

23 JULY 1971

LINEAR ACCELERATION AT COORDINATE 84

FREQUENCY-RESPONSE FUNCTION AMPLITUDE

+1.60E+1
+1.20E+1
+8.00E+0
+4.00E+0
0.0

PHASE

+4.00E+2
+2.00E+2
0.0

0.0 10.0 20.0 30.0 40.0 50.0 60.0

FREQUENCY- RAD/SEC

FIGURE A-19

FIGURE A-20

H3T GUST RESPONSE, 10 MODES

29 JULY 1971

LINEAR ACCELERATION AT COORDINATE 84

POWER SPECTRUM

+2.80E+1
+2.40E+1
+2.00E+1
+1.60E+1
+1.20E+1
+8.00E+0
+4.00E+0
0.0

0.0 10.0 20.0 30.0 40.0 50.0

FREQUENCY- RAD/SEC

H3T GUST RESPONSE, 10 MODES

29 JULY 1971

LINEAR ACCELERATION AT COORDINATE 84

FREQUENCY-RESPONSE FUNCTION AMPLITUDE

+8.00E+0
+6.00E+0
+4.00E+0
+2.00E+0
0.0

PHASE

+4.00E+2
+2.00E+2
0.0

0.0 10.0 20.0 30.0 40.0 50.0

FREQUENCY- RAD/SEC

FIGURE A-20

FIGURE A-21

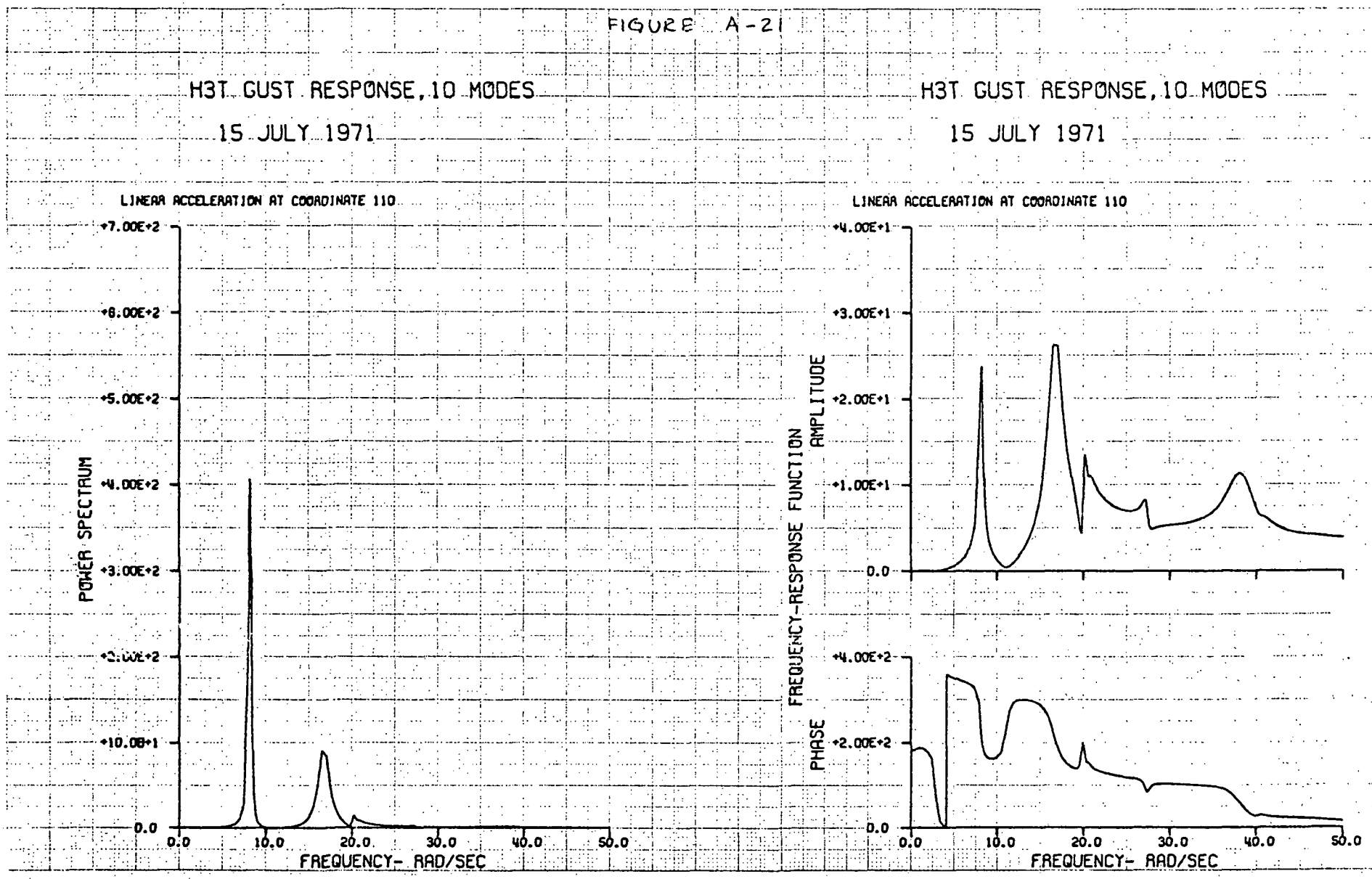

FIGURE A-21

JUDSON BIGELOW INC. CHART NO. 02 CA

FIGURE A-22

H3T GUST RESPONSE, 10 MODES

23 JULY 1971

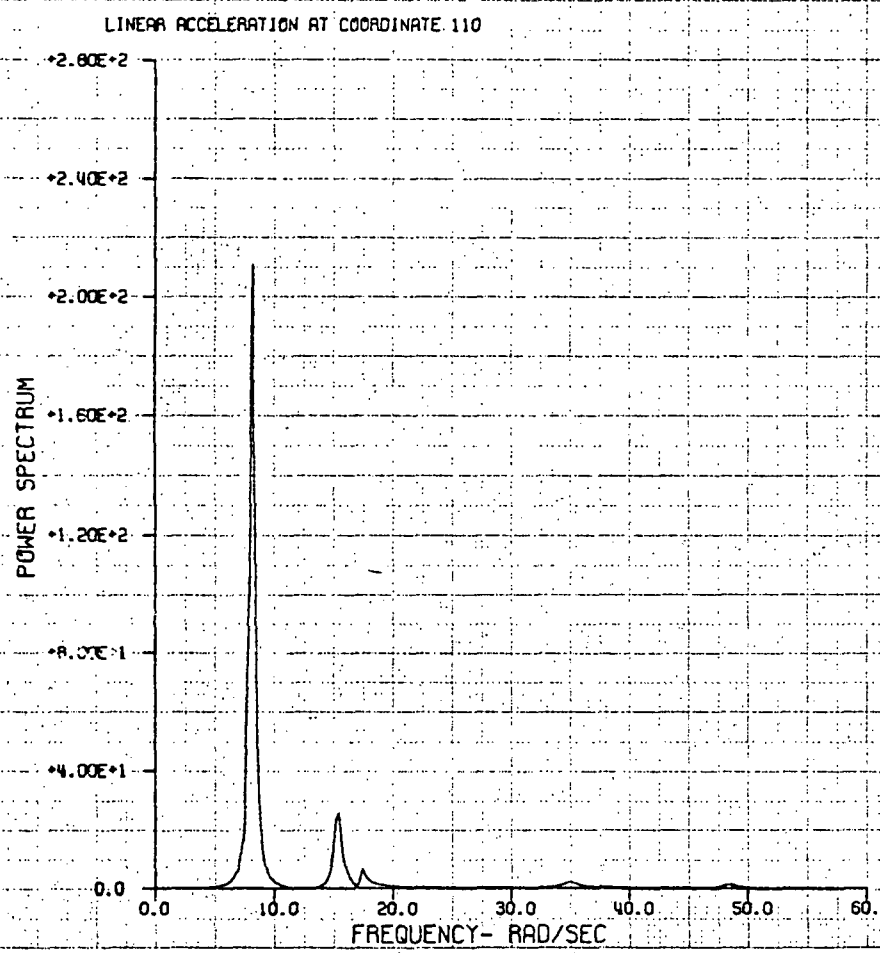

H3T GUST RESPONSE, 10 MODES

23 JULY 1971

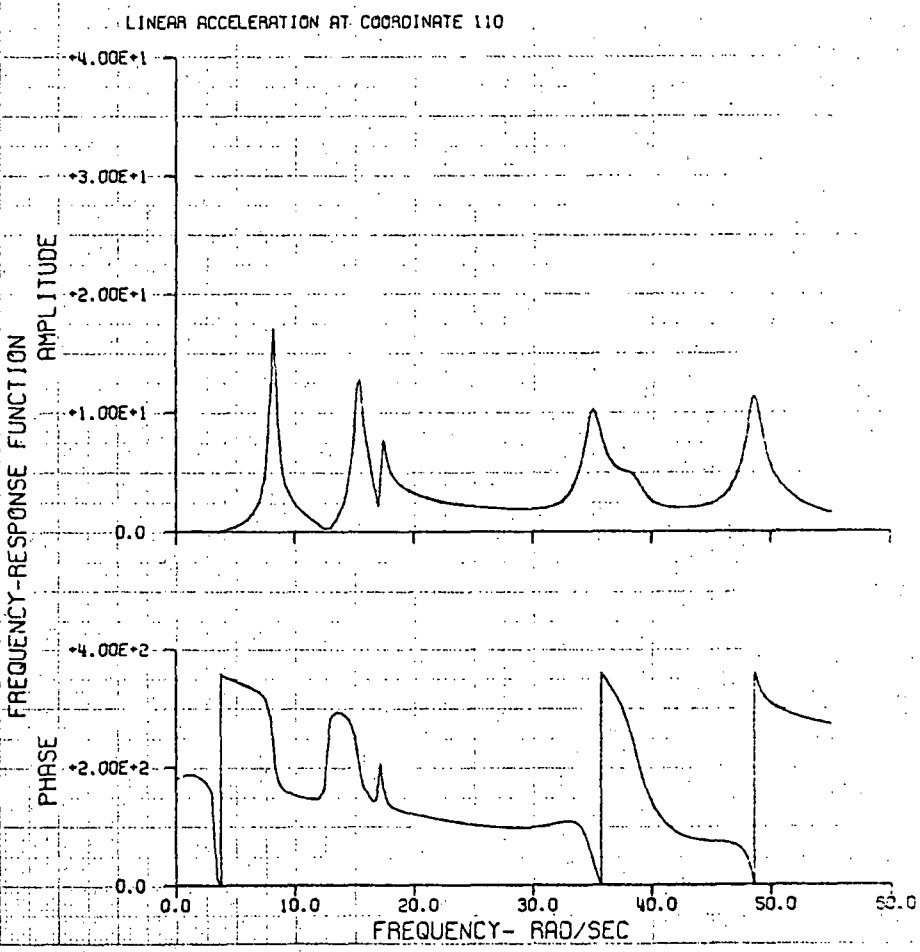

FIGURE A-22

JUDSON BIGELOW INC. CHART NO. 02 CA

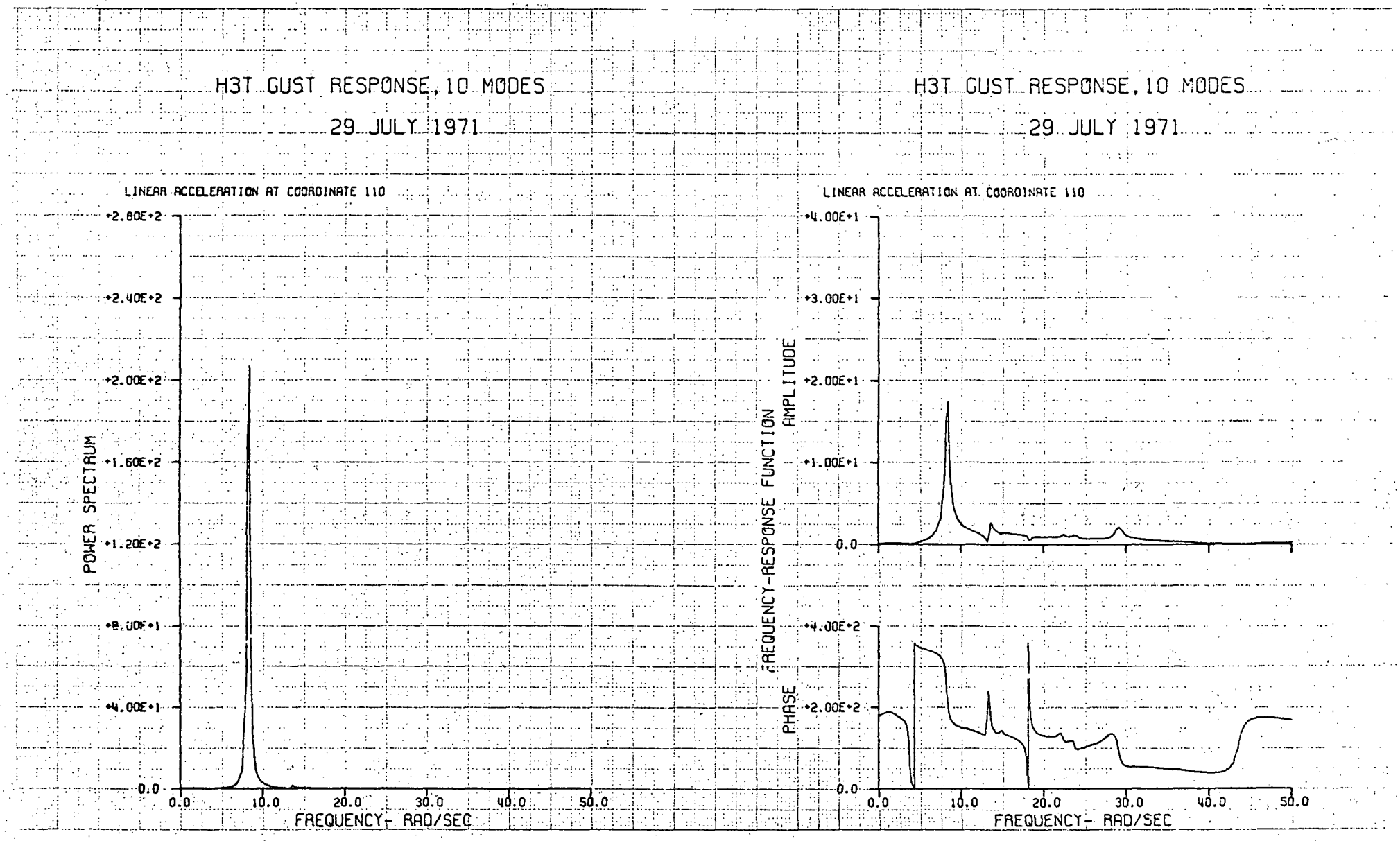

FIGURE A-23

JUDSON BIGELOW INC. CHART NO. 02 CA

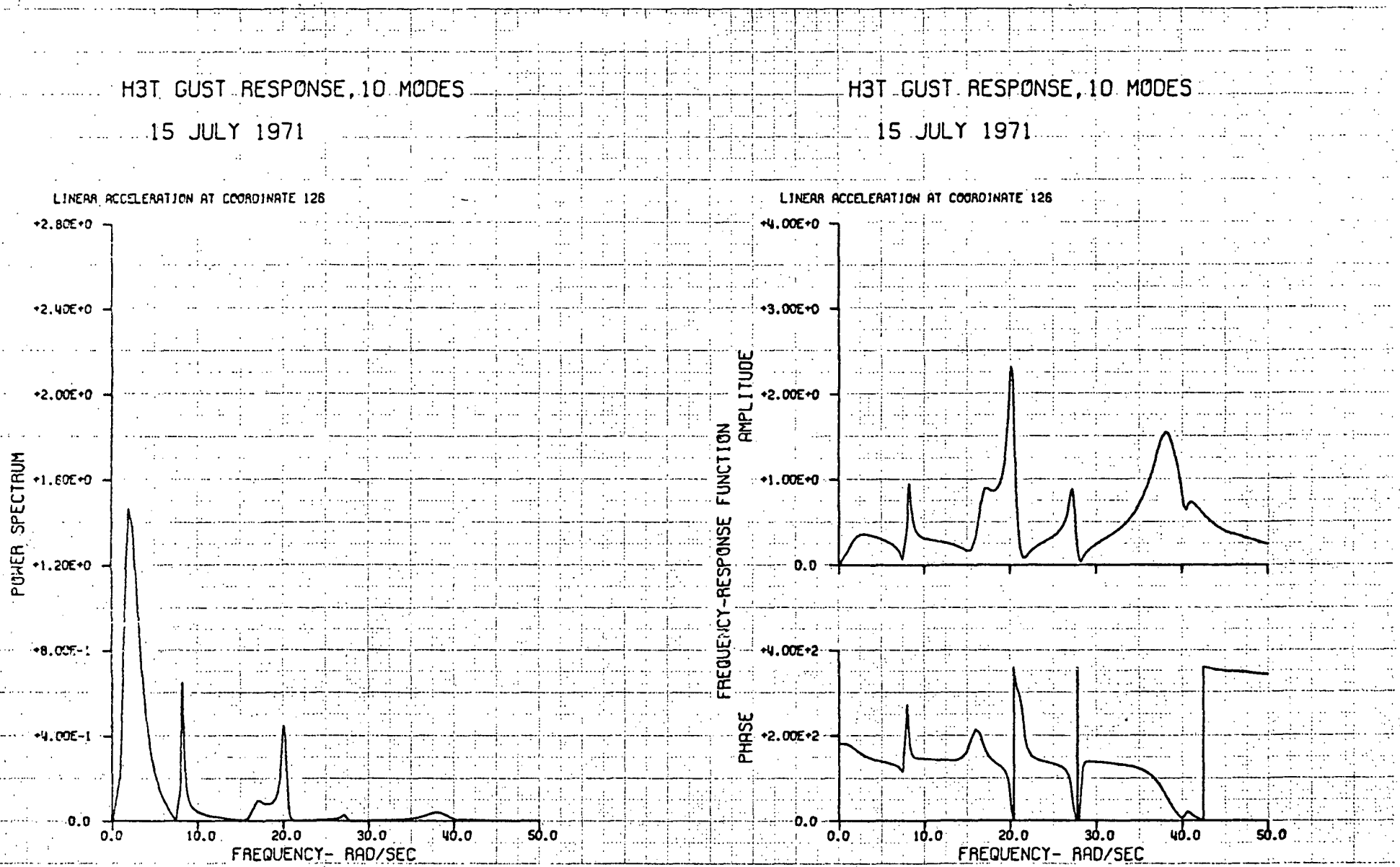

FIGURE A-24

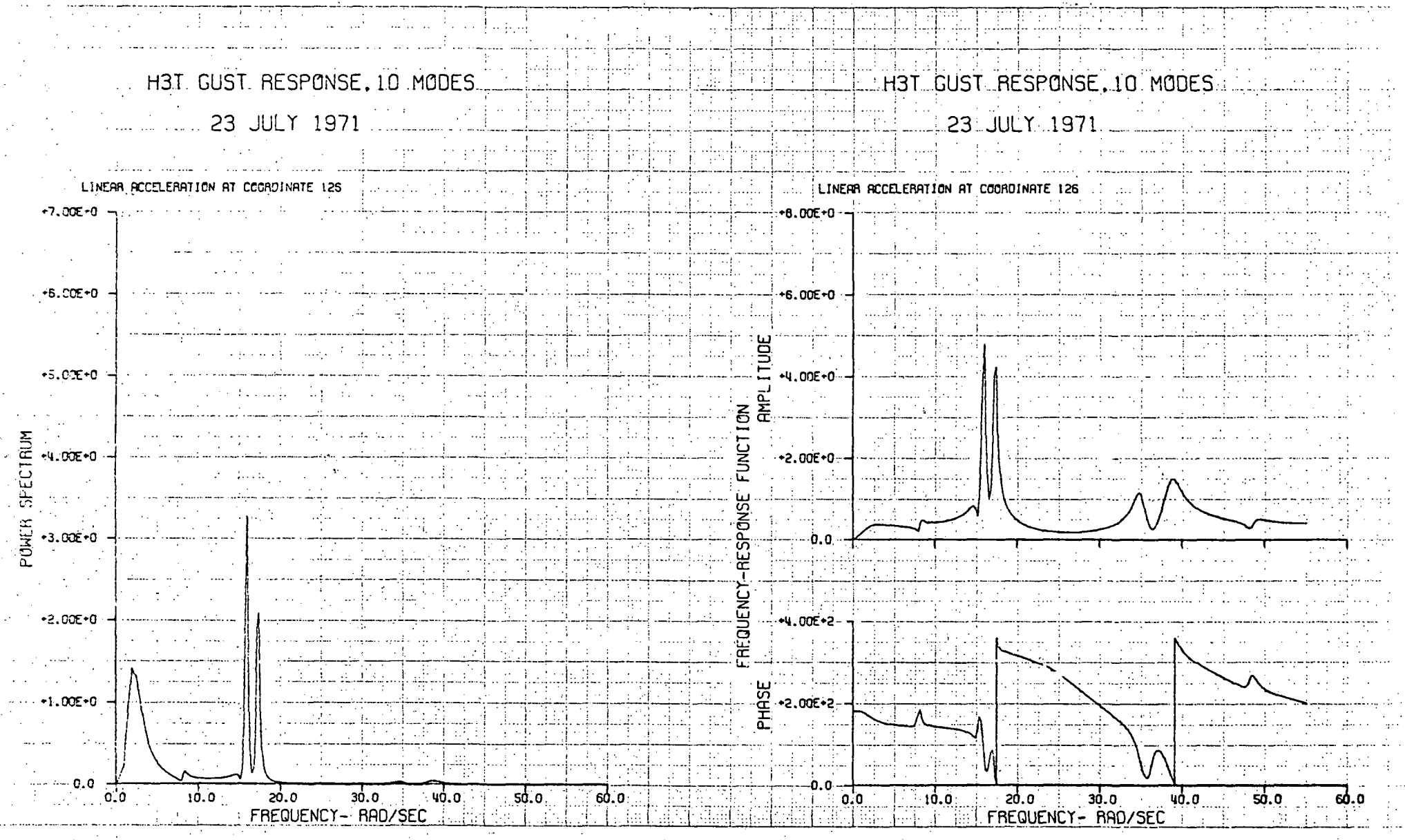
H3T GUST RESPONSE, 10 MODES
23 JULY 1971
LINEAR ACCELERATION AT COORDINATE 125
POWER SPECTRUM
+7.00E+0
+6.00E+0
+5.00E+0
+4.00E+0
+3.00E+0
+2.00E+0
+1.00E+0
0.0
0.0
10.0
20.0
30.0
40.0
50.0
60.0
FREQUENCY- RAD/SEC
H3T GUST RESPONSE, 10 MODES
23 JULY 1971
LINEAR ACCELERATION AT COORDINATE 126
FREQUENCY-RESPONSE FUNCTION
AMPLITUDE
+8.00E+0
+6.00E+0
+4.00E+0
+2.00E+0
0.0
PHASE
+4.00E+2
+2.00E+2
0.0
0.0
10.0
20.0
30.0
40.0
50.0
60.0
FREQUENCY- RAD/SEC

FIGURE A-25

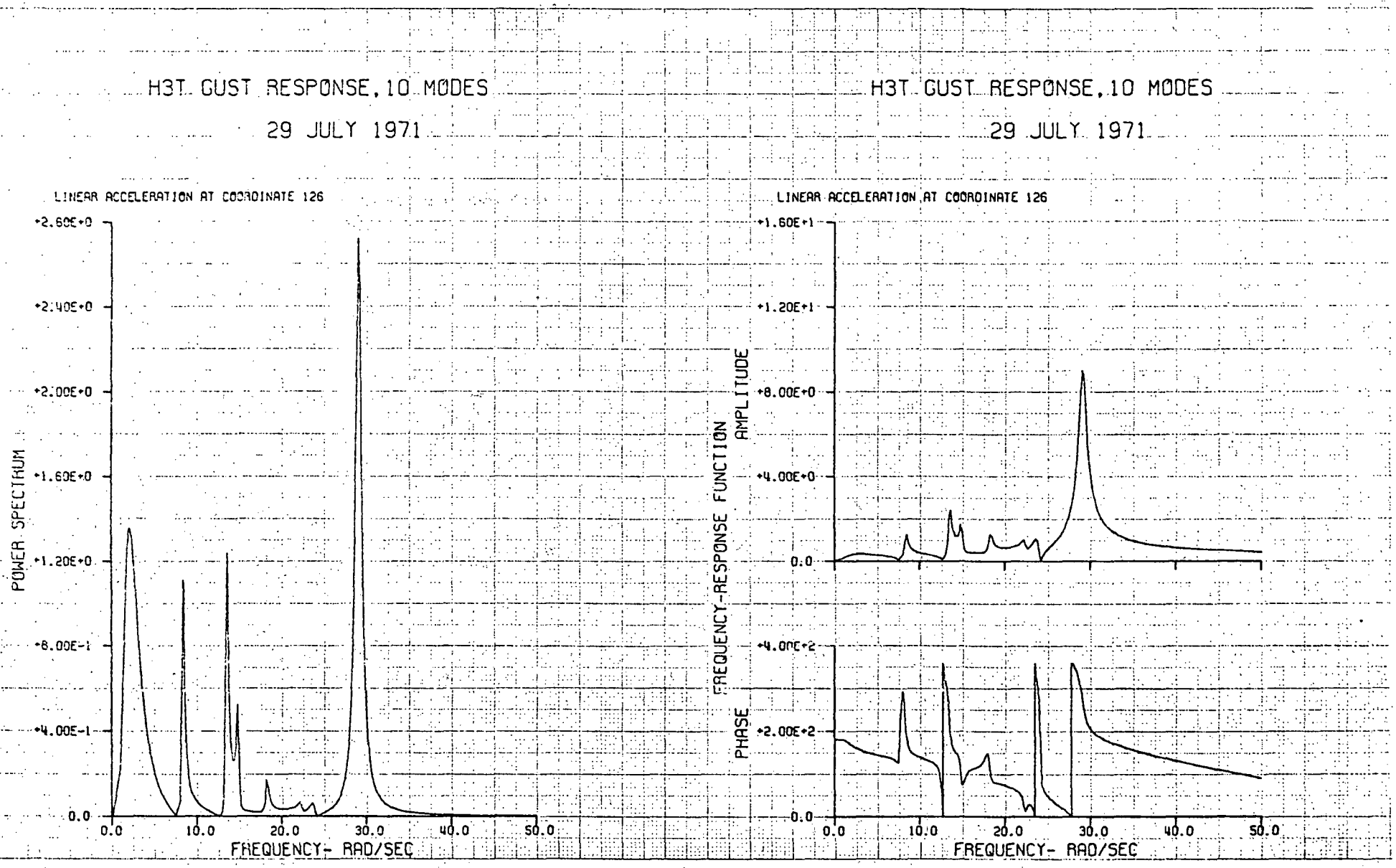
H3T GUST RESPONSE, 10 MODES
29 JULY 1971
LINEAR ACCELERATION AT COORDINATE 126
POWER SPECTRUM
+2.80E+0
+2.40E+0
+2.00E+0
+1.60E+0
+1.20E+0
+8.00E-1
+4.00E-1
0.0
0.0
10.0
20.0
30.0
40.0
50.0
FREQUENCY- RAD/SEC
H3T GUST RESPONSE, 10 MODES
29 JULY 1971
LINEAR ACCELERATION AT COORDINATE 126
FREQUENCY-RESPONSE FUNCTION
AMPLITUDE
+1.60E+1
+1.20E+1
+8.00E+0
+4.00E+0
0.0
PHASE
+4.00E+2
+2.00E+2
0.0
0.0
10.0
20.0
30.0
40.0
50.0
FREQUENCY- RAD/SEC

FIGURE A-26

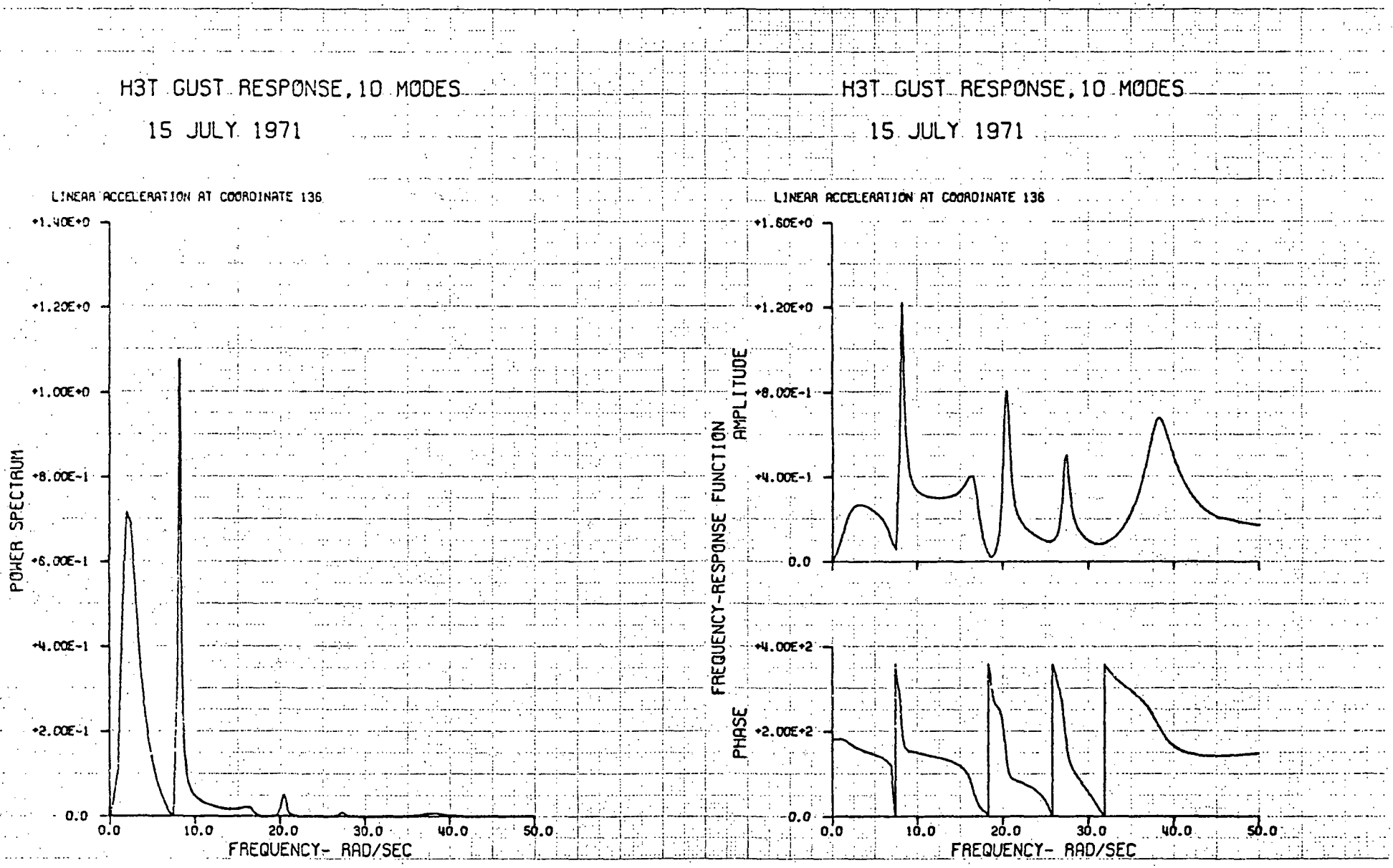
H3T GUST RESPONSE, 10 MODES
15 JULY 1971
LINEAR ACCELERATION AT COORDINATE 136
POWER SPECTRUM
+1.40E+0
+1.20E+0
+1.00E+0
+8.00E-1
+6.00E-1
+4.00E-1
+2.00E-1
0.0
0.0
10.0
20.0
30.0
40.0
50.0
FREQUENCY- RAD/SEC
H3T GUST RESPONSE, 10 MODES
15 JULY 1971
LINEAR ACCELERATION AT COORDINATE 136
FREQUENCY-RESPONSE FUNCTION
AMPLITUDE
+1.60E+0
+1.20E+0
+8.00E-1
+4.00E-1
0.0
PHASE
+4.00E+2
+2.00E+2
0.0
0.0
10.0
20.0
30.0
40.0
50.0
FREQUENCY- RAD/SEC

FIGURE A-27

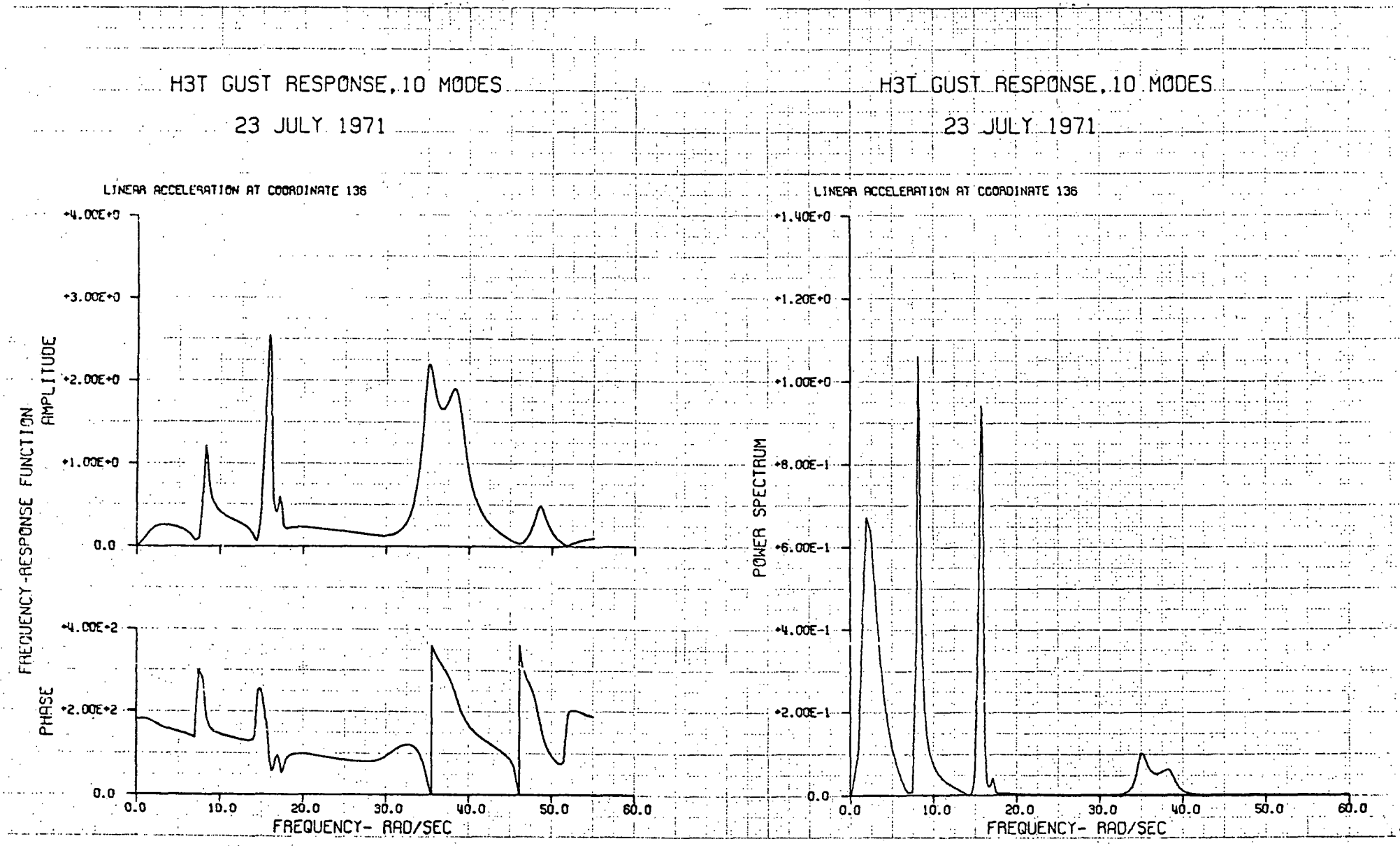
H3T GUST RESPONSE, 10 MODES
23 JULY 1971
LINEAR ACCELERATION AT COORDINATE 136
FREQUENCY-RESPONSE FUNCTION AMPLITUDE
+4.00E+0
+3.00E+0
+2.00E+0
+1.00E+0
0.0
PHASE
+4.00E+2
+2.00E+2
0.0
0.0
10.0
20.0
30.0
40.0
50.0
60.0
FREQUENCY- RAD/SEC
H3T GUST RESPONSE, 10 MODES
23 JULY 1971
LINEAR ACCELERATION AT COORDINATE 136
POWER SPECTRUM
+1.40E+0
+1.20E+0
+1.00E+0
+8.00E-1
+6.00E-1
+4.00E-1
+2.00E-1
0.0
0.0
10.0
20.0
30.0
40.0
50.0
60.0
FREQUENCY- RAD/SEC

FIGURE A-28

JUDSON BIGELOW INC. CHAR

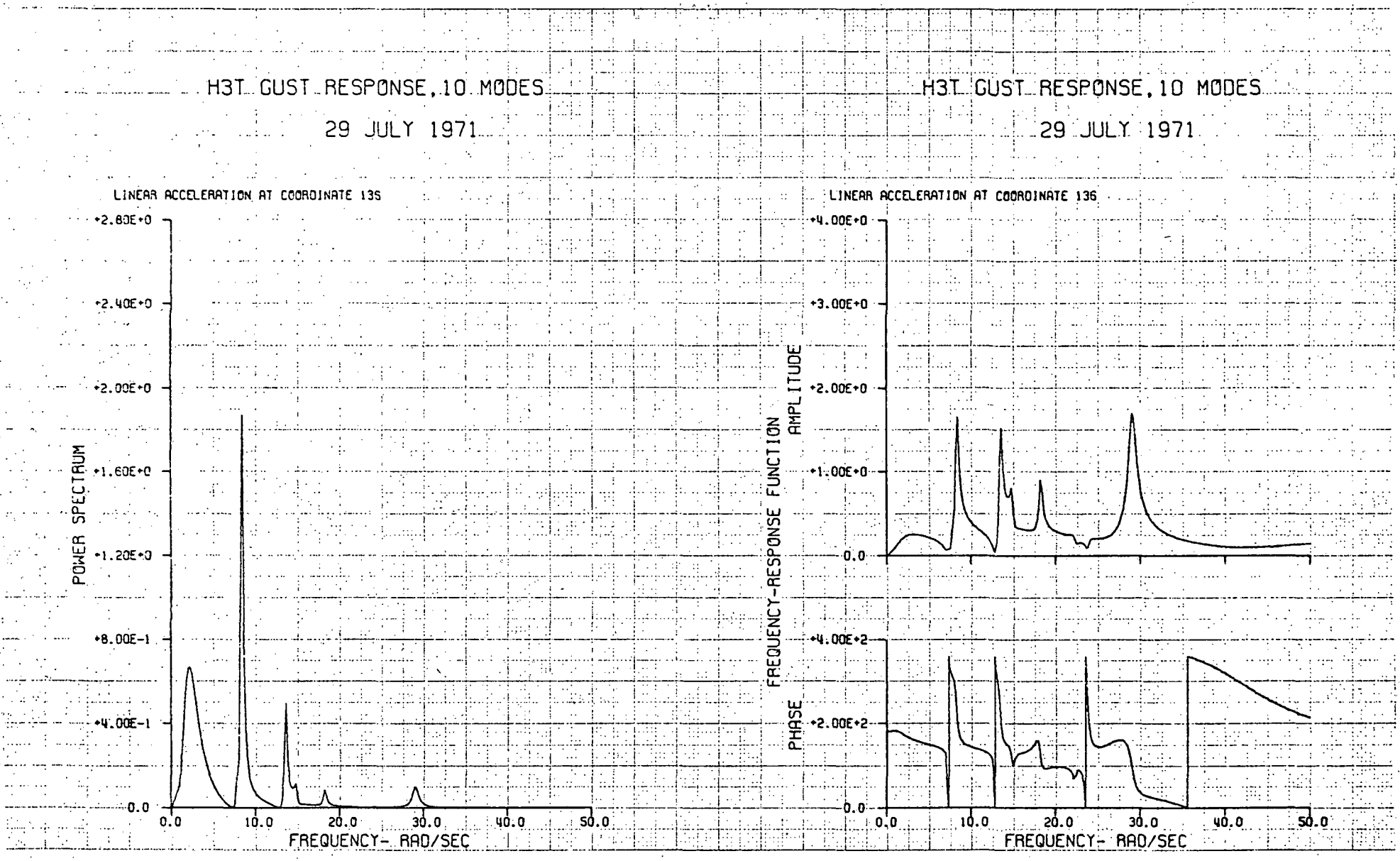

FIGURE A-29

JUDSON BIGELOW INC. CHART NO. 02 CA

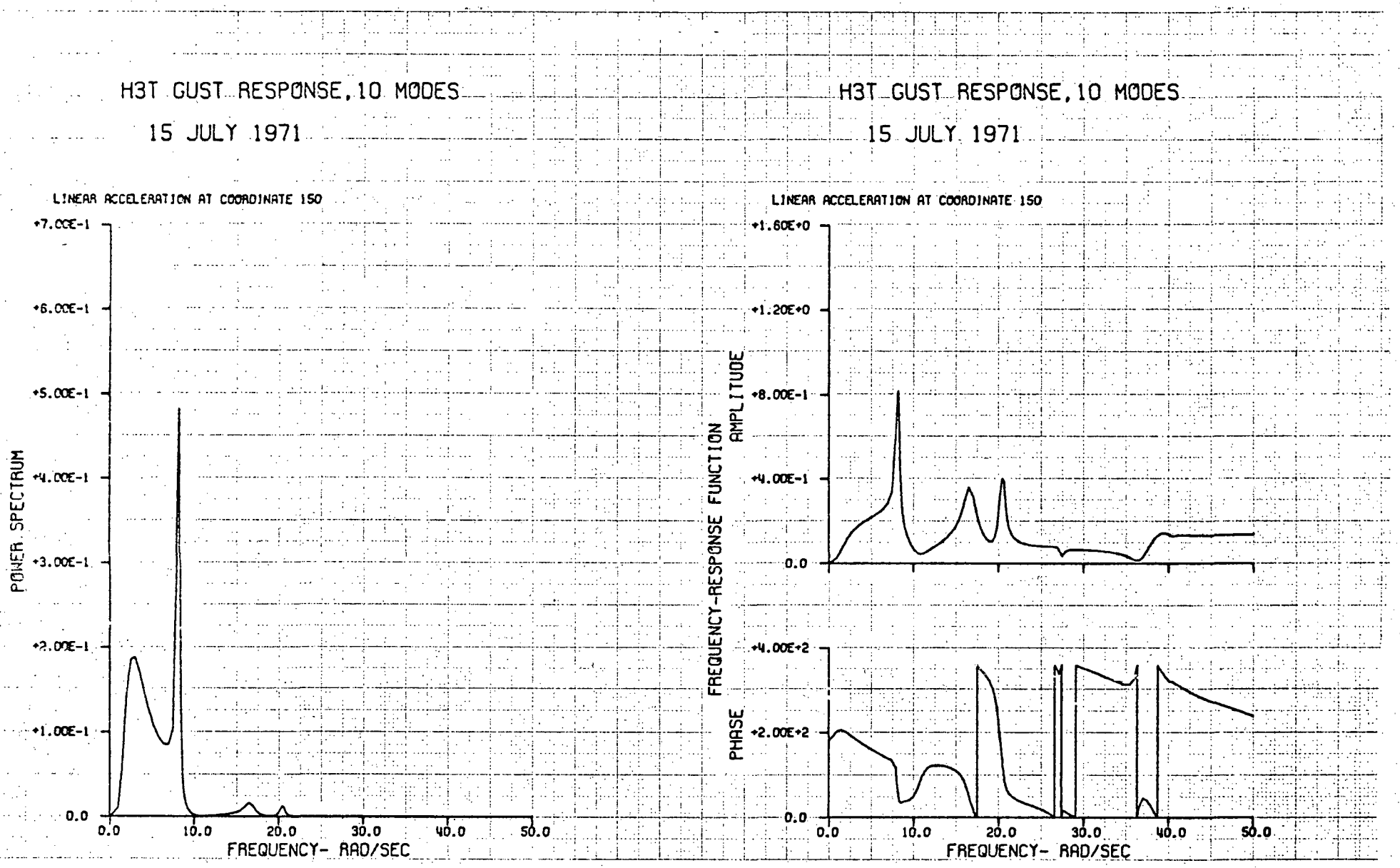

FIGURE A-30

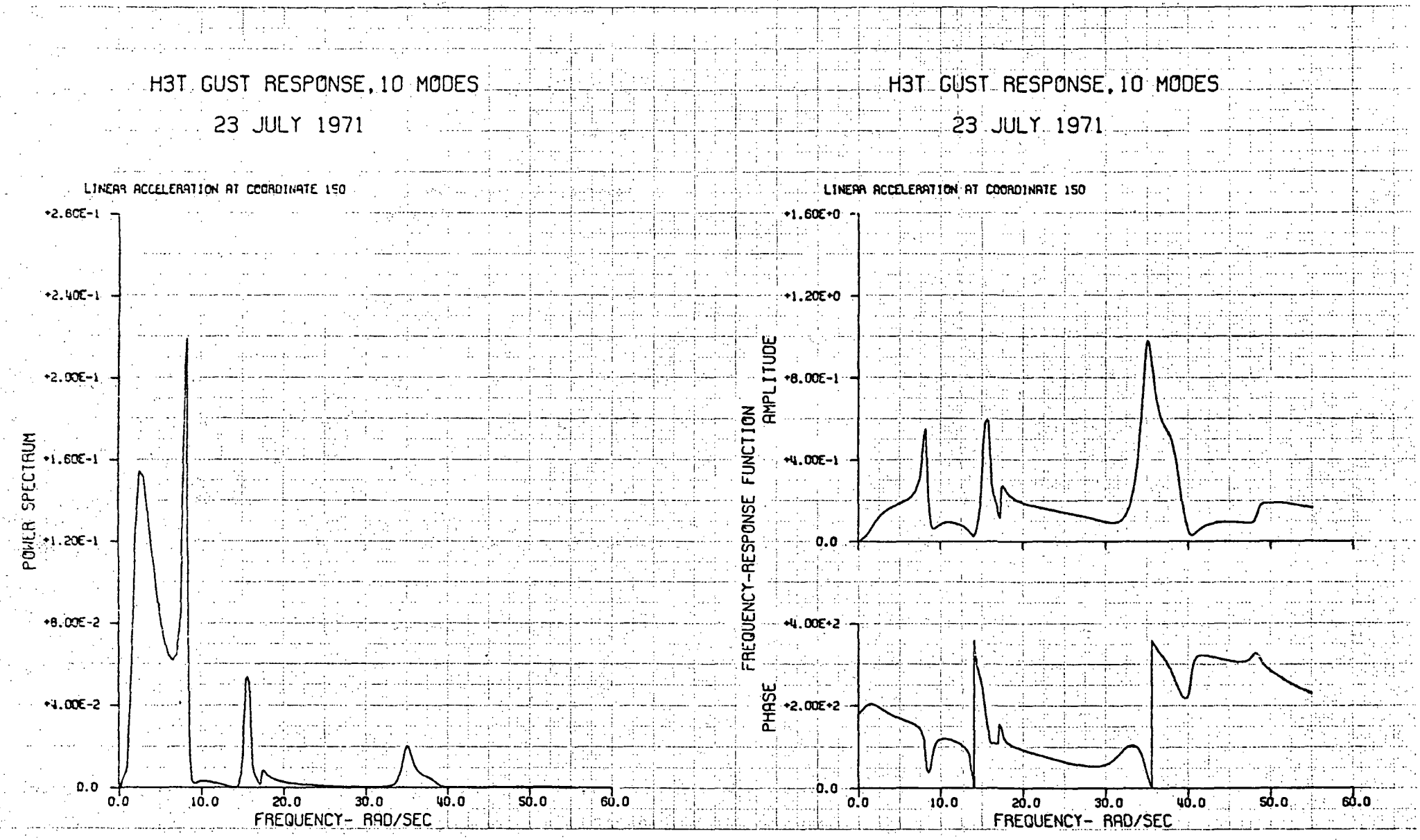
H3T GUST RESPONSE, 10 MODES
23 JULY 1971
LINEAR ACCELERATION AT COORDINATE 150
POWER SPECTRUM
+2.80E-1
+2.40E-1
+2.00E-1
+1.60E-1
+1.20E-1
+8.00E-2
+4.00E-2
0.0
0.0
10.0
20.0
30.0
40.0
50.0
60.0
FREQUENCY- RAD/SEC
H3T GUST RESPONSE, 10 MODES
23 JULY 1971
LINEAR ACCELERATION AT COORDINATE 150
FREQUENCY-RESPONSE FUNCTION
AMPLITUDE
+1.60E+0
+1.20E+0
+8.00E-1
+4.00E-1
0.0
PHASE
+4.00E+2
+2.00E+2
0.0
0.0
10.0
20.0
30.0
40.0
50.0
60.0
FREQUENCY- RAD/SEC

FIGURE A-31

JUDSON BIGELOW INC.

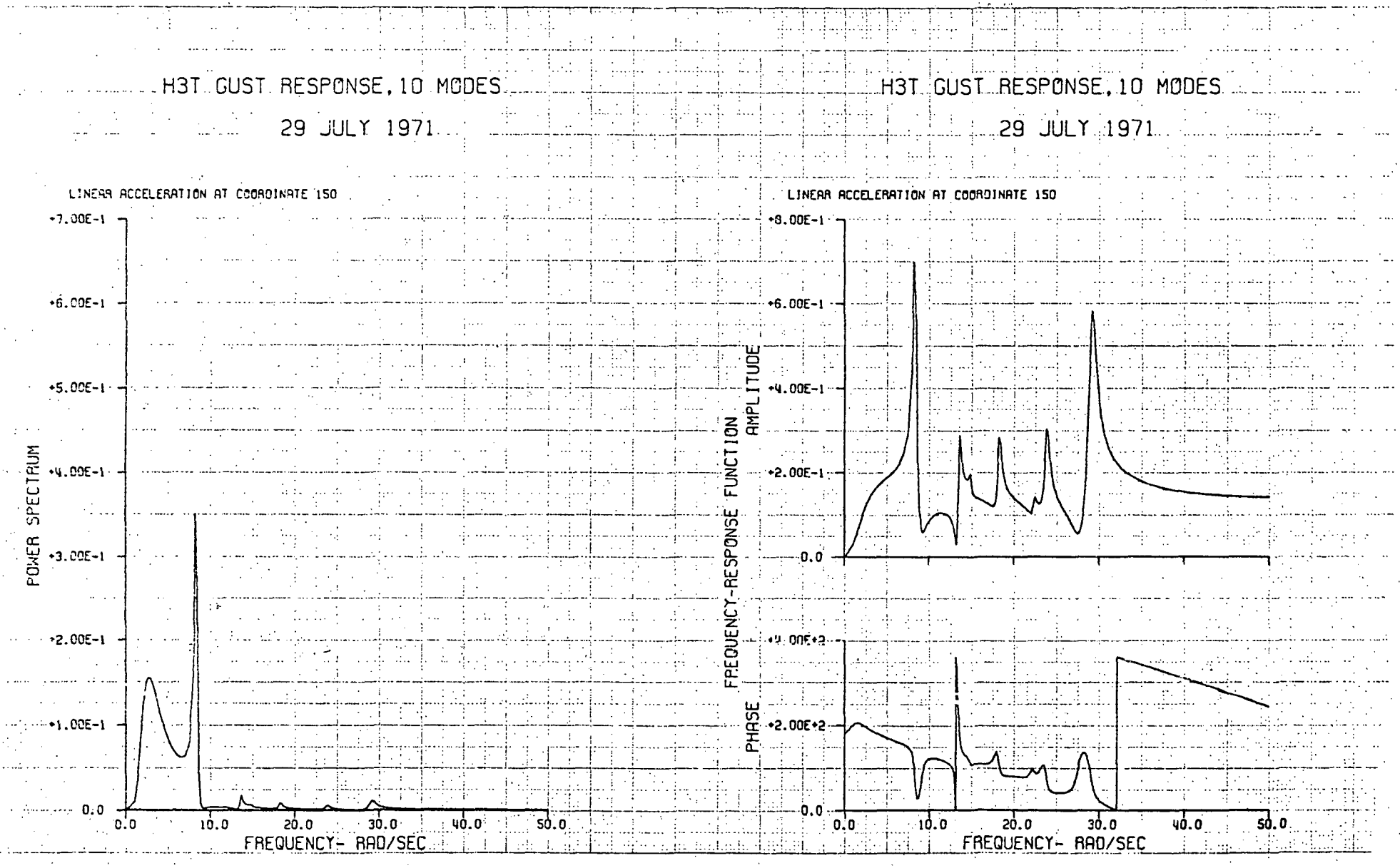

FIGURE A-32

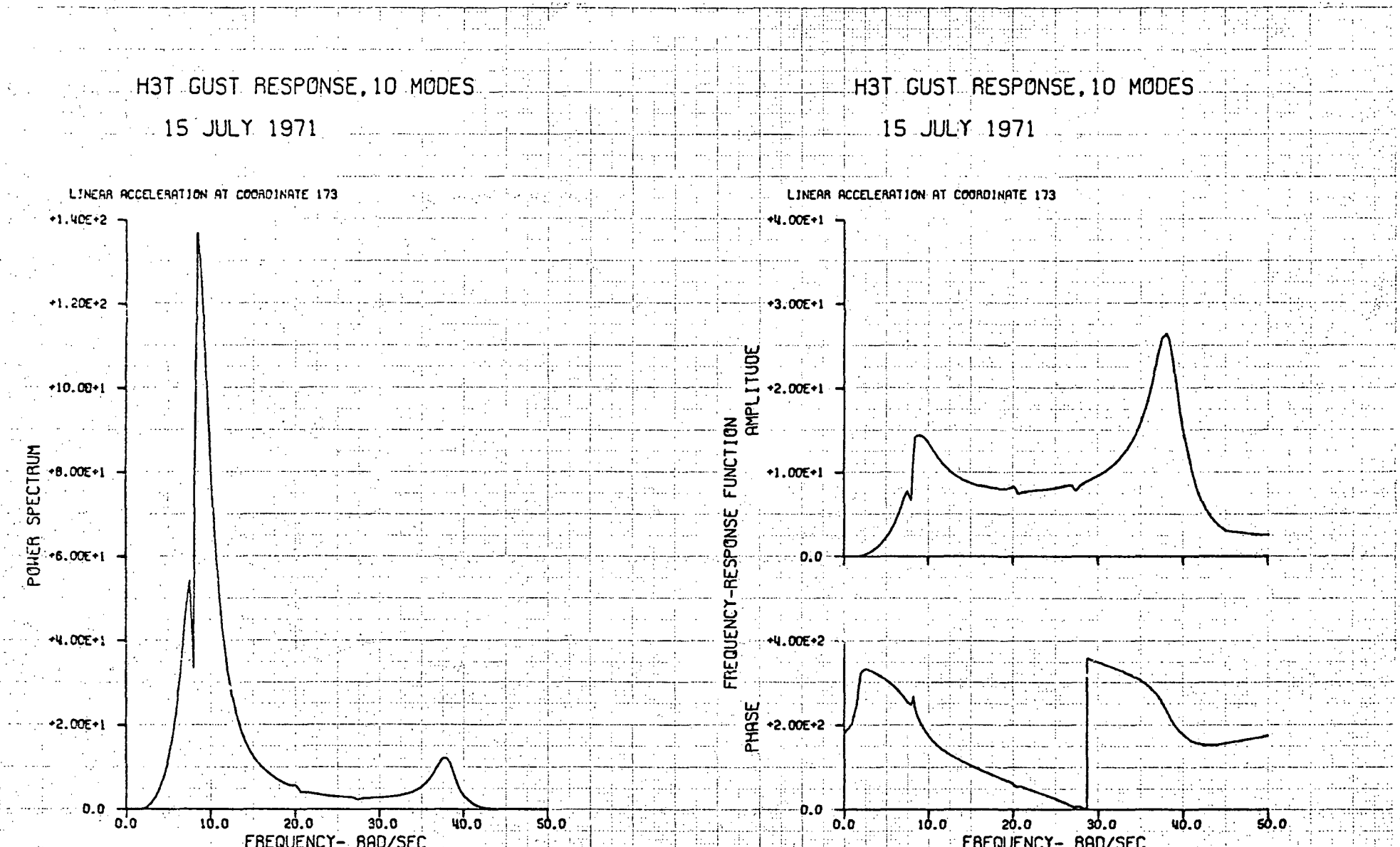
H3T GUST RESPONSE, 10 MODES
15 JULY 1971
LINEAR ACCELERATION AT COORDINATE 173
POWER SPECTRUM
+1.40E+2
+1.20E+2
+10.00+1
+8.00E+1
+6.00E+1
+4.00E+1
+2.00E+1
0.0
0.0
10.0
20.0
30.0
40.0
50.0
FREQUENCY- RAD/SEC
H3T GUST RESPONSE, 10 MODES
15 JULY 1971
LINEAR ACCELERATION AT COORDINATE 173
FREQUENCY-RESPONSE FUNCTION AMPLITUDE
+4.00E+1
+3.00E+1
+2.00E+1
+1.00E+1
0.0
PHASE
+4.00E+2
+2.00E+2
0.0
0.0
10.0
20.0
30.0
40.0
50.0
FREQUENCY- RAD/SEC

FIGURE A-33

JUDSON BIGELOW INC. CHART NO. 02

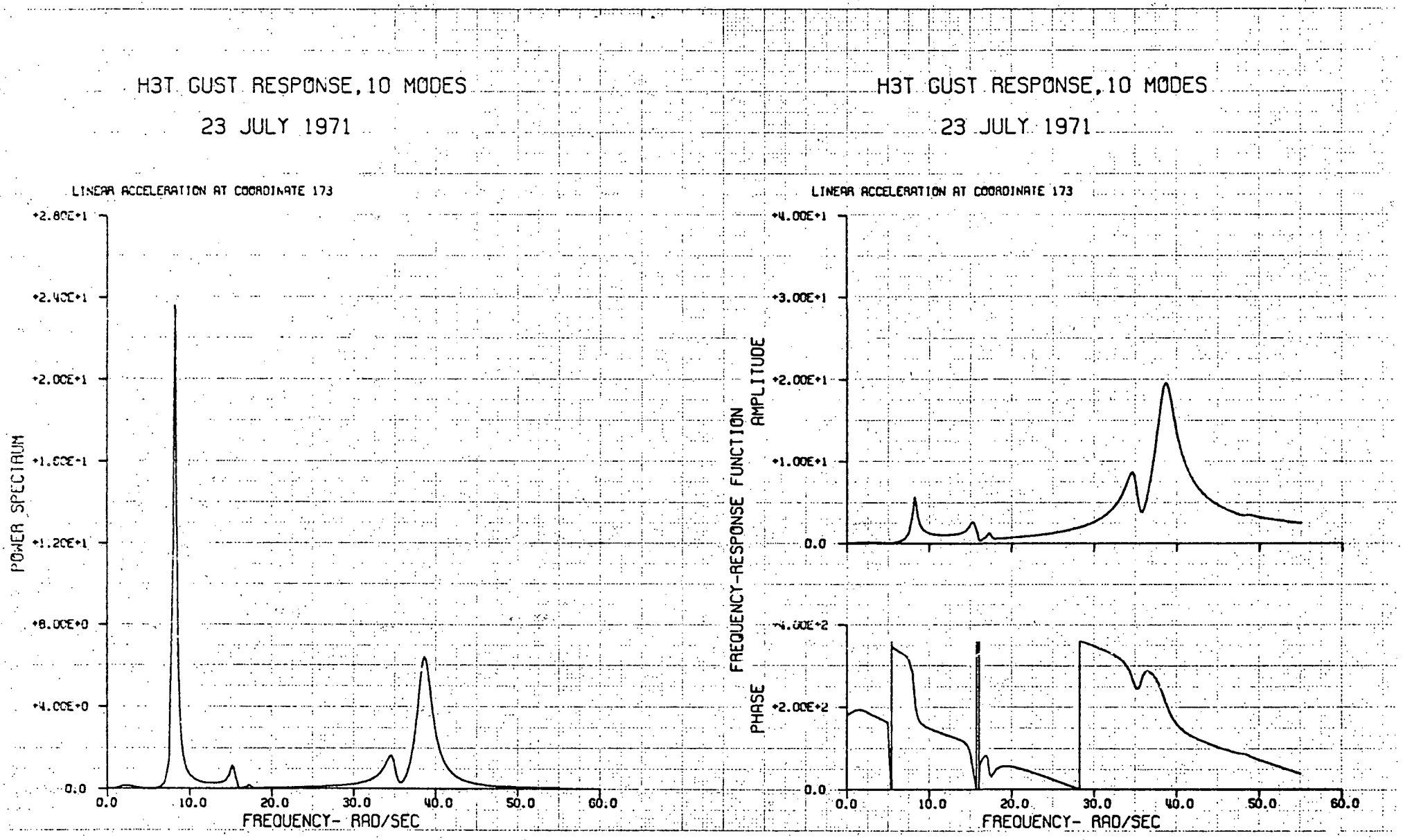

FIGURE A-34

JUDSON BIGELOW INC. CHART NO. 02 CA

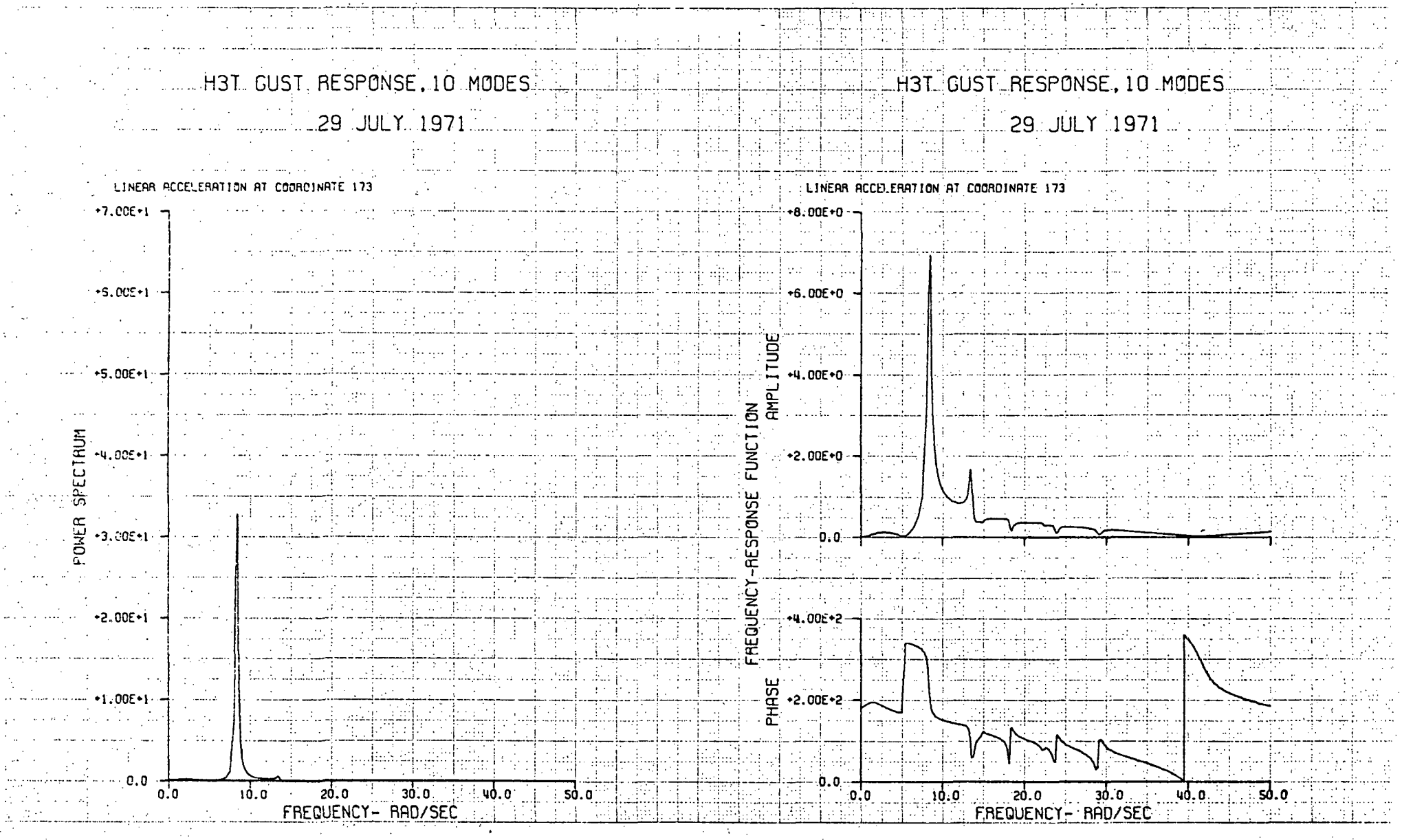

FIGURE A-35

JUDSON BIGELOW INC. CHART NO. 0

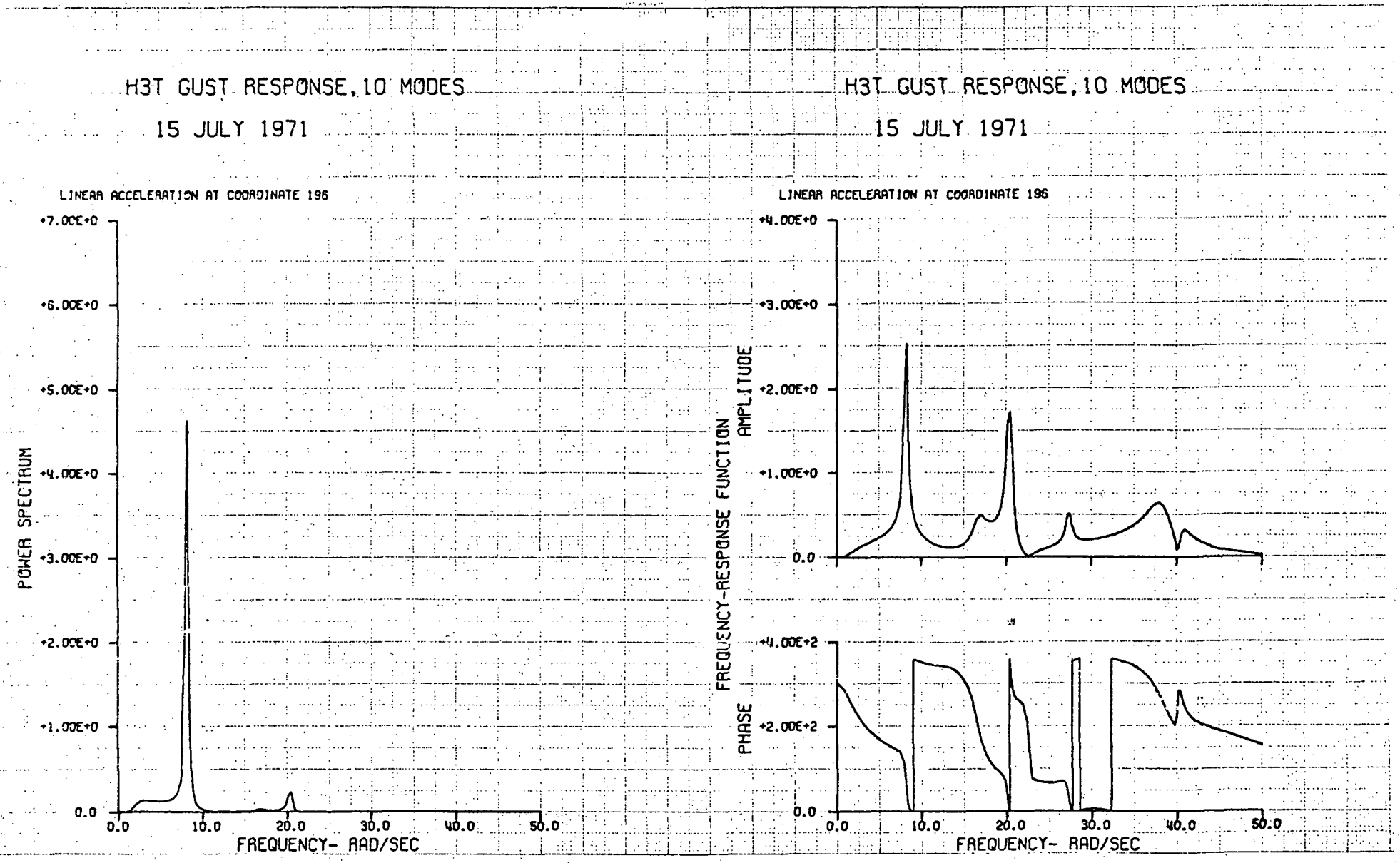

FIGURE A-36

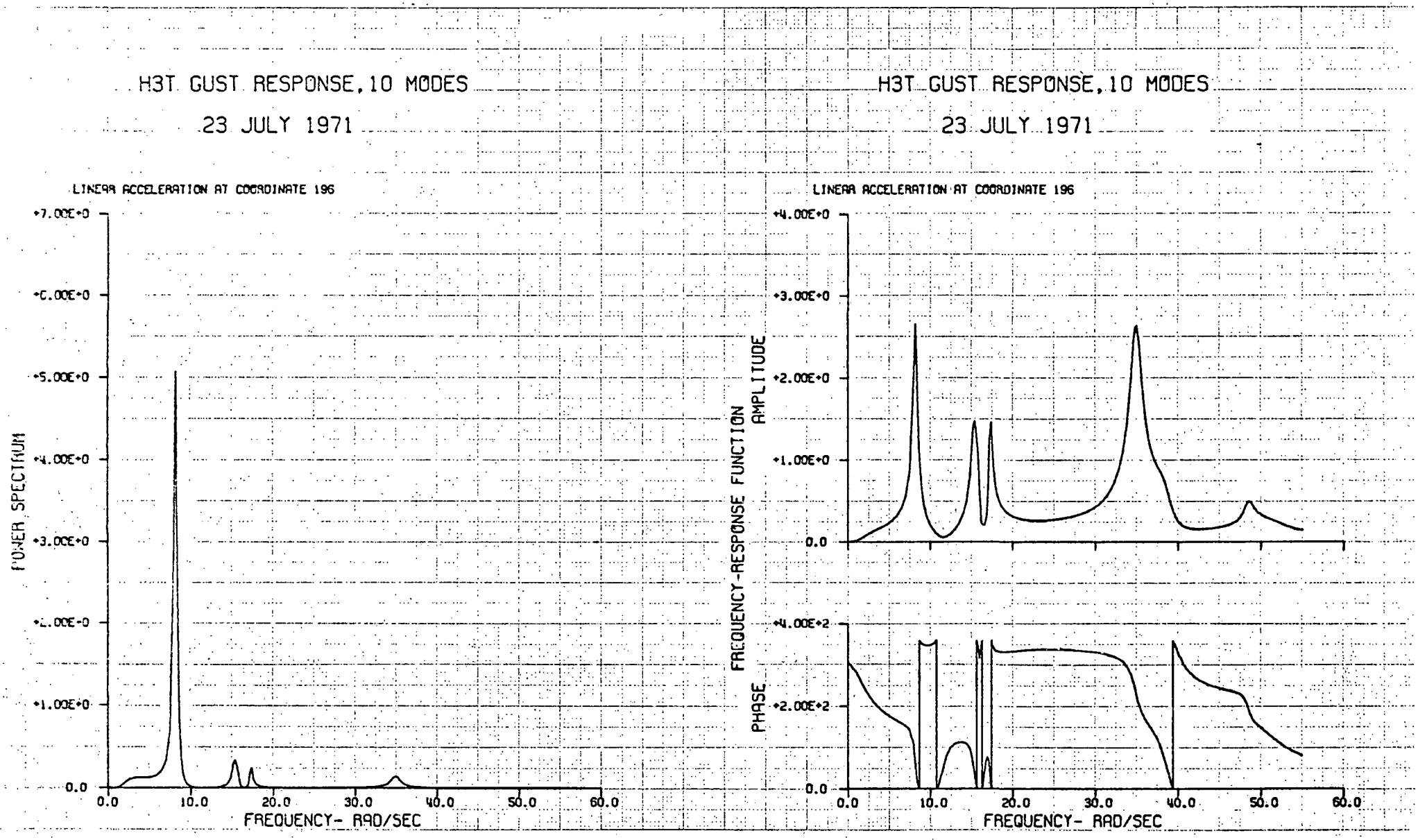
H3T GUST RESPONSE, 10 MODES
23 JULY 1971
LINEAR ACCELERATION AT COORDINATE 196
POWER SPECTRUM
+7.00E+0
+6.00E+0
+5.00E+0
+4.00E+0
+3.00E+0
+2.00E+0
+1.00E+0
0.0
0.0
10.0
20.0
30.0
40.0
50.0
60.0
FREQUENCY- RAD/SEC
H3T GUST RESPONSE, 10 MODES
23 JULY 1971
LINEAR ACCELERATION AT COORDINATE 196
FREQUENCY-RESPONSE FUNCTION
AMPLITUDE
+4.00E+0
+3.00E+0
+2.00E+0
+1.00E+0
0.0
PHASE
+4.00E+2
+2.00E+2
0.0
0.0
10.0
20.0
30.0
40.0
50.0
60.0
FREQUENCY- RAD/SEC

FIGURE A-37

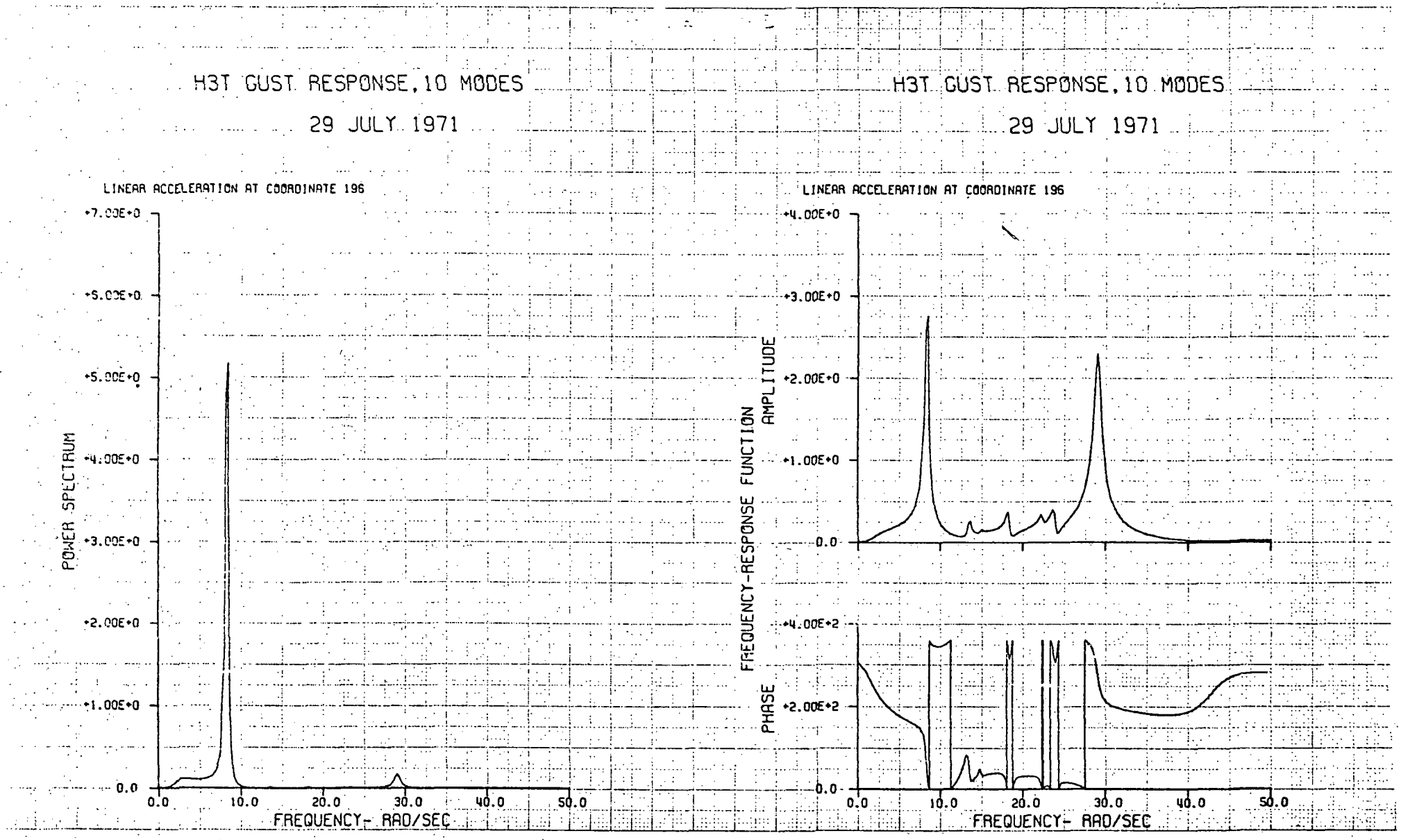
H3T GUST RESPONSE, 10 MODES
29 JULY 1971
LINEAR ACCELERATION AT COORDINATE 196
POWER SPECTRUM
+7.00E+0
+6.00E+0
+5.00E+0
+4.00E+0
+3.00E+0
+2.00E+0
+1.00E+0
0.0
0.0
10.0
20.0
30.0
40.0
50.0
FREQUENCY- RAD/SEC
H3T GUST RESPONSE, 10 MODES
29 JULY 1971
LINEAR ACCELERATION AT COORDINATE 196
FREQUENCY-RESPONSE FUNCTION
AMPLITUDE
+4.00E+0
+3.00E+0
+2.00E+0
+1.00E+0
0.0
PHASE
+4.00E+2
+2.00E+2
0.0
0.0
10.0
20.0
30.0
40.0
50.0
FREQUENCY- RAD/SEC

FIGURE A-38

APPENDIX B

1/10 SCALE DYNAMIC MODEL

PRELIMINARY STRESS ANALYSIS

APPENDIX B

PRELIMINARY STRESS ANALYSIS

TABLE OF CONTENTS

STRUCTURAL ANALYSIS

Structural analysis for the 1/10 scale model design was limited to checking the critical areas for buckling under a 1.5 g limit axial load with the vehicle in an upright launch attitude. A factor of safety of 1.5 to ultimate load was used. The stress analysis effort consisted of determining the approximate number and location of stiffening frames or stringers required. No additional stress calculations were considered necessary because the basic dimensions of the model were scaled down from the prototype which had been designed for critical flight loads and would therefore be adequate for any of the relatively low vibration loads induced during mode surveys. In view of the preliminary nature of the model design, no more detailed stress analyses appeared justifiable.

An overall static equilibruim load distribution of the mated configuration under the ultimate 2.25 g load condition is shown below.

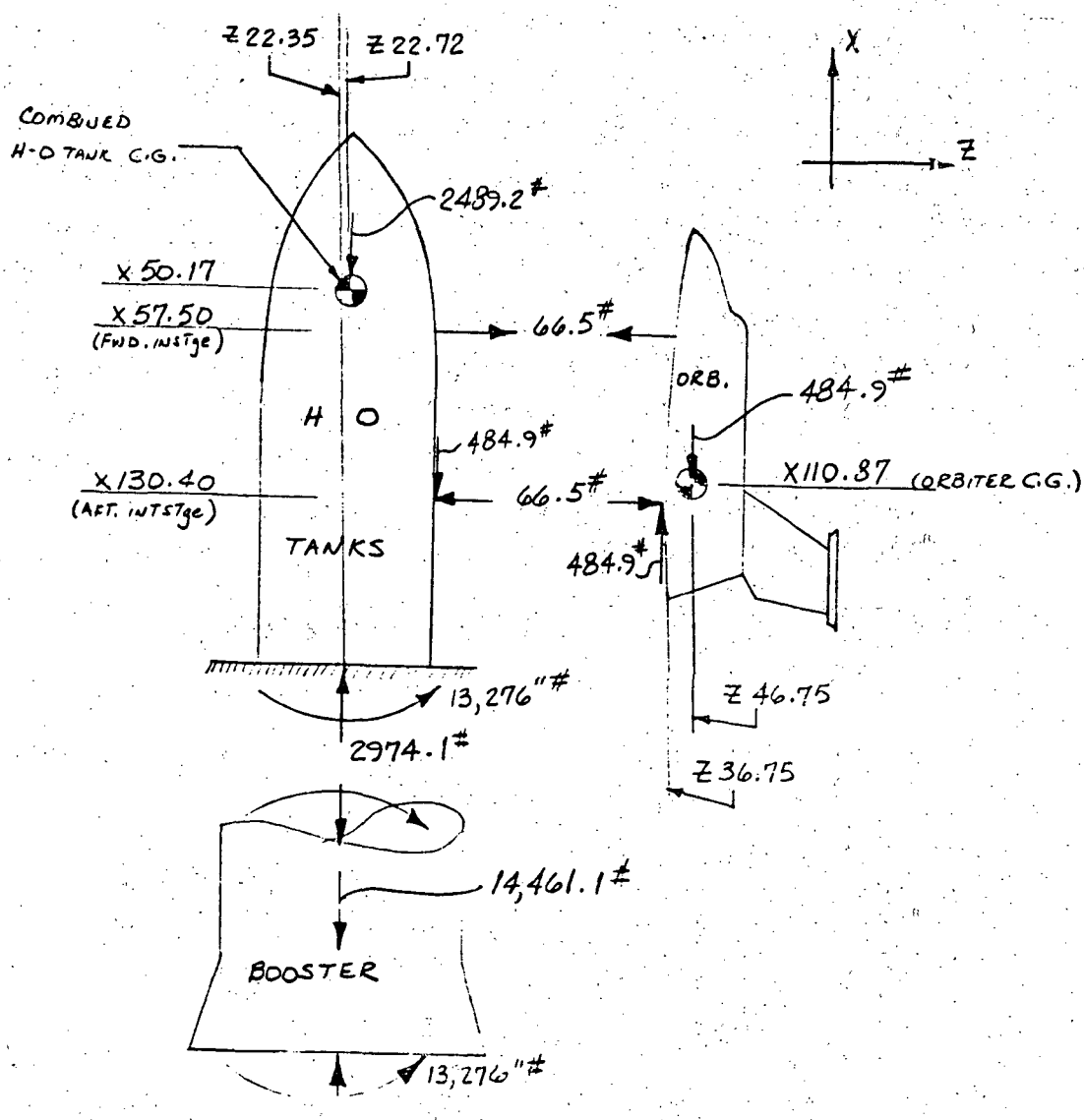

STRESS ANALYSIS

H-O External Tanks

The oxidizer tank utilizes monocoque type construction. The area aft of x station 50.0 is critical for compression buckling and requires intermediate frames spaced between $2\frac{1}{4}$ and 3 5/8 in. This area includes the fwd. intertank skirt, LH_2 tank, and aft interstage skirt. Major bulkheads are located at the fwd. interstage location (x57.5), the aft interstage location (x130.4) and the lag redistribution frame (x112.7). Basic skin is aluminum alloy, .015" thick; it is locally thicker aft of the fwd. interstage location in the upper quadrant for increased buckling capability due to compression bending.

Booster

The booster LO_2 and RP-1 tanks are of monocoque structure construction. Thickness of the LO_2 tank is .167 in., and the RP-1 tank thickness is .139 in. The intertank structure aft of (x270.0) and fwd. of (x302.0) requires no intermediate frames and has an effective thickness of .041 in. The skirt aft of (x329.7) which houses the engine support beams is effectively .025" thick, but requires intermediate frames and stiffeners to prevent buckling. There are Seven main engines, one in the center and six outer engines which are supported by twelve support beams that run between a central six-sided cannister that houses the center engine and the outer shell.

Model Configuration
NAS 1-10635-4

STRESS ANALYSIS

ORBITER

The orbiter fuselage between x57.0 and x130.40 basically consists of thin gage aluminum sheet with corner longerons made up of angle sections upper and lower. The skins are stiffened by intermediate frames at a pitch of approximately 2" with major bulkheads at the forward interstage fitting (x57.50) and the aft interstage location (x130.40). The forward portion of the fuselage is to be mass simulated as is the wing structure. The aft end of the fuselage model shall be simulated in such a manner as to effectively reproduce the true mass and stiffness distribution of the engines, support structure and tail structure.

- EXTERNAL TANKAGE

MODEL CONFIGURATION
1/25/72 PJC

DESIGN CONDITION: HANDLING, 1.50g (X-DIRECTION)

FACTOR of SAFETY (ULTIMATE) = 1.50 ∴ ULTIMATE HANDLING = 2.25g

(ALL STATIONS SHOWN ARE ORBITER STATIONS.)

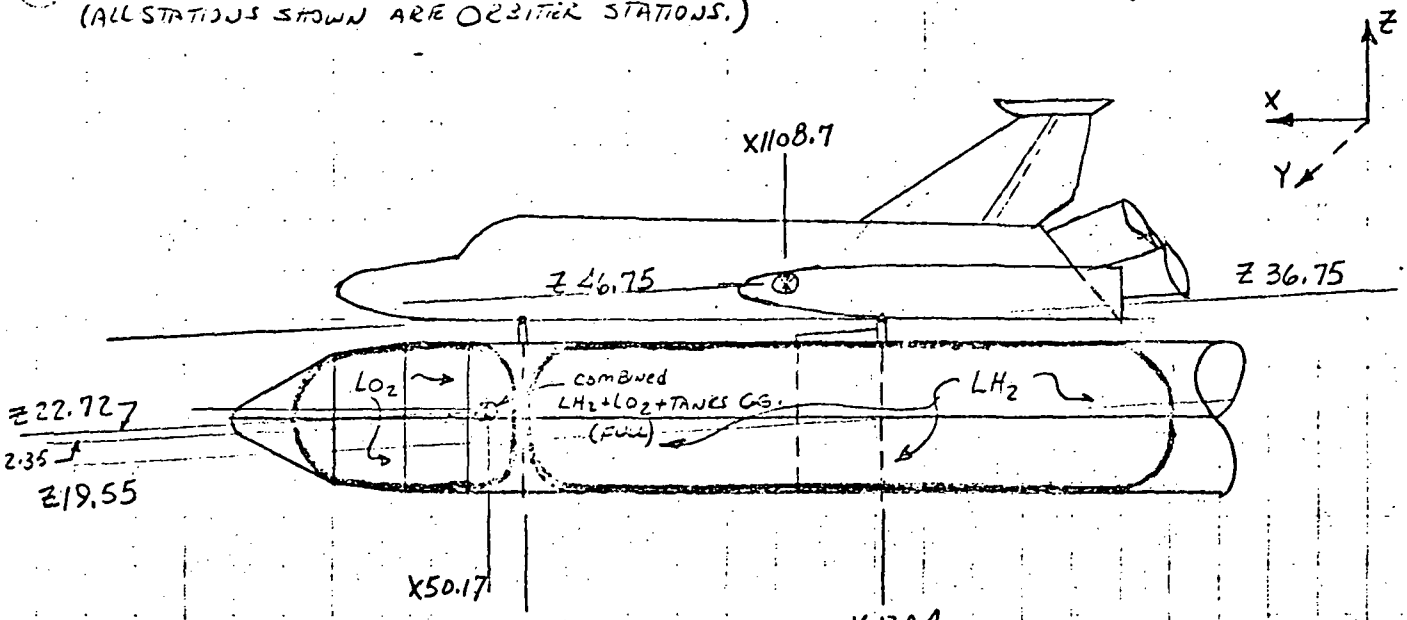

ITEM	1g (LB) MODEL WEIGHT	1.5g (LB.) (LIMIT)	2.25g (LB) (ULTIMATE)
TANKS (FULL)	1106.3	1659.5	2489.2
ORBITER	215.5	323.3	484.9

LOADS USED IN MODEL STRESS ANALYSIS

Case a) 2.25g HANDLING CONDITION ~ ULTIMATE

TANKS SUPPORTED AXIALLY (X) by ORBITER

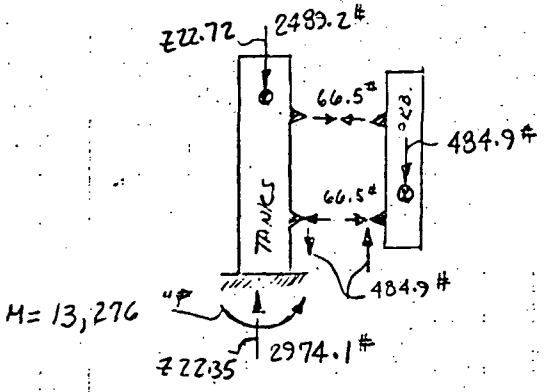

$R = \frac{484.9^{\#} \times 100''}{729''} = 66.5^{\#}$

$M = 66.5^{\#} \times 729'' + 484.9^{\#} \times 14.4'' + 2489.2^{\#}(.37'') = 13,276\ ''^{\#}$

Case b) 2.25g (ULTIMATE) HANDLING CONDITION ~ TANKS HUNG FROM INTERSTAGE PTS OF "HELD" ORBITER

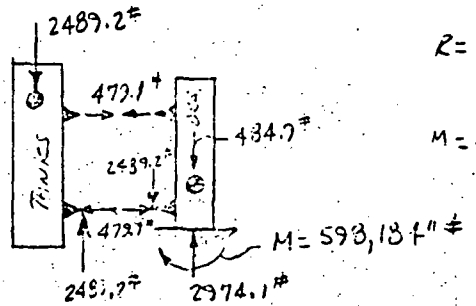

$R = \frac{2489.2^{\#} \times 14.03''}{729''} = 479.1^{\#}$

$M = 472.1^{\#}(729'') + 2489.2^{\#}(\quad'') = 59,818\ ''^{\#}$

case a)

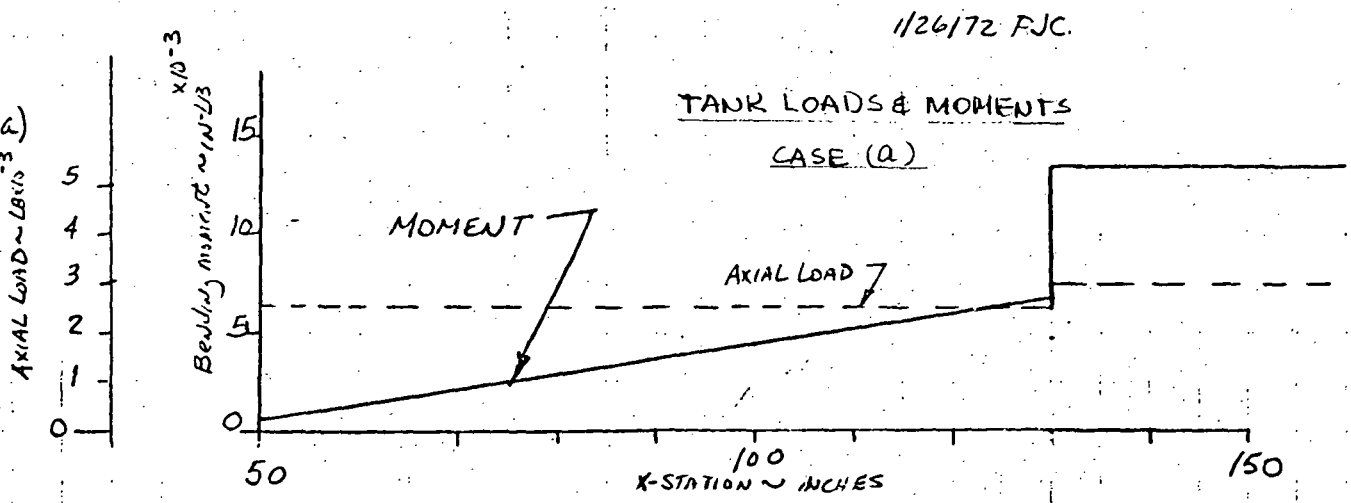

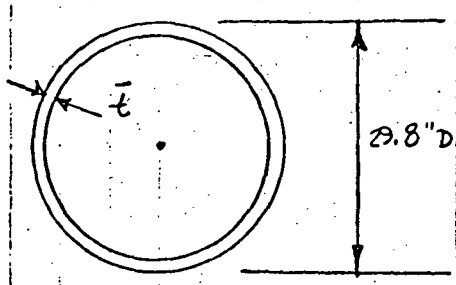

EQUATION FOR STRESS

Assume that $t = .016$" ALUMINUM

$A = 2\pi r t = \pi D t$

$I = \pi r^3 t = \frac{\pi D^3 t}{8}$

$S = I/c = \pi r^2 t = \frac{\pi D^2 t}{4}$

$$\therefore f = \frac{P}{A} + \frac{Mc}{I} = \frac{P}{\pi D t} + \frac{MD}{\frac{2\pi D^3 t}{8}} = \frac{P}{\pi D t} + \frac{4M}{\pi D^2 t} = \frac{1}{\pi D^2 t}[PD + 4M]$$

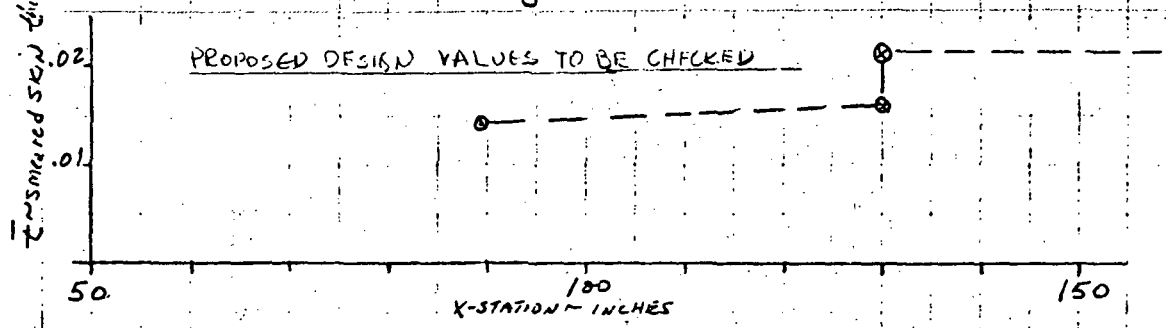

$$F_{cr} = .194\, E t/r = \frac{.194 \times 10.5 \times 10^6 \times t}{29.8/2} = 136.7 \times 10^3\, t$$

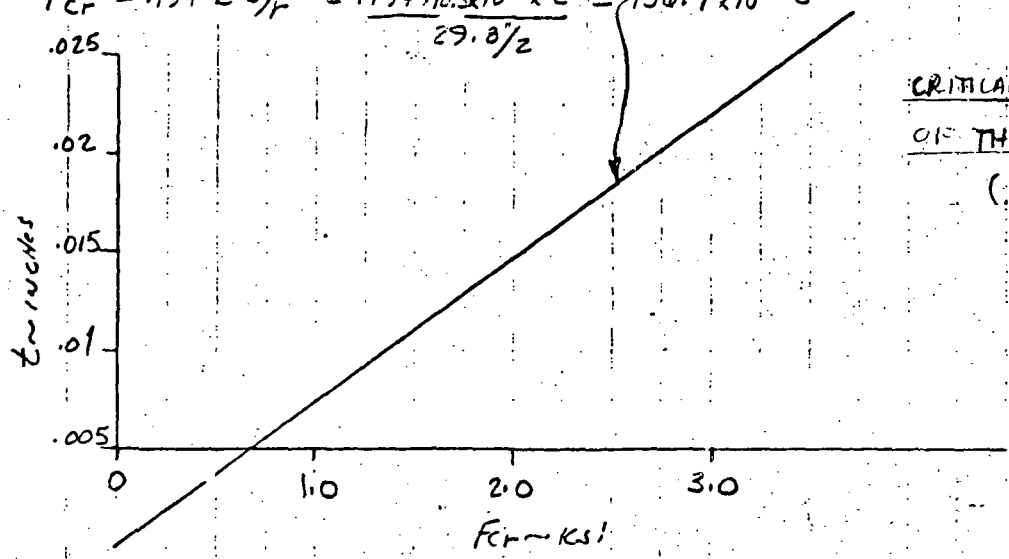

CRITICAL STRESS FOR BUCKLING OF THIN CYLINDRICAL TUBE (BRUHN)

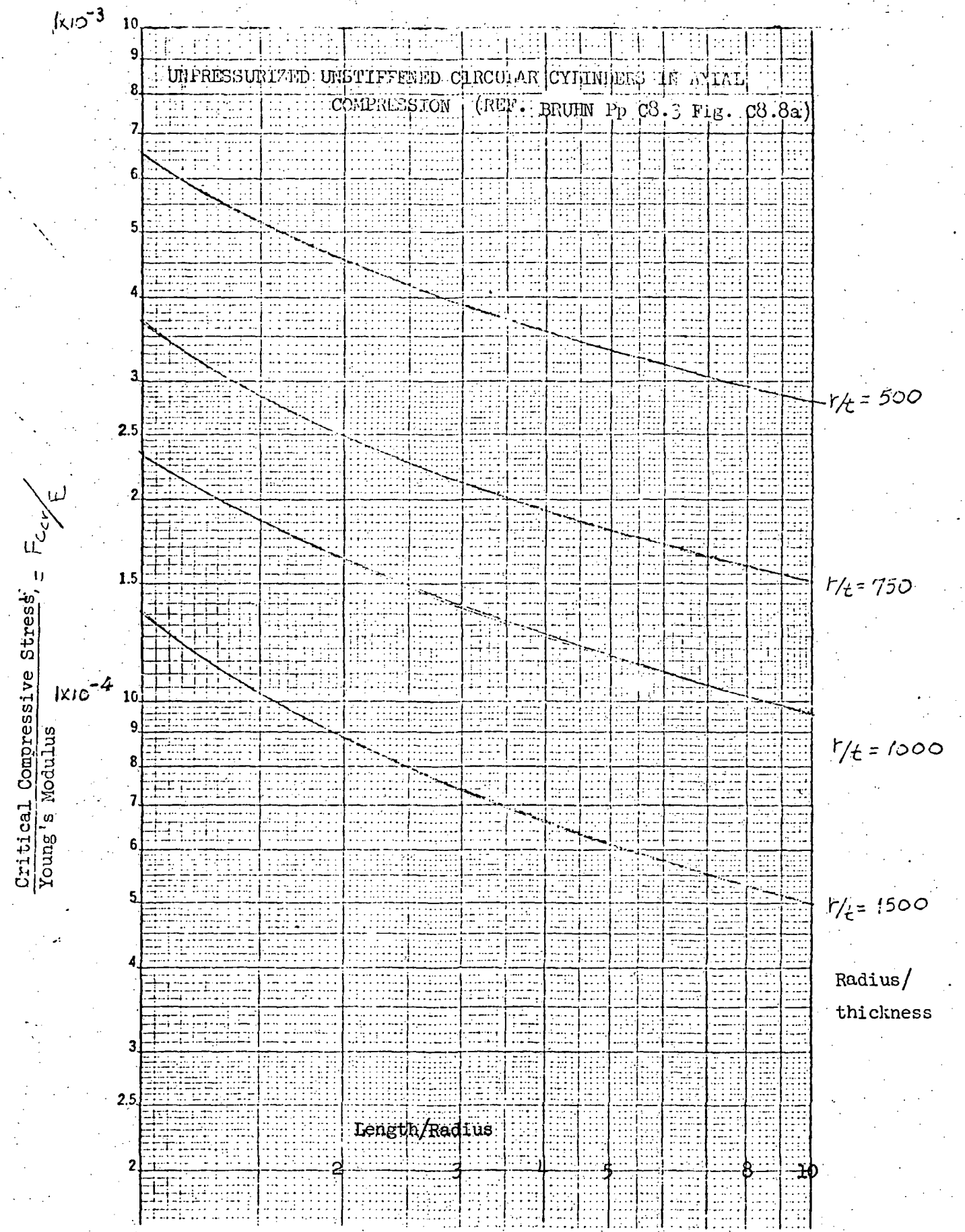
UNPRESSURIZED UNSTIFFENED CIRCULAR CYLINDERS IN AXIAL COMPRESSION (REF. BRUHN Pp C8.3 Fig. C8.8a)
1x10-3
1x10-4
Critical Compressive Stress / Young's Modulus = Fcr/E
r/t = 500
r/t = 750
r/t = 1000
r/t = 1500
Radius/ thickness
Length/Radius
10
9
8
7
6
5
4
3
2.5
2
1.5
2
3
4
5
8
10

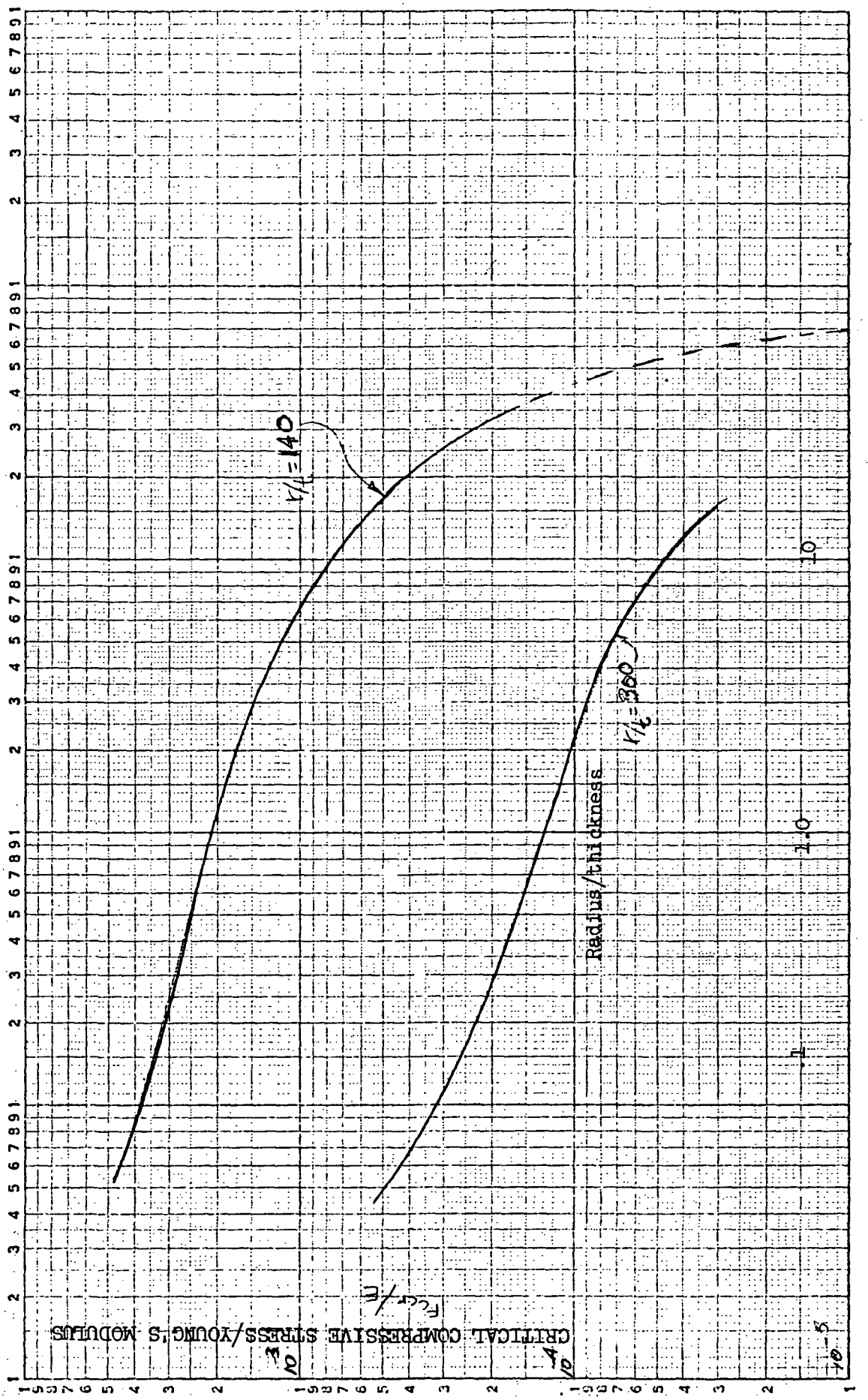
CRITICAL COMPRESSIVE STRESS/YOUNG'S MODULUS
Length/Radius
(L/r)
Radius/thickness
r/t=140
r/t=360
1.0
10
10^{-3}
10^{-4}
10^{-5}

2/2/72 PJC

DETERMINING FRAME SIZE REQUIRED

PANEL INSTABILITY STRENGTH: ref. Bruhn, P. C9.11, & Shanley, P. 67

$(EI)_{frame} = \frac{MD^2}{16000L}$ = req'd stiffness of Frame to prevent general instability of a stiffened shell in Bending.

$\therefore$ @ STATION $\cong$ 100 inches, $(EI)_f = \frac{(450)(29.8)^2}{16000\,(1.86)} = \frac{3956.18}{29.76} = \underline{\underline{134.3}}$ LB-IN^2

$\therefore I_f$ (required) $= \frac{134.3}{10.5\times10^6} = \underline{\underline{12.8\times10^{-6}}}$ IN^4

try a Section AS Follows:

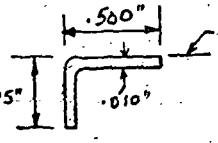

$A = .010\,(.500 + .365) = .00865$ IN^2

$Ay = (.01)(.50)(.005) + (.01)(.365)(.1925) = .000727625$

$Ay^2 = (.005)(.005)^2 + (.00365)(.1925)^2 = 135.380\times10^{-6}$

$I_{o\,x-x} = 1/12\,(.5)(.01)^3 + 1/12\,(.01)(.365)^3 = 40.564\times10^{-6}$ in^4

$\therefore \bar{y} = \frac{.727625}{8.65} = \underline{\underline{.0841}}$''

@ $I_{NA}{}_{x-x} = 10^{-6}(40.564 + 135.380) - .00865\,(.0841)^2 = (175.944 - 61.194)\times10^{-6} = \underline{\underline{114.75\times10^{-6}}}$ IN4

try section as follows:

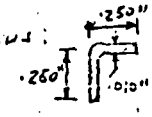

$A = .010\,(.250 + .240) = .00490$ IN^2

$Ay = (.01)(.250)(.005) + (.01)(.240)(.130) = .0003245$ $\therefore \bar{y} = \frac{.3245}{4.90} = .06622$''

$Ay^2 = .0025(.005)^2 + .0024(.13)^2 = 40.622\times10^{-6}$

$I_{o\,x-x} = 1/12\,(.25)(.01)^3 + 1/12\,(.01)(.24)^3 = 11.541\times10^{-6}$

$\therefore I_{NA}{}_{x-x} = 10^{-6}(52.163) - \underbrace{.0049\,(.06622)^2}_{21.487\times10^{-6}} = \underline{\underline{30.676\times10^{-6}}}$ IN4 ← use this

@ Section @ $\cong$ 1400 inches, I_f (req'd) $= \frac{(13,275)(29.8)^2}{16\,000\,(7.45)\,(10.5\times10^6)} = \underline{\underline{9.42\times10^{-6}}}$ IN4

2/3/72 PJC

HO EXTERNAL TANK

SKIN SIZING & FRAME SPACING BASED ON AXIAL LOAD - TO AVOID BUCKLING CONSIDERATIONS ONLY, ASSUMING that upper SKIN (UNcomp.) will be modified

ORBITER STA.	RADIUS	TANK LOWER THICKNESS	AXIAL LOAD	f_c Comp. stress	$E \times 10^{-6}$	f_c/E	r/t	L/r	L
50	14.9 IN.	.014 IN.	2490 LB	1900 PSI	10.5 PSI	1.81×10^{-4}	1064	.15	2.25 IN
60	14.9	.014	2490	1900	10.5	1.81×10^{-4}	1064	.15	2.25 IN
75	14.9	.015	2490	1770	10.5	1.69×10^{-4}	993	.185	2.75 IN
710	14.9	.016	2490	1660	10.5	1.58×10^{-4}	931	.240	3.60 IN
120	14.9	.016 ADJ.	2735 ADJ. (LOAD INCREASE AREA)	1825	10.5	1.74	931	.200	3.00 IN
130	14.9	.016	2975	1985	10.5	1.89	931	.17	2.50 IN

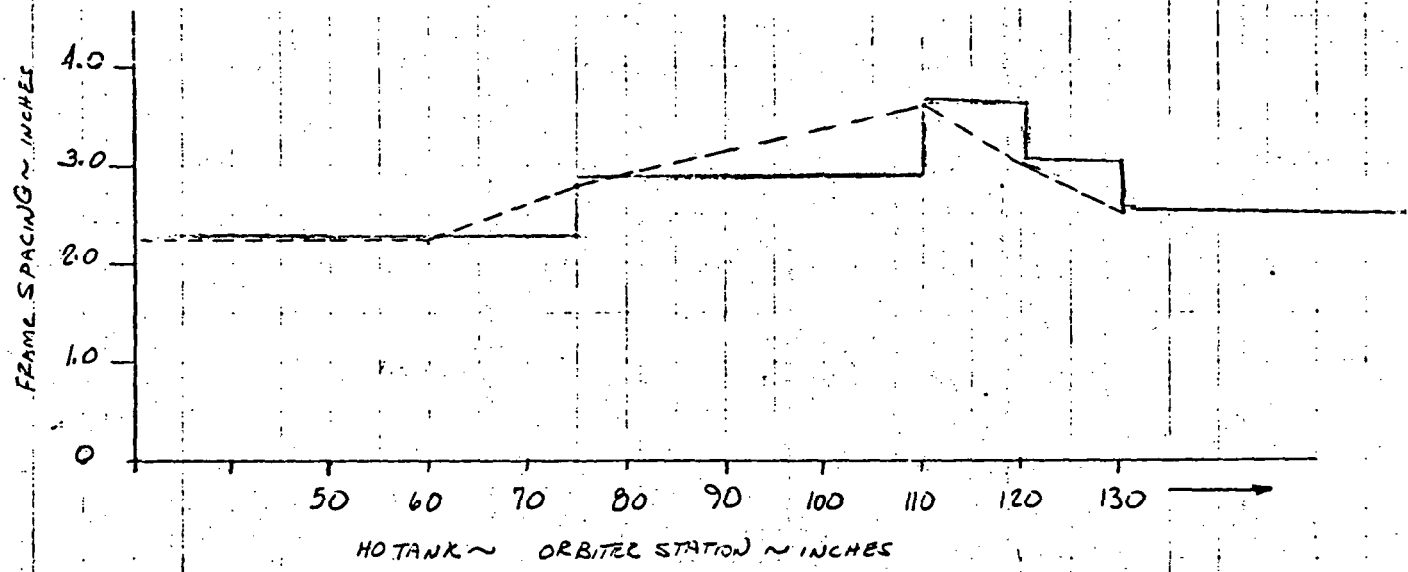

MODEL CONFIGURATION

BOOSTER DESIGN LOADS FOR 2/4/72 PJC

MODEL SUPPORTED AT BASE OF BOOSTER

ITEM	X-STATION LOCATION	LOAD (LB)/1g		2.25g (ULTIMATE)
1) ORBITER + HOTANKS	~181.0	1321.8		2974.1 #
2) STRUCTURE (DRY)	~185.8	40.3	105.3 # combined	236.9 #
3) N_2	~190.8	65.0		
4) LOX + DRY STRUCTURE	~240	4113.0		9254.2 #
5) FREON + DRY STRUCTURE	~286.3	74.7		168.1 #
6) RP-1 + DRY STRUCTURE	~315.0	1722.8		3876.3 #
7) ENGINES	~351.2	282.9	404.7 # combined	910.6 #
8) DRY STRUCTURE	~361.0	121.8		
		Σ = 7742.3 LB		Σ = 17420.2 #

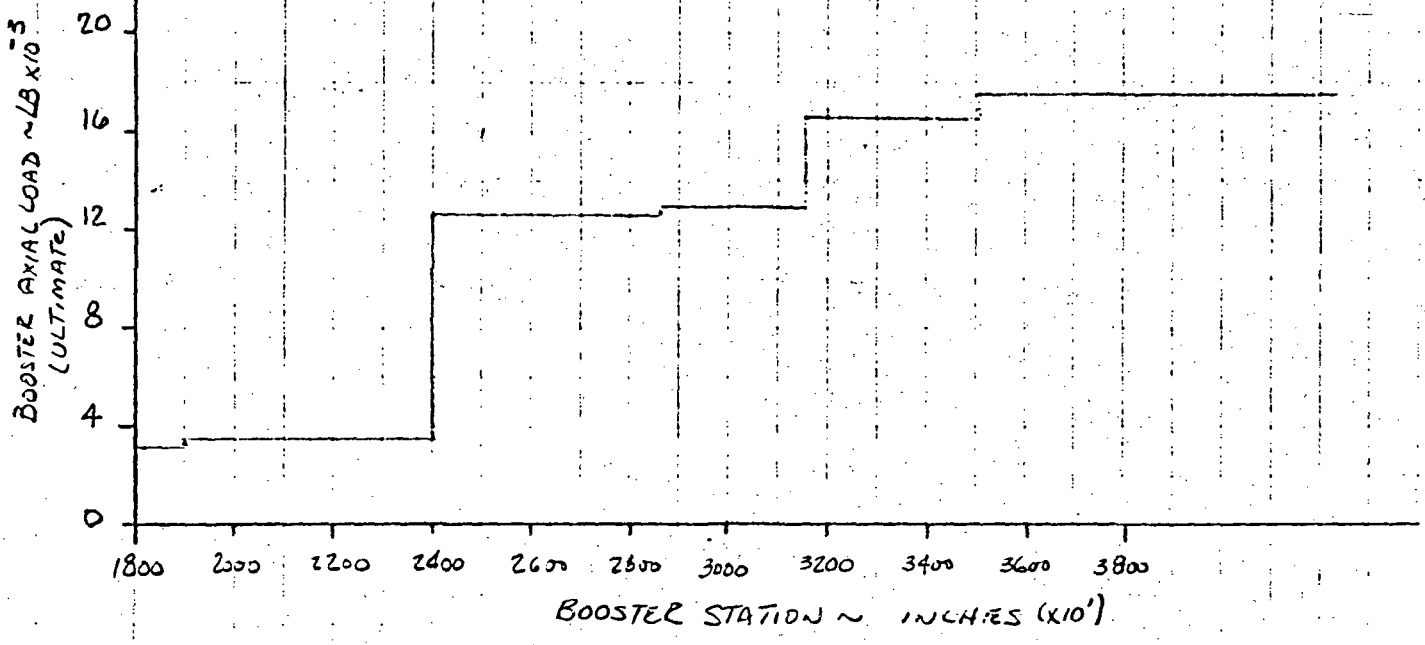

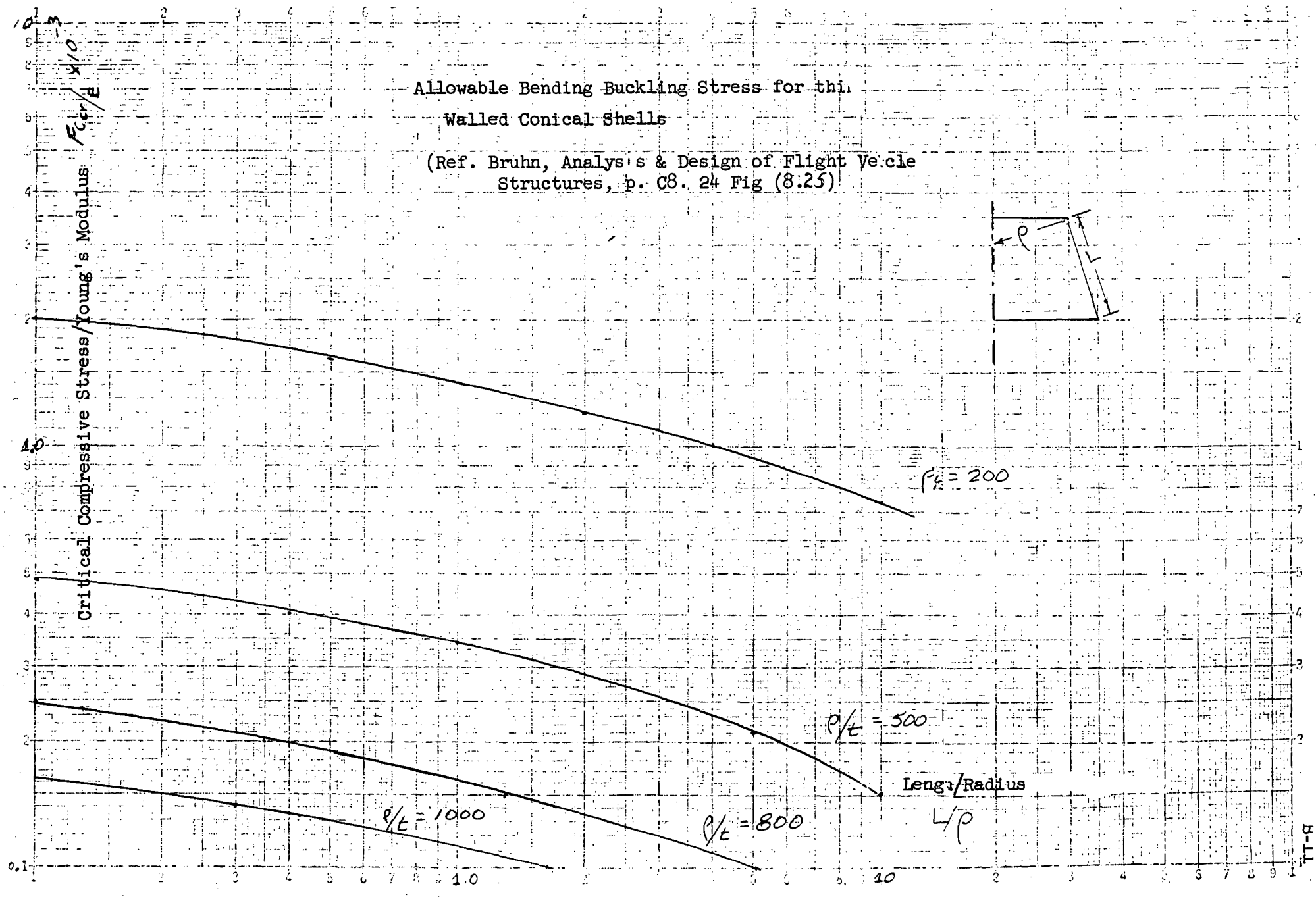
Allowable Bending Buckling Stress for thi
Walled Conical Shells
(Ref. Bruhn, Analys s & Design of Flight Ve cle
Structures, p. C8. 24 Fig (8.25)
Critical Compressive Stress/Young's Modulus $F_{c_{cr}}/E \times 10^{-3}$
$\rho/t = 200$
$\rho/t = 500$
$\rho/t = 800$
$\rho/t = 1000$
Length/Radius
L/ρ
1.0
10
0.1
B-11

2/7/72 PJC

SKIN SIZING & FRAME SPACING FOR BOOSTER

STATION	RADIUS	thickness	AXIAL LOAD	(f) COMP. STRESS	$(\times 10^{-6})$ E	$(\times 10^4)$ f/E	F/t	L/r	L
				PSI	PSI				
~191.0	14.9 IN	.016 IN	3211#	2150	10.5	2.05	931	.15	2.25 IN
~227.5	19.8 IN	.140 IN	3211#	185	10.5	.18	141	APPROX. 65 EXTRAPOLATED VALUE	1287 IN
~240.0	19.8 IN	.167 IN	12,465#	600	10.5	.57	118	APPROX 50 EXTRAP. VALUE	990 IN
700 → ~ 3020	19.8 IN	.041 IN	12633#	2480	10.5	2.36	483	2.0	39.6 IN
3020 → ~ 3297	19.8 IN	.139 IN	16,510#	960	10.5	.91	142	APPROX. 45 EXTRAPOLATED VALUE	891 IN
3297 SKIRT	19.8 IN	.025 IN	16510#	5310	10.5	5.06	792	.05	1.00 IN.

FROM ABOVE, FRAMES ARE ONLY REQUIRED FORWARD OF STA 191 & AFT OF 330

BOOSTER (AFT END)

SIZING of FRAME SPACING Required AT BOOSTER BASE

2/9/72 PJC

(Ref. P. 7)

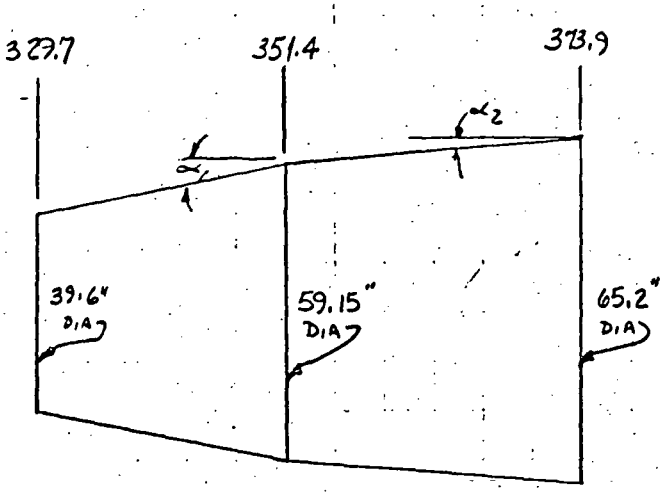

STA. 329.7 → 351.4 ($L = 21.7$") $P = 16,510$ LB. ; $t = .025$"

$\alpha_1 = TAN^{-1} \frac{9.775}{21.7} = TAN^{-1}.45046 = 24°15'$ & $\cos\alpha_1 = .91176$

$\therefore \rho = \frac{39.6}{2(.91176)} = 21.716$ IN & $\rho/t = \frac{21.716}{.025} = 869$ & $L = \frac{21.7}{.91176} = \underline{23.8}$ IN & $L/\rho = \frac{23.8}{21.716} = 1.1$

$\therefore \frac{F_c}{E} = .14 \times 10^{-3}$ $\therefore F_c = .14 \times 10^{-3} \times 10.5 \times 10^6 = 1470$ PSI

$P_{ACT} = 16510$ LB & $A = \pi Dt = \pi(39.6)(.025) = 3.110$ IN^2 & $\therefore F_{ACT.} = \frac{16510}{3.110} = \underline{5310}$ PSI

NOW 5310 PSI > 1470 PSI $\therefore$ FRAMES ARE Needed

ASSUMPTIONS USING CYLINDRICAL DATA:

(@ x 329.7) $r/t = \frac{19.8}{.025} = 792$; $f/E = \frac{5310}{10.5 \times 10^6} = \underline{5.06 \times 10^{-4}}$ $\therefore L/r \cong .065$ $\therefore L = \underline{1.30}$"

(x 351.4) $r/t = \frac{29.575}{.025} = 1183$; $f = \frac{16510}{\underbrace{\pi(59.15)(.025)}_{4.645}} = \underline{3560}$ psi & $f/E = 3.39 \times 10^{-4}$ $\therefore L/r = .055$ & $L = 1.625$"

STA. 329.7
DIA. = 39.6"

XSTA. 351.4
DIA = 59.15"

Assume that longitudinal stiffeners are to be added:

$C_1 = \pi D_1 = \pi(39.6) = 124.41"$

$C_2 = \pi D_2 = \pi(59.15) = 185.83"$

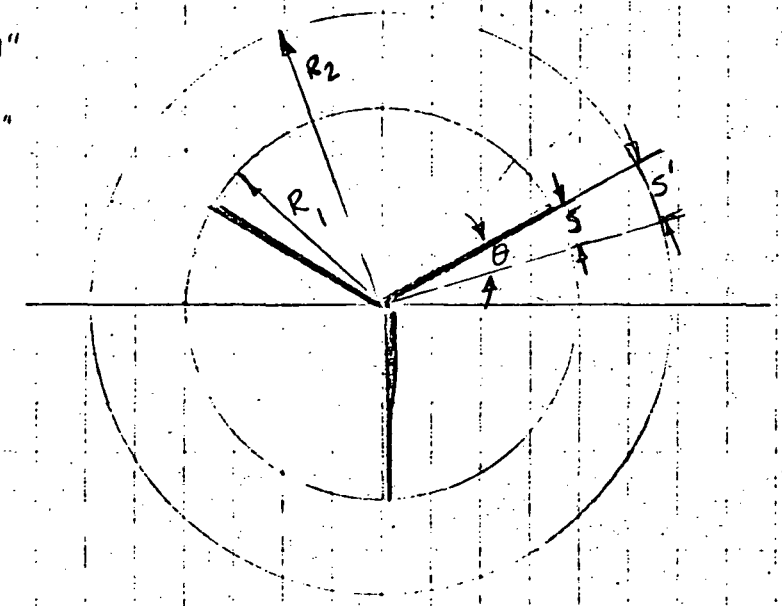

Arc Length $(S) = \frac{\pi r \theta}{180} = \frac{\pi D \theta}{360}$ $\therefore \theta = \frac{360 S}{\pi D}$

STA. 329.7 :

S (in)	πD	360/πD	θ Deg.	Deg-min
1.0	124.41	2.894	2.834	2°-54'
2.0	↕	↕	5.788	5°-47'
3.0			8.682	8°-41'
4.0			11.576	11°35'

$D_2/D_1 = \frac{59.15}{39.6} = 1.494$ ✓ o.k. chad

STA 351.4

S' (in)	πD	360/πD	θ Deg.
1.494	185.83	1.937	2.894
2.988	↕	↕	5.788
4.482			8.682
5.975			11.576

AFT BOOSTER STRUCTURE
STA 329.7 → 351.4

MODEL CONFIGURATION
2/12/72 PJC

Assume we use stiffeners @ 2.00" spacing at sta. 329.7. This is equivalent to about 3.00" spacing at station 351.4

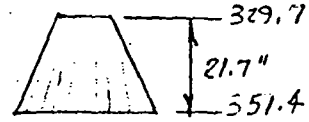

Now Let's try to find the frame spacing we need to attain our goal.

Ref. GSM, P. B5.21-1 : based on an "Average" Section

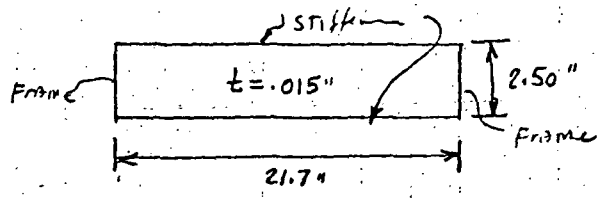

$$z = b^2/rt = \frac{(2.5)^2}{(24.7)(.015)} = \frac{6.25}{.371} = 1.69 \quad \therefore K_{c_{cr}} \cong 4.0$$

$$\therefore F_{c_{cr}} = K_{c_{cr}} E (t/b)^2 = 4.0 \times 10.5 \times 10^6 \left(\frac{.016}{2.5}\right)^2$$

$$\therefore F_{c_{cr}} = 3780 \text{ psi}$$

$$F_{\substack{ACT \\ Avg.}} = 1/2(3560 \text{ psi} + 5310 \text{ psi}) = 4435 \text{ psi} \quad \text{: this is not acceptable}$$

and a closer stiffener spacing is req'd (2.3" would be adequate)

ORBITER

MODEL CONFIGURATION

2/16/72 PJC

MODEL AREAS AND INERTIAS

REQUIRED TO MATCH PROTOTYPE

$E = 10 \times 10^6$ PSI Assumed

PROTOTYPE STATION	PROTOTYPE $(EA)_P (\times 10^{-9})$	MODEL $(EA)_m (\times 10^{-6})$	MODEL A_m (IN^2)	PROTOTYPE $(EI)_P (\times 10^{-12})$	MODEL $(EI)_m (\times 10^{-6})$	MODEL I_m (IN^4)
318	.199	1.99	.199	.300	30	3.0
570	.199	1.99	.199	.300	30	3.0
570 - 704	.258	2.58	.258	.470	47	4.7
704 - 832.5	.372	3.72	.372	.780	78	7.8
832.5 - 929.5	.444	4.44	.444	1.05	105	10.5
929.5 - 1006	.503	5.03	.503	1.26	126	12.6
1006 - 1162	.566	5.66	.566	1.56	156	15.6
1162 - 1237	.625	6.25	.625	1.87	187	18.7
1237 - 1314	.670	6.70	.670	2.06	206	20.6
1314 - 1382	.690	6.90	.690	2.16	216	21.6
1382 - 1413	.690	6.90	.690	2.16	216	21.6

COMPARISON OF DESIGN AND PROTOTYPE ORBITER AREA AND INERTIA AT STATION 57

MODEL CONFIGURATION
2/17/72 PJC

STA 570

ASSUME ALL STIFFNER AREAS ARE ANGLE SECTIONS of 3/8" × 3/4" × .020"

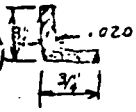

ref. GSM, P. 23.33-445 - LOCATION OF d (NEUTRAL AXIS) AND ρ (RADIUS OF GYR.)

$b_w/b_F = 1.0$; $b_F/t = \frac{.75}{.020} = 37.5$ ∴ $\rho_{yy} = k b_F = .319 \times .750 = .239$ & $d = J \times b_F = .266 \times .75 = .200$" (NEUTRAL AXIS LOCATION)

∴ $I = \rho^2 A = (.239)^2 (.020)(1.981) = .00169$ IN⁴

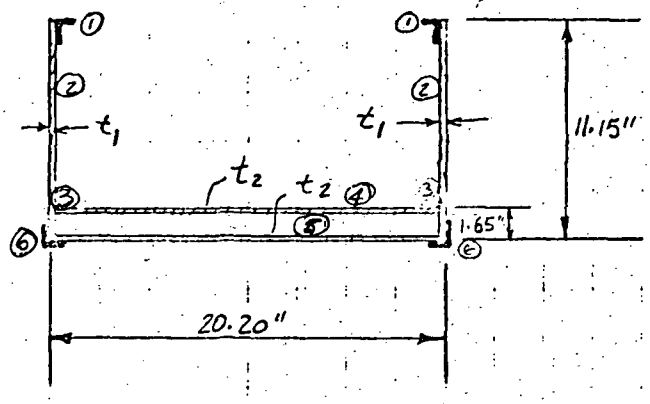

1/10 SCALE SIZE

1ST ASSUMPTION: $t_1 = .005$" & $t_2 = .005$"

Section	n	AREA $A_{(IN^2)} = nA$	$Y_{ref(IN)}$	AY	AY^2	I_{OX-X}
1	2	.0592	10.95	.75774	8.29725	.00338
2	2	.1115	5.575	.62161	3.46548	1.15518
3	0	NEG.	NEG.	◄	———	——— ►
4	1	.1010	1.650	.16665	.27497	NEG.
5	1	.1010	.0025	.00025	NEG.	NEG.
6	2	.0592	.200	.01384	.00277	.00338
Σ		.4319		1.56009	12.04047	1.16310

$$\bar{y} = \frac{1.56009}{.4319} = 3.45229"$$

$$I_{XX_{NA}} = 1.16310 + 12.04047 - \underbrace{.4519(3.45229)^2}_{5.38583} = 7.81769 \text{ IN}^4$$

MODEL CONFIGURATION
2/22/72 PJC

ORBITER

MODEL AREA AND INERTIA AT STA 1314

try AGAIN: Assume $t_1 = .050"$ $t_{②} = .008"$ $t_{③} = t_{④} = .006"$ & $t_{⑤} = .030"$

SECTION	h	A	y_{ref}	Ay	Ay^2	I_{o-o}
1	2	.14500	13.345	1.93503	25.82284	Neg.
2	2	.21648	6.795	1.47098	9.99531	3.30248
3	1	.12108	4.060	.49158	1.99581	Neg
4	1	.12108	.033	.00400	.00013	Neg
5	2	.08820	.210	.01852	.00389	Neg
Σ		.69184		3.92011	37.81798	3.30248

$$\bar{y} = \frac{3.92011}{.69184} = \underline{5.66621"}$$

$$I_{NA}_{x-x} = 41.12046 - \underbrace{.69184(5.66621)^2}_{22.21217} = 18.908\ in^4 \angle 21.6\ Reg'd$$

try $t_{①} = .060"$ $t_{②} = .008"$ $t_{③} = t_{④} = .006"$ & $t_{⑤} = .025"$

Section	h	A	y_{ref}	Ay	Ay^2	I_{o-o}
1	2	.1728	13.340	2.30515	30.75070	Neg
2	2	.21648	6.790	1.46990	9.98055	3.30248
3	1	.12108	4.055	.49078	1.99008	Neg
4	1	.12108	.028	.00339	.00009	Neg
5	2	.07375	.200	.01475	.00295	Neg.
Σ		.70519		4.28417	42.72517	3.30248

$$\bar{y} = \frac{4.28417}{.70519} = \underline{6.0752"}$$

$$I_{NA}_{x-x} = 46.02765 - \underbrace{.70519(6.0752)^2}_{26.02719} = \underline{20.00}\ in^4 \angle 21.6\ Reg'd$$

but close enough

(≈ F.S. 1314 Section required)

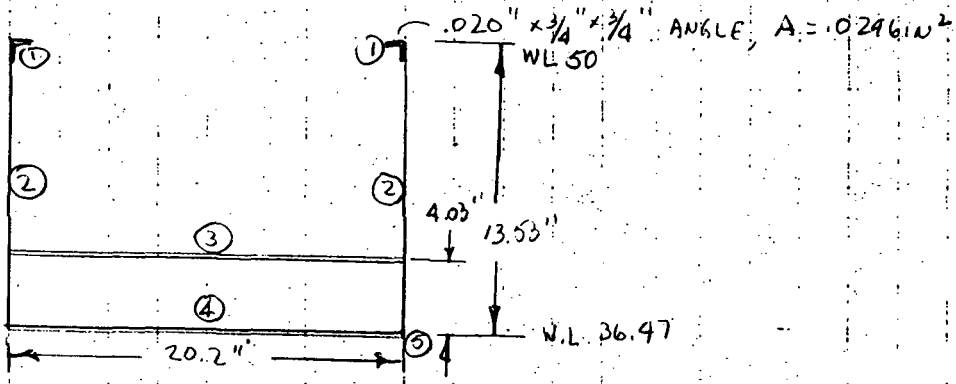

ORBITER 2/23/72 PJC

MODEL A AND I AT STA 76.8 Lower W.L. = 38.85 − .032009 [x − 57.0]

XSTA 76.825 Avg. Irq'd = 7.8 in 4 = 38.85 − .032009 [76.825 − 57.0] (19.825)

Assume $t_{①}$ = .020" $t_{②}$ = .008" $t_{③} = t_{④}$ = .006" $t_{⑤}$ = .010"

Section	h	A	Yref	AY	AY²	$I_{o\,x-x}$
1	2	.0592	11.595	.68642	7.95904	Neg.
2	2	.18856	5.903	1.11307	6.57039	2.18228
3	1	.12108	2.285	.27667	.63217	Neg.
4	1	.12108	.013	.00157	.00002	Neg.
5	2	.0298	.175	.00522	.00091	Neg.
Σ		.51972		2.08295	15.16253	2.18228

(17.34481)

$\bar{y} = \frac{2.08295}{.51972} = 4.00783"$

$I_{x-x\,NA} = 17.34481 - .51972(4.00783)^2 = 8.9967\ in^4$ vs. 7.8 in 4 req'd (8.34811)

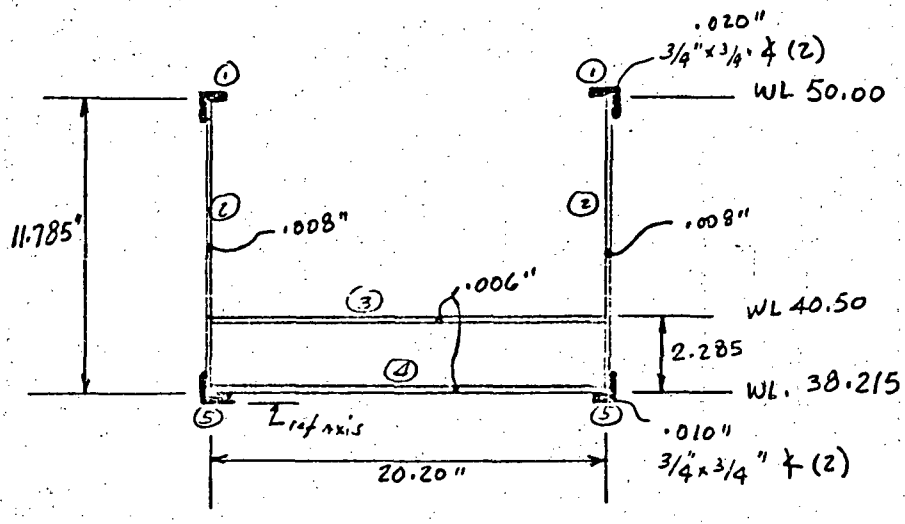

MODEL CONFIGURATION
2/23/72 PJC

ORBITER
MODEL I AND A AT STA 108.4

$t_{①} = .040"$ ✗
$t_{②} = .008"$
$t_{③} = t_{④} = .006"$
$t_{⑤} = .015"$ ✗

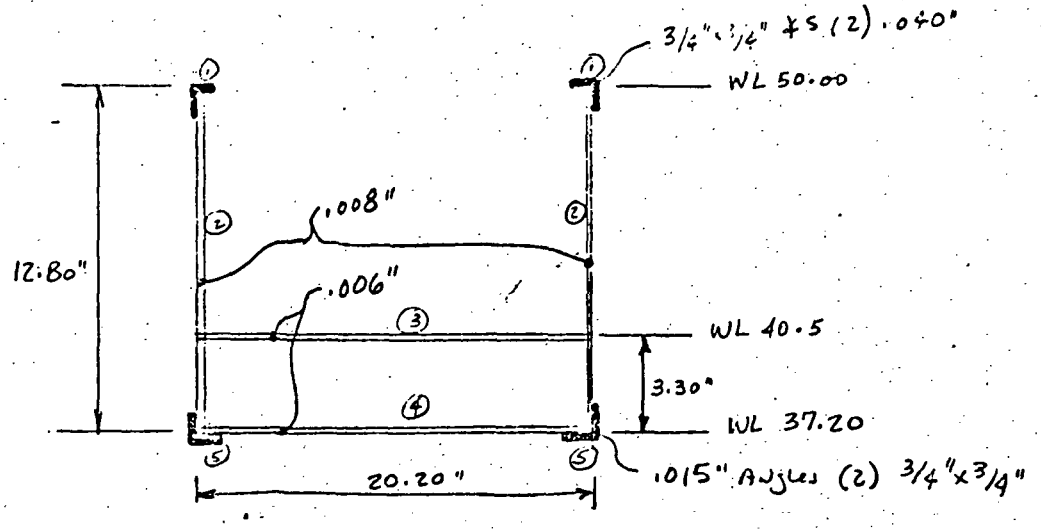

SECTION	n	A	Yref	Ay	Ay²	$I_{o\,x-x}$
1	2	.11680	12.57	1.46818	18.45490	Neg.
2	2	.2048	6.42	1.31482	8.44108	2.79626
3	1	.12108	3.32	.40199	1.33457	Neg.
4	1	.12108	.018	.00218	.00004	Neg.
5	2	.04455	.190	.00846	.00161	Neg.
Σ		.60831		3.19563	28.23220	2.79626

$$\bar{y} = \frac{3.19563}{.60831} = 5.25329" \qquad \bar{y}^2 = 27.59706$$

$$\therefore I_{NA\,x-x} = 31.02846 - .60831\,(27.59706) = 14.24089\ in^4 \text{ vs. } 15.6 \text{ req'd W.k.}$$

PROPOSED

ORBITER MODEL FUSELAGE GAGES

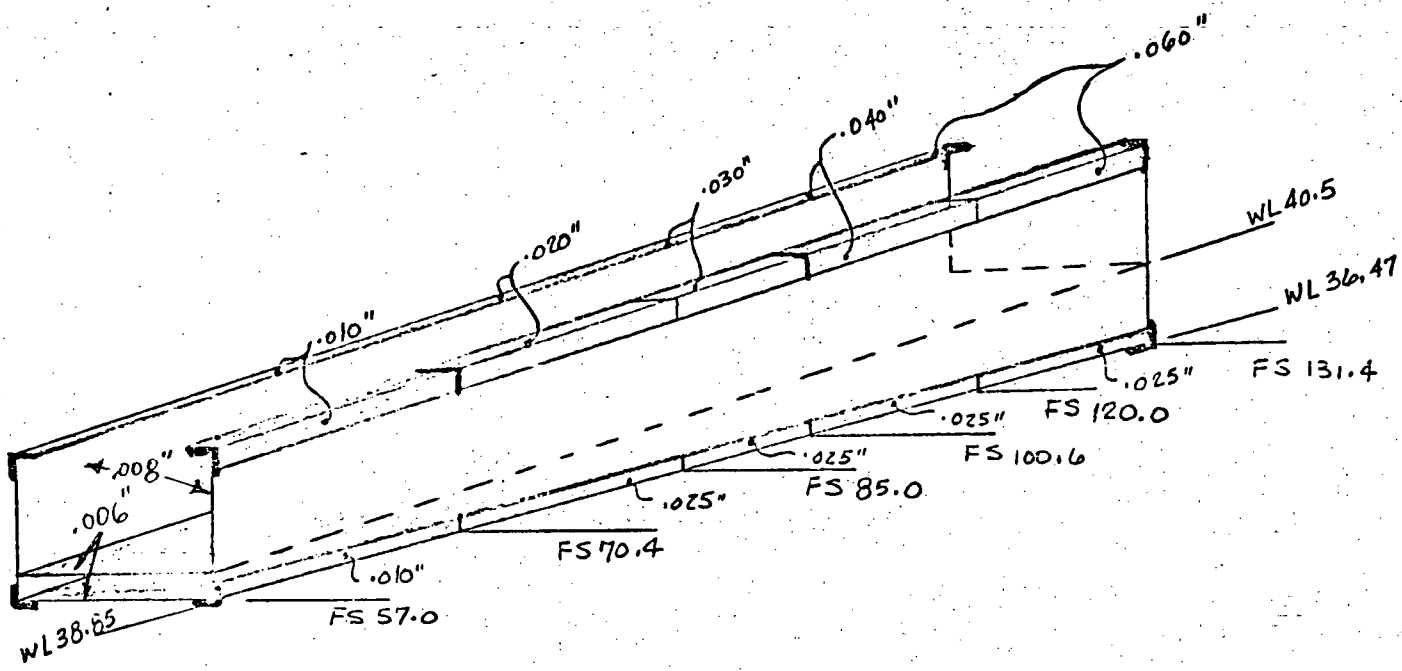

2/24/72 PJC

ORBITER DESIGN LOADS

ORBITER: 2.25g (ULTIMATE) (Reversible)
INERTIA LOADING

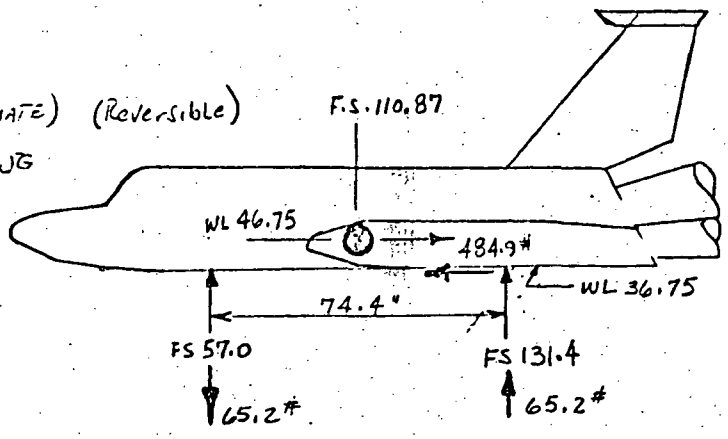

$R = \frac{484.9^{\#}(10.00")}{74.40"} = 65.2^{\#}$

ORBITER VEHICLE BODY DISTRIBUTION:

FS STA.	1g WEIGHT (LB)	2.25g WEIGHT (ULT.) (LB)	
250	2.575	5.80	
350	3.248	7.30	
450	10.368	23.30	
550	17.158	38.60	
650	10.625	23.90	
750	10.085	22.70	
850	9.728	21.90	
950	9.538	21.50	
1050	9.593	21.60	
1150	10.239	23.00	
1250	57.839	130.10	(R.H. & L.H. WINGS INCLUDED)
1350	9.607	21.60	
1450	40.510	91.10	
1550	14.426	32.50	(INCLUDES TAIL & CONTENTS)
Σ	215.549	484.9	

"AVERAGE" BODY LOAD DISTRIBUTION

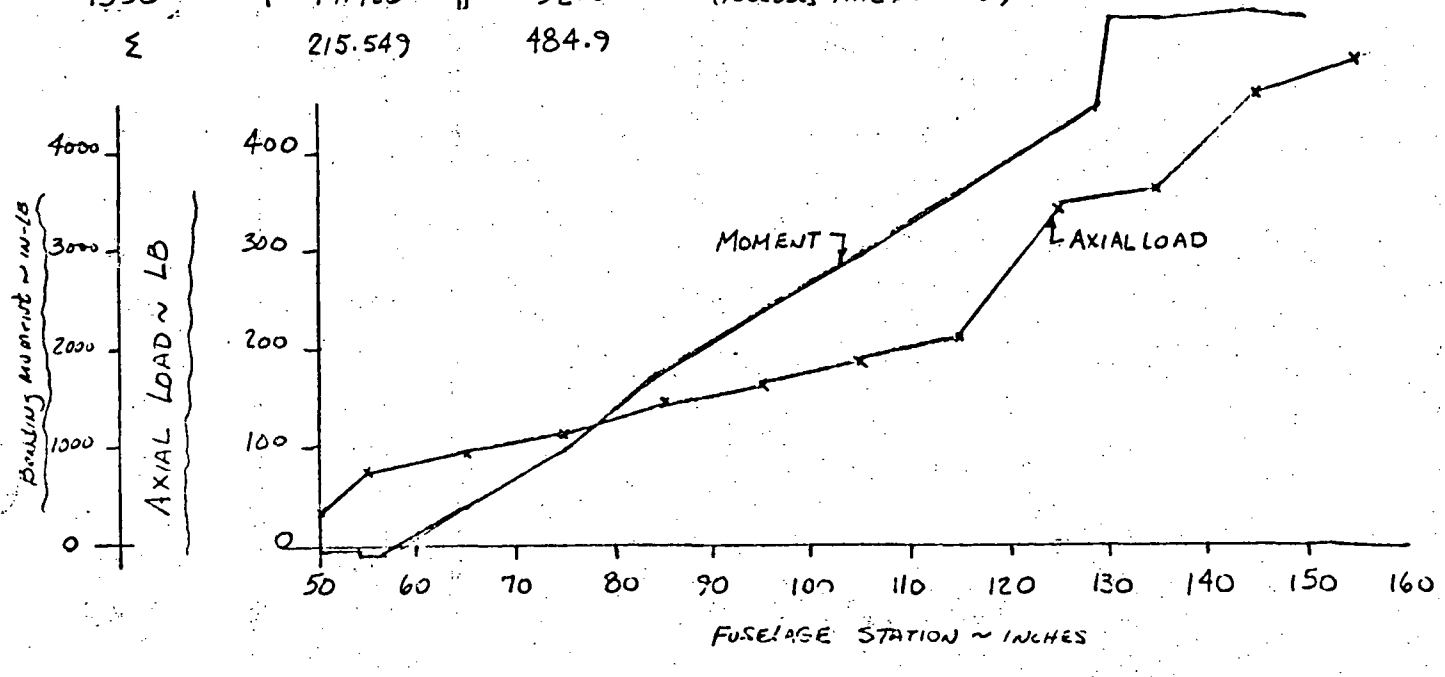

ORBITER "ACTUAL" BODY DISTRIBUTION WITH 45K PAYLOAD - AXIAL LOAD

W.L. 46.75 = ref Plane

NO.	LIMIT (lg) Weight (LB)	ULTIMATE (2.25 SF) Weight	$(\bar{X})$ F.S.	$(\bar{Z})$ W.L.	ΔWL (46.75 ref.)
1	2.575	5.80	24.29	47.20	+ .45
2	3.248	7.30	34.98	46.64	- .11
3	10.368	23.30	45.67	50.70	+ 3.95
4	17.158	38.60	54.36	47.93	+ 1.18
5	10.623	23.90	65.01	48.75	+ 2.00
6	10.085	22.70	74.96	48.68	+ 1.93
7	9.738	21.90	84.99	48.56	+ 1.81
8	9.539	21.50	95.01	48.32	+ 1.57
9	9.593	21.60	105.02	48.06	+ 1.31
10	10.239	23.00	115.29	47.45	+ .70
11	14.661	33.00	124.91	44.71	- 2.04
(WINGS) 12	43.178	97.20	127.97	40.04	- 6.71
13	9.607	21.60	135.07	44.41	- 2.34
14	40.510	91.10	144.62	47.61	+ .86
15	6.492	14.60	150.15	73.89	+ 27.14
16	7.934	17.80	151.11	44.12	- 2.63
Σ	215.543	484.90			

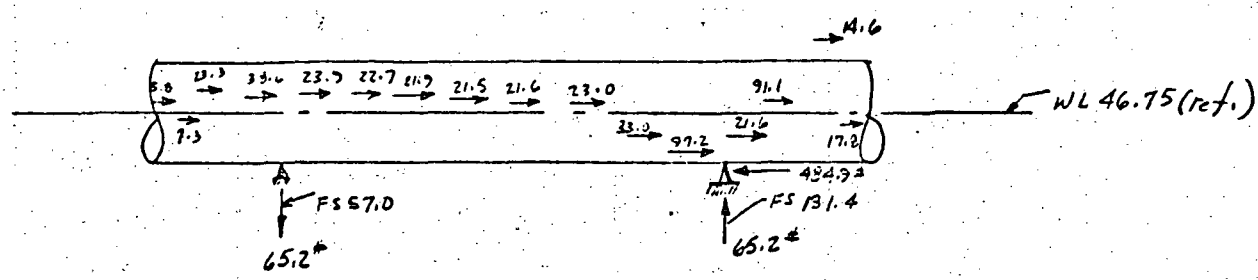

MODEL CONFIGURATION

2/28/72 RJC

ORBITER WEIGHT MODEL FOR DESIGN

NO.	2.25 g weight	($\bar{x}$) F.S. (IN.)	(46.75 ref.) ΔW.L. (IN.)	(comp. upward=+) ΣM (IN-LB)
1	5.80	24.29	+.45	0
2	7.30	34.98	-.11	+ 2.60
3	23.30	45.67	+3.95	+ 1.80
R_1=65.2# 4	38.60	54.36	+1.18	+ 93.80
→ 5	→	57.00	→	→ + 139.40
	23.90	65.01	+2.00	- 382.90
6	22.70	74.96	+1.93	- 983.80
7	21.90	84.99	+1.81	- 1733.30
8	21.50	95.01	+1.57	- 2347.00
9	21.60	105.02	+1.31	- 2965.90
10	23.00	115.29	+.70	- 3607.20
11	33.00	124.91	-2.04	- 4218.30
R_2=65.2# 12	97.20	127.97	-6.71	- 4485.20
→	→	131.40	→	- 5361.00
13	21.60	135.07	-2.34	- 5361.00
14	91.10	144.62	+.86	- 5411.50
15	14.60	150.15	+27.14	- 5334.10
16	17.80	151.11	-2.63	- 4937.90
				- 4984.70

GRUMMAN AEROSPACE CORPORATION